Investigation of MOSkin detectors for use in dosimetry of a HDR brachytherapy source

Anna Hayton
B.Sc. (Hons)

A thesis submitted in (partial) fulfilment
of the requirements for the degree of
Master of Applied Science
(Medical and Health Physics)

School of Applied Sciences
College of Science, Engineering and Health
RMIT University

December 2011

Declaration

I certify that except where due acknowledgement has been made, the work is that of the author alone; the work has not been submitted previously, in whole or in part, to qualify for any other academic award; the content of the thesis is the result of work which has been carried out since the official commencement date of the approved research program; any editorial work, paid or unpaid, carried out by a third party is acknowledged; and ethics procedures and guidelines have been followed.

Anna Hayton

2011

Acknowledgements

I would like to acknowledge the immense guidance provided by both my supervisors. A/Prof Annette Haworth and Dr Duncan Butler, without whose ongoing support the project would not have been finished. I would also like to thank Dr Alex Merchant and Dr Rick Franich for providing support through RMIT University.

I would like to thank the staff at the Peter MacCallum Cancer Centre, in particular the staff of the Physical Sciences Department including Mr Stephen Todd, Dr Joseph Pillainayagam, Dr Jim Hagekyriakouy and Dr Tomas Kron. I would also like to thank the radiation therapists, especially Ms Sylvia van Dyk, for their careful construction of the IOBT applicator.

This project would not have been possible without the generous supply of MOSkin detectors provided by the Centre for Medical Radiation Physics at the University of Wollongong and in particular I would like to thank Dr Dean Cutajar for his assistance.

I would like to thank my employers and the staff at The Australian Radiation Protection and Nuclear Safety Agency, for their support and guidance throughout my research.

Finally I would like to thank my family, in particular my mother and Michael for being patient in their support during this project.

Table of Contents

List of Figures

List of Tables

Abstract

Dose verification is an important part of all radiotherapy. Dose measurements in high dose rate brachytherapy can be challenging for a number of reasons. The steep dose gradient around HDR sources necessitates a dosimeter with a very small detection volume. Also, the logistics of placing a dosimeter in a clinically meaningful position requires they have a small physical size. In this thesis we explore the use of two detectors for measurement of the backscatter factor for an application involving the treatment of colorectal cancer. These treatments involve excising the tumour then delivering a radiation dose directly to the tumour bed during surgery using an Intra-Operative Brachytherapy applicator. In these cases the radiation dose is sometimes delivered in the absence of backscatter material which can lead to a lower dose being delivered than predicted by the treatment planning computer.

Two dosimeters currently in use in brachytherapy are TLDs and MOSFETs. The use of TLDs in medical dosimetry is well established, they have a small physical size and an approximately tissue equivalent atomic number. MOSFETs have a less extensive history in medical dosimetry but their use is gaining popularity. MOSFETs have a small detection volume and are capable of giving readings in real time, making them ideal candidates for measurements around HDR brachytherapy sources.

A number of MOSkin detectors were provided for this project. The MOSkin is a variation on the MOSFET detector, the main difference being a lack of epoxy bubble covering the MOSFET chip. The uncertainty in a single measurement with a MOSkin detector was estimated by examining the following dosimetric characteristics – stability, accumulated dose response, linearity, angular response, energy response, dose rate response and temperature response. Similar characteristics were also examined for TLD rods in order to make a comparison. Measurements were made using a HDR Ir-192 source, a kilovoltage treatment unit and a high

energy linac. Measurements were then made, using both TLD rods and MOSkins, to calculate the reduction in dose that results from a lack of backscatter material when using an IOBT applicator.

The largest variation in the response of the MOSkins was from accumulated dose, change in radial angle and radiation energy. For each of these characteristics the response was repeatable and therefore predicted by determining a correction factor from measurements. The largest variation in the response of the TLD rods was from changes in radiation energy which again was repeatable allowing the calculation of a correction factor. Using the IOBT applicator without adequate scatter material resulted in a reduction in delivered dose as measured with both the TLD rods and MOSkins and confirmed with previously published data calculated using Monte Carlo methods. MOSkin devices provide a useful measurement tool in the presence of high dose gradients, however, the dosimetric characteristics of the detector must be accounted for when estimating the uncertainty.

1 Introduction

1.1 Brachytherapy

Brachytherapy (from the Greek word *brachys*, meaning short and *therapeia*, meaning treatment) is a form of radiation therapy primarily used in the treatment of cancer. In brachytherapy treatments the dose of radiation is delivered by placing a radiation source within or in close proximity to the tumour volume. This is in contrast to external beam radiation therapy (EBRT), also known as teletherapy (from the Greek word tele, meaning far), where a linear accelerator is used to deliver the radiation dose from outside the body.

Brachytherapy has two main advantages over EBRT. The first is that placing the source either inside or in close proximity to the tumour volume means that the radiation does not have to pass through surrounding healthy tissue, as it does with EBRT, prior to reaching the tumour volume. The second is that brachytherapy sources have steep dose gradients meaning a high local dose of radiation can be delivered to the tumour volume and the majority of radiation is attenuated before it reaches surrounding healthy tissue.

1.2 High Dose Rate Brachytherapy

High Dose Rate (HDR), brachytherapy uses radioactive sources with a dose rate of greater than 12 Gyh^{-1}[1]. Modern HDR brachytherapy treatments are delivered using remote afterloading units, an example of these, the Nucletron microSelectron unit is shown in Figure 1.1.

Figure 1.1 The Nucletron microSelectron HDR treatment delivery unit used at the Peter MacCallum Cancer Centre.

The radioactive source is stored in a shielded safe inside the unit when it is not in use. For treatment delivery the radioactive source is sent out on the end of a wire through guide tubes. The guide tubes are connected to catheters which are either inserted directly in to the tumour volume or they can be connected to an applicator. The radioactive source is stepped through the treatment volume in the catheters under computer control. The positions in the catheters the radioactive source stops at are known as ‘dwell positions’. The location of each dwell position and the time the radioactive source remains in that dwell position is determined using a computer treatment planning system to achieve the desired dose distribution. A known limitation of some computer treatment planning systems is that dwell times are calculated with the assumption that the source is completely surrounded by scatter material. If this is not the case the dose delivered is less than reported by the treatment planning system.

1.3 HDR Intra-Operative Brachytherapy

Intra-Operative Brachytherapy (IOBT), describes brachytherapy in which catheters or an applicator are placed near to or in contact with the tumour volume, or tumour bed following surgical removal of the tumour, during surgery. IOBT is used for selected cases of rectal cancer in combination with surgery and HDR brachytherapy at the Peter MacCallum Cancer Centre[2]. For these treatments the tumour is excised then an IOBT applicator is placed on the tumour bed. The catheters of the applicator are connected to the delivery tubes of the HDR after loader. It is not practical to take a CT image for treatment planning purposes because the patient is undergoing surgery, therefore a suitable library treatment plan is used to deliver the dose of radiation, typically 10 Gy to the surface of the applicator, before the surgery is completed. The patient's body provides scatter material below the IOBT applicator but it is not practical to provide a significant amount of extra scatter material above the applicator to provide full scatter conditions.

1.4 Dosimetry in Brachytherapy

Detectors in brachytherapy may be used for in-vivo dosimetry, a method for verifying the dose delivered to the patient, and may be used for dose measurements, for example when there is some doubt in the accuracy of the dose predicted by the planning computer. Whatever the purpose, dosimeters in brachytherapy generally need to be small in size due to the steep gradients surrounding a radioactive source.

Detectors that have been used for in vivo dosimetry include thermoluminescent dosimeters (TLDs), diodes, radiochromic film and Metal Oxide Semiconductor Field Effect Transistors (MOSFETs)[3].

TLDs have been widely used in medical dosimetry for over fifty years[4]. They are solid state detectors commonly consisting of lithium fluoride (LiF) in a lattice structure, and their

capability to record and store the absorbed dose is due to impurities in the LiF lattice in the form of magnesium, titanium, copper or phosphorus. They are available in a variety of forms, including chips, rods, powder and ribbons. TLDs can be used repeatedly and do not require auxiliary cables or equipment during the irradiation[5]. They do however, require a reproducible heating and cooling cycle during the read out and a time consuming annealing process post irradiation before the next measurement can be made. They are also able to store the measured dose for long periods of time with relatively little loss of signal due to fading[5].

Radiochromic film, unlike conventional film, is insensitive to visible light but changes colour with absorbed ionising radiation dose. The change in colour is due to a chemical reaction that results in the formation of a highly coloured dye salt when the film is exposed to ionising radiation[6]. The film does not require any subsequent processing and film dosimetry has the advantage of providing a 2D dose distribution[7]. There are several disadvantages to radiochromic film, these include a sensitivity to ultraviolet light and humidity[6], a non linear dose response and energy response[8, 9]. The scanning technique used to read the film can also introduce uncertainties such as fluctuations in the light source of the flatbed scanner[9] and changing the film orientation during scanning can also introduce uncertainty[8].

Diode dosimeters are semiconductor detectors. Incident radiation causes the production of electron hole pairs, the movement of which induces a current[10]. They have a high spatial resolution when compared to ionisation chambers but like all semiconductor detectors, their sensitivity is dependent on temperature, dose rate and energy[11].

MOSFETs are also semiconductor detectors. Radiation doses are recorded via a threshold voltage that is altered by damage to the detector caused by incident radiation. They have an extremely small dosimetric volume and the ability to permanently store the accumulated dose or give a measurement in real time, i.e. as the treatment is being delivered[12]. The

disadvantage is that they have a limited useful lifetime that is dependent on accumulated dose. A new type of MOSFET, known as the MOSkin, offers a skin dose equivalent detection depth of 70 μm[13].

1.5 Scope of this project

This project investigated the use of two detectors in the measurement of dose for brachytherapy applications. Specifically, the measurement of the reduction in dose due to the absence of backscatter material above an IOBT applicator was addressed. Measurements were made with two detector types, TLD rods and MOSkins. TLD rods were used because they have a history of use in medical dosimetry, and can be used repeatedly with proper post irradiation annealing. The decision to use MOSkins was based on several factors. Their use as medical dosimeters is relatively new, they have a small detection volume which is ideal for use in steep dose gradients and they can give real time measurements, an ability most other detectors lack.

1.5.1 Thesis

This aim of this project was to first determine the response of MOSkin dosimeters for a number of characteristics relevant to dosimetry in brachytherapy including stability, linearity, angular, energy and temperature response. These characteristics were also measured for a batch of TLD rods so a comparison between the MOSkins and TLD rods could be made and also to test the experimental design before the MOSkins were used so that their useful lifetime was not wasted.

Both the MOSkins and TLD rods were then used to measure the reduction in dose resulting from inadequate scatter material above an IOBT applicator, which can occur clinically. These measurements were then compared to a theoretically calculated reduction in dose.

1.5.2 Overview of Thesis

In Chapter 2 of this thesis a literature review of TLDs and MOSFETs is provided, detailing their known responses to various dosimetric characteristics. This chapter also provides a literature review of brachytherapy in particular IOBT and the challenges involved.

In Chapters 3 and 4 the process of measurements taken to characterise the TLD rods and MOSkins is described, respectively.

In Chapter 5 the measurements made using the IOBT applicator in the presence and absence of backscatter material, using the TLD rods, MOSkins and dual MOSkins are described. In Chapter 6 the capabilities and uncertainties of each detector are summarised and their suitability as dosimeters in brachytherapy applications are discussed, along with suggestions for future work to build on the work presented in this thesis.

2 Dosimeters and Clinical Intra-Operative Brachytherapy

2.1 Thermoluminescent Dosimeters

Thermoluminescent dosimeters (TLDs), are integrating solid crystal radiation detectors. The materials used to make TLDs for the purpose of medical dosimetry include lithium fluoride (LiF), calcium fluoride (CaF_2) and calcium sulphate ($CaSO_4$). TLDs have an extremely long useful lifetime but their main disadvantages are they require a time consuming annealing process between irradiations and are not capable of giving measurements in real time.

The TLDs used in this project were TLD rods (type TLD-100, Harshaw, USA). TLD 100 refers to Lithium Fluoride doped with Magnesium and Titanium (LiF:Ti,Mg). The effective atomic number of Lithium Fluoride is 8.2, which is similar to the effective atomic number of water of 7.4[10], making TLD 100 material suitable for medical dosimetry. The TLD rods had a total volume of $6mm^3$, (dimensions 6 mm × 1 mm × 1 mm).

2.1.1 Thermoluminescent Dosimeter Theory

Pure Lithium Fluoride forms a regular crystal lattice structure, the addition of impurities giving it thermoluminescent qualities. For TLD 100, the addition of magnesium creates the electron traps and the addition of titanium is required for the generation of luminescence centres[5].

At room temperature the structure of the TLD crystal is such that all electrons remain in the valence band and the material is non-conducting. When the material is exposed to ionizing radiation, electrons from the valence band gain enough energy to jump to the conduction band. Most of these electrons fall back to the valence band, but a small percentage are caught in electron traps with energies between that of the valence and conduction band. Each electron trap has a specific lifetime that is dependent on the energy depth of the trap. Shallow traps, or those with the lowest energies, will empty spontaneously at room temperature with a

half-life of approximately 10 minutes. Other deeper traps may empty spontaneously but have a half-life of more than 100 years.

For the electron trap to empty the electron must move from the trap to the conduction band by gaining energy, this is achieved by heating the material. Once in the conduction band the electron then moves back to the valence band with the emission of visible light. A schematic of the thermoluminescence process is shown in Figure 2.1

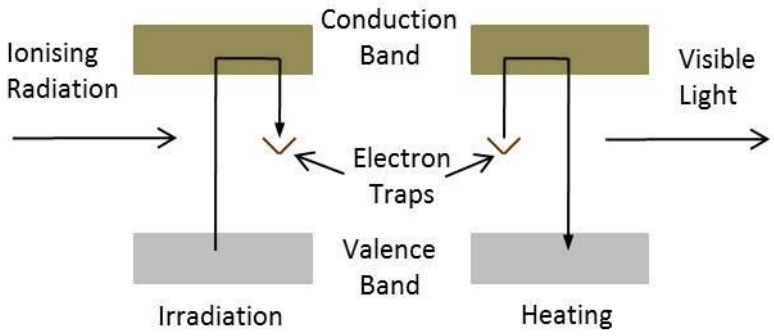

Figure 2.1 Diagram of the thermoluminescence process.

The total ionizing radiation absorbed by the TLD is calculated by measuring the total light emitted when all electron traps are emptied. The radiation absorbed by the detector is proportional to the visible light emitted by the relation described in Equation 2.1[5].

$$I_{ir} = f I_{vl} \qquad \text{Equation 2.1}$$

Where I_{ir} *is the intensity of the ionising radiation incident on the TLD*

I_{vl} *is the intensity of the visible light emitted by the TLD*

f *is a complex function that relates to the material, geometry and radiation and thermal history of the specific TLD material*[5].

To empty all electron traps the TLD is heated through a range of temperatures and the intensity of the light emitted is measured as a function of temperature. A plot of the intensity of emitted light versus temperature produces a graph known as a glow curve. A glow curve is actually made up of several component glow curves. Each component glow curve represents a

different trap energy. The shallow traps are represented by the first peak as the shallower the trap the lower the temperature required to empty it. Figure 2.2 shows a typical TLD 100 glow curve and its deconvolution into four glow peaks[14].

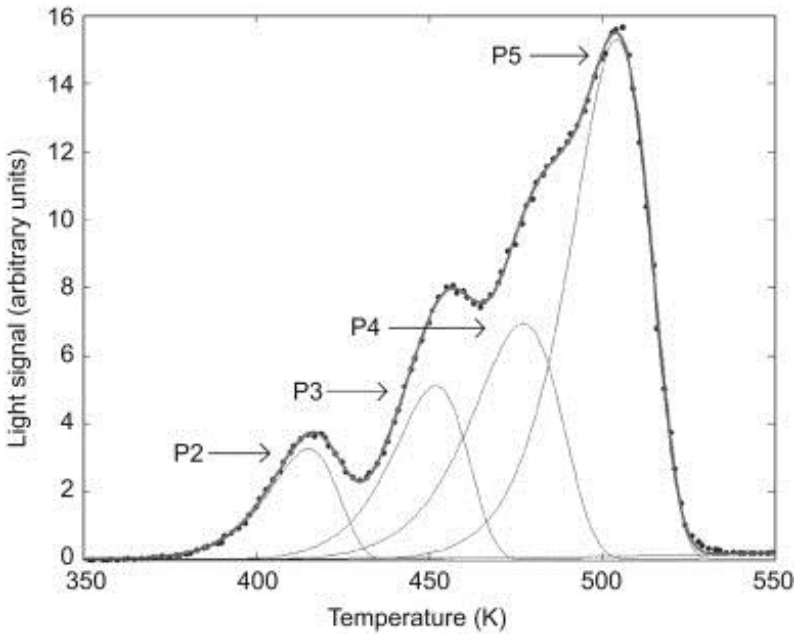

Figure 2.2 A typical TLD 100 glow curve and its deconvolution into four glow peaks[14].

Each component glow curve is assigned a peak number which relates to the approximate energy gap of the electron trap. Kron et al[5], described each peak of the glow curve from TLD 100 material in terms of the approximate energy gap, read out temperature, approximate contribution to read out and half-life at room temperature, see Table 2.1.

Peak Number	Approximate Energy Gap (eV)	Read Out Temperature (°C)	Approximate Contribution to Read Out[1]	Half Life at Room Temperature
I	1.04	70	0.0	10 mins
II	1.07	105	0.2	20 hours
III	1.05	130	0.3	6 months
IV	1.53	170	1.0	10 years
V	2.21	195	0.1	80 years

1 normalised to the readout contribution of peak V

Table 2.1 Glow curve peak data for TLD 100 material taken from Kron et al[5].

As the peak number increases, so does the approximate energy gap. As the approximate energy gap increases more energy is required to empty the trap, meaning the read out temperature also increases with increasing peak number. The half-life refers to the likelihood of the electron trap emptying spontaneously at room temperature. The smaller the energy gap the shorter the half-life, meaning the half-life also increases with increasing peak number. Peak I and II have half-lives of 10 mins and 20 hrs respectively, so it is important to be consistent with the time at which the TLDs are read out post irradiation. Reading the dose prior to 20 hrs for some measurements and post 20 hrs for other measurements means that the contribution to the dose from peak II may vary significantly across measurements introducing a large unnecessary uncertainty. Peaks II-V can be identified as deconvoluted peaks in Figure 2.2.

Figure 2.3 shows a glow curve from one of the TLD rods used in this project. The shoulder on the left hand side of the curve is evidence of the separate component glow curves.

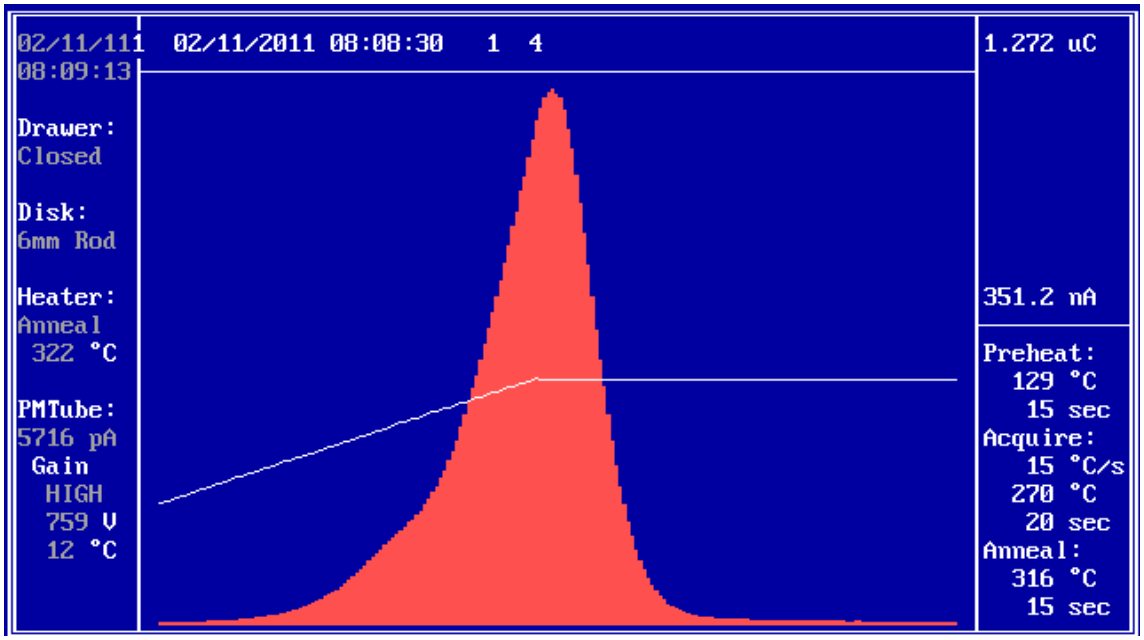

Figure 2.3 Screen shot of a glow curve from a TLD rod used in this project. The white line indicates the relative temperature at which each part of the glow curve is produced.

The measured emitted light, or light reading, from the TLD material must be converted into absorbed dose. The factor used to convert this raw measurement into absorbed dose depends on the characteristics of the TLD material. This will determine its sensitivity, linearity with dose, dose rate, energy and angular response. These factors will vary for different thermoluminescent materials as well as the form of the thermoluminescent detector. In this project these factors were determined by commissioning the TLD rods and are described in Chapter 3.

2.2 Thermoluminescent Dosimeter Characteristics

2.2.1 Sensitivity

The sensitivity of any batch of TLDs depends on the material composition and the thermal history[5]. The number of impurities added to the lattice structure will affect the sensitivity. Intentionally introduced impurities such as magnesium and titanium will increase the number of electrons that can become trapped for a given dose, increasing the visible light output upon heating. The heating pattern during the read out and the annealing process also has an effect on the sensitivity. Even slight changes to the heating pattern during the annealing process can alter the sensitivity significantly. For example, the sensitivity can be increased if cooling after the annealing process is rapid[5]. For this reason the heating rates and temperatures reached during the annealing process must be reproduced precisely each time the dosimeters are used, as failure to do so will introduce further uncertainty into dose measurements. A major advantage of TLDs is that they can be used repeatedly, however, care must be taken during the annealing process to maintain detector stability over repeated use.

2.2.2 Linearity

If the raw response of a detector can be multiplied by a constant to convert it to absorbed dose then the response of the detector is said to be linear with dose. TLD 100 rods display good linearity between 0.01 Gy and 3 Gy[5]. Above 3 Gy they display an overestimation of dose, supralinearity which can be explained by the track model[5, 15]. Electron-hole pairs are formed along the tracks of secondary ionising particles, these electron-hole pairs can form luminescent centre. The track model states that when the dose is high these tracks become closer together meaning the electron-hole pairs are also closer together. When the material is heated some of the electrons recombine with the new luminescent centres created resulting in the emission of light[16]. This light is additional to the light that is emitted from the

intentional luminescent centres in the material meaning the relationship of response (emitted light), to dose at these high dose levels is not linear.

At doses above approximately 200 Gy the sensitivity of the detector decreases due to radiation damage, which is permanent[5].

2.2.3 Dose Rate Response

According to Kron[5], TLD 100 detectors show no dose rate response up to 10^8 Gys^{-1}, however, this reflects the findings of studies with an accuracy of 5% or worse. Tochilin et al[17], also reported dose rate independence of LiF materials, up to 10^9 Gys^{-1} with an accuracy of 10%.

2.2.4 Angular Response

Kron[5], states that no wall effects or directional dependence of the reading can be expected for symmetrical detectors or powders. If however, the detector does not have equal dimensions in all directions, then attenuation and light self absorption may alter the response with incidence angle. The TLD rods used in this project had dimensions of 6 mm × 1 mm × 1 mm, meaning they have only one axis of symmetry and it should be possible to observe a non-isotropic response around either of the two other axes.

2.2.5 Energy Response

The variation in response of TLDs depends on a variety of factors such as effective atomic number, dopants and impurities, thermal history, read out process, absorbed dose and detector size[18]. Theoretically the photon energy response of TLD materials is given by Equation 2.2[15].

$$S(E) = \frac{\left(\mu_{en}/\rho\right)_{TLD}}{\left(\mu_{en}/\rho\right)_{WATER}} \eta(E) \qquad \text{Equation 2.2}$$

Where $S(E)$ *is the photon energy dependence*

μ_{en}/ρ *are mass energy absorption coefficients*

$\eta(E)$ *is the relative thermoluminescent response*

Figure 2.4 shows the photon energy response for LiF and Water, calculated using Equation 2.2 assuming n(E) = 1, and mass energy absorption coefficients obtained from the Physical Measurement Laboratory, NIST[19], normalised to the ratio at 2000 keV.

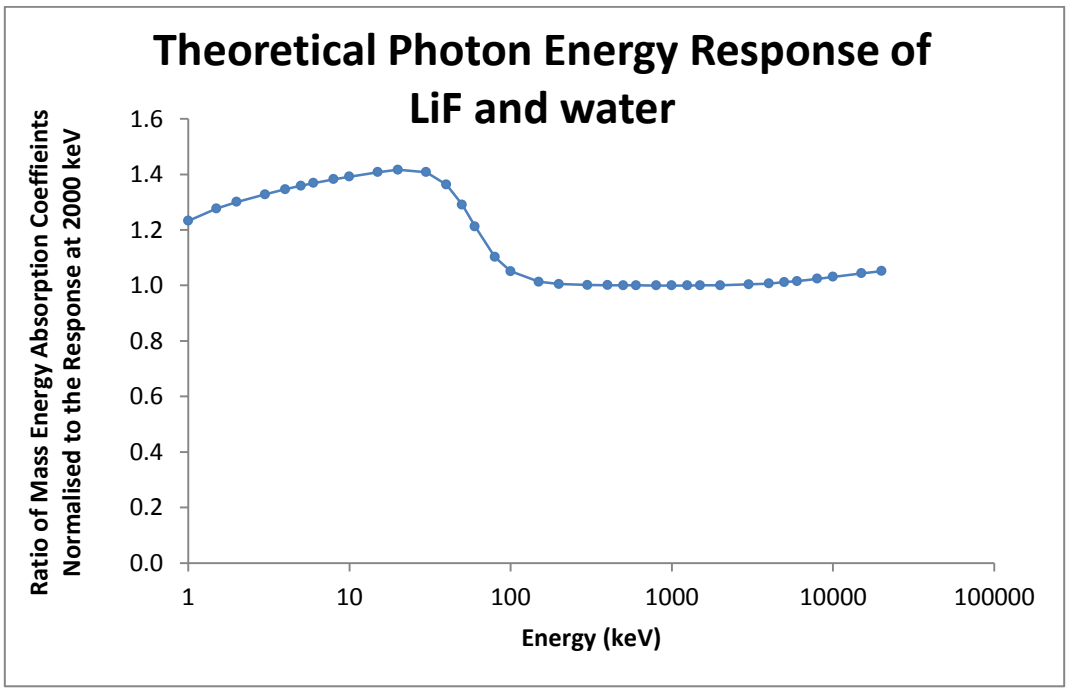

Figure 2.4 The photon energy response of LiF and water calculated using Equation 2.2, with mass energy absorption coefficients obtained from the Physical Measurement Laboratory[19], normalised to the ratio at 2000 keV.

At high energies TLD 100 is approximately tissue equivalent due to its effective atomic number (approximately equivalent to soft tissue (7.4)[20]). At lower energies where the photoelectric effect predominates, slight differences in atomic number result in a rapid change in response with energy compared to water. This is displayed in Figure 2.4 where the theoretical response of LiF remains relatively constant for photon energies above 100 keV but below 100 keV the response increases rapidly until a maximum over response of approximately 1.42 is reached at 20 keV. Below 20 keV the response falls slightly due to self absorption of the soft energy within the TLD rod. The theoretical response in Figure 2.4 has been calculated using $\eta(E)=1$ which may not be the case for the specific LiF material. This theoretically predicted maximum over response of 1.42 times the response at 2000 keV is in agreement with experimental findings

that have measured the maximum over response of TLD 100 material to be between 1.3 and 1.7 times the response at 2000 keV[4, 5].

The HDR Ir-192 source used for brachytherapy treatments emits a spectrum of photons with energies ranging from 201 keV to 884 keV[21]. The effective energy from a HDR Ir-192 source decreases with increasing depth in water due to the increase in fluence of low energy scatter photons. At a distance of 10 mm in water the effective energy is 337 keV and at a distance of 100 mm the effective energy is 221 keV[21]. Using a linear relationship between points calculated from Figure 2.4, these energies correspond to a theoretical response of 1.001 and 1.004 times the response at 2000 keV respectively.

The response of TLD 100 material to variations in irradiation energy has been reported by a number of authors [4, 5, 18]. Of particular interest is the finding of Meigooni et al[22], and Thomason et al[23].

Meigooni et al[22] reported the response of TLD 100 chips to various effective energies in water relative to the response at 4 MV on a linac. They found that the response was 1.41, 1.23 and 1.10 at 100 keV, 250 keV and 392 keV respectively, relative to the response at 4 MV. In contrast to this Thomason et al[23], found that the energy response of TLD 100 material varied by less than 1.0% when irradiated at distances between 10 mm (337 kV) and 100 mm (221 kV) from an Ir-192 source in water. It was suggested by Thomason et al[24] that the discrepancies between results due to differences in the experimental set ups, namely, the presence of an air gap in the Meigooni set up[24]. This point was disputed by Meli et al[25].

In Chapter 3, the characteristics of the TLDs provided for this project were determined for direct comparison with published data.

2.3 MOSFET Detectors

MOSFETs, or Metal Oxide Semiconductor Field Effect Transistors, are transistor components commonly used in electronic devices. They were first developed in 1959 by Atalla and Kahng[26] and during the 1960s they were used in computer logic circuits. In 1974 the response of the devices to ionising radiation and their capability to measure integrated dose was first published[27]. The devices began to be used in radiotherapy measurements in the 1980s[28].

2.3.1 MOSFET Detector Theory

MOSFET detectors are semiconductor devices. They consist of a base of p-type silicon which is connected to three electrical terminals known as the source, gate and drain. The source and drain are connected directly to the p-type silicon while the gate is connected to a thin layer of insulating silicon dioxide connected to the p-type silicon. A schematic of a MOSFET device is shown in Figure 2.5.

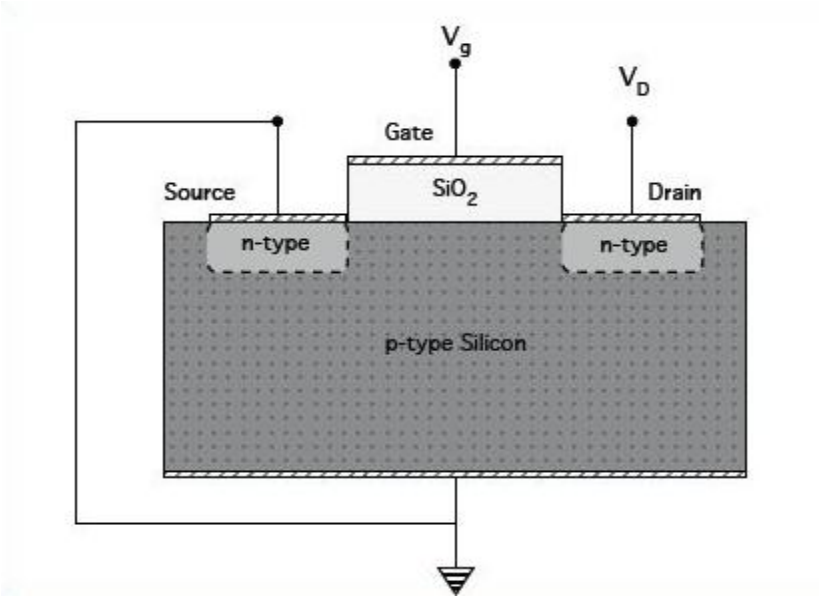

Figure 2.5 A schematic diagram of a MOSFET device illustrating the relative position of the gate, silicon dioxide and semiconductor material.

For the MOSFET to function, a bias voltage must be applied to the gate, V_g. This causes the layer of silicon dioxide to become electron rich. It also causes an inversion layer to form at the

silicon dioxide/p-type silicon interface. The inversion layer forms a channel connecting the source and drain which allows a current to flow. When the MOSFET is exposed to ionising radiation, electron-hole pairs form in the silicon dioxide. The electrons move out the gate electrode and the holes move towards the interface with the p-type silicon. At the interface the holes become trapped in long term sites. This trapping of holes causes a negative threshold shift. Measurements are made with MOSFET detectors by recording the threshold voltage before and after irradiation, with the change in threshold voltage being proportional to the absorbed dose of radiation.

2.3.2 Development of Commercial MOSFETs for use as Medical Dosimeters

In 1985 Hughes[29] used a RADFET, a radiation-sensitive MOSFET, to monitor the dose received during a radiotherapy treatment for breast cancer. Interest in MOSFET devices as medical dosimeters grew with Thomson and Nielsen marketing the first clinical dosimetry system in the 1990s[28]. Two other companies also manufacture MOSFET detectors for medical dosimetry; Sicel Technologies (Morrisville, NC, USA) manufacture the OneDose dosimetry verification system involving a single use disposable MOSFET and the Centre for Medical Radiation Physics, CMRP, (University of Wollongong, NSW, Australia) manufacture the MOSkin and Clinical Dose Verification System. Thomson and Nielsen now manufacture a number of MOSFET products the most recent of which is the microMOSFET and Portable dose verification system.

The MOSFET detectors used in this project were MOSkins. In comparison to the traditional design of MOSFET detectors where the MOSFET chip sits on top of a substrate enclosed in a bubble of epoxy, the new MOSkin detector has the MOSFET chip sitting below the surface of the substrate enclosed by a layer of build-up material. The differences between the older epoxy style MOSFET detectors and new MOSkin detector are illustrated in Figure 2.6.

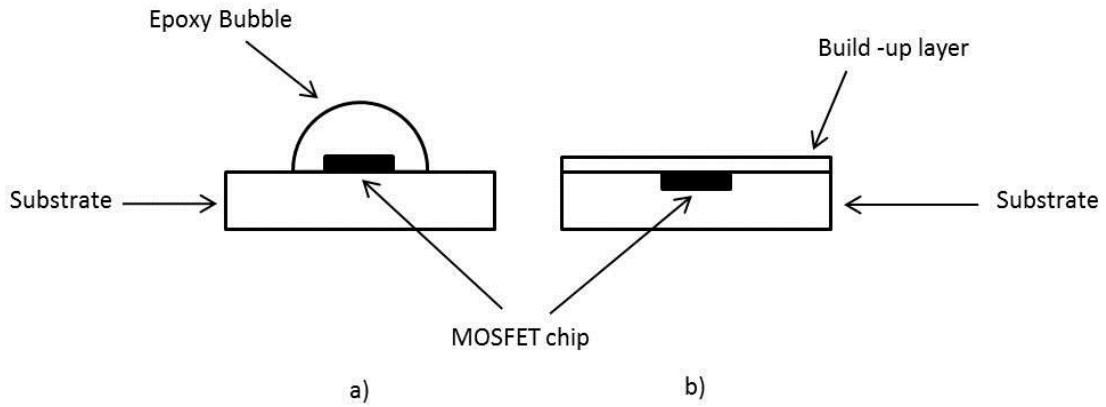

Figure 2.6 Diagram of the cross section of a) 'epoxy bubble' style MOSFET detector and b) new MOSkin detector.

The epoxy bubble covering of the MOSFET chip on the older style MOSFET detector was subject to variations in size leading to variations in the water equivalent detection depth. The build-up layer covering the MOSFET chip in the new MOSkin detector can be manufactured to a specific thickness with good reproducibility, meaning the water equivalent detection depth can be altered depending on the detectors application[13].

2.4 MOSFET Detector Characteristics

2.4.1 Short Term Response/Reproducibility

Short term response, or reproducibility, refers to the tendency for consecutive measurements of equal doses to produce varying measurements. When a measurement is made using a MOSFET detector the measuring circuit injects a small amount of charge into the MOSFET chip. This injection of charge creates a temporary perturbation in the charge distribution which will decay in a few minutes[30]. This perturbation leads to small variations in measurements of equal doses.

Kwan et al[31], found the reproducibility of MOSkin detectors to be 3.2% in comparison with Thompson and Nielsen detectors which are reported to be between 1.0% and 2.0%[30, 32].

2.4.1.1 Creep Up

'Creep Up' is a term used to describe the situation when a second measurement is made in close succession to a first measurement, before the perturbations created as a result of the injection of charge from the first measurement have decayed sufficiently. In this situation the second injection of charge causes an amplification of the charge perturbation resulting in an elevation of the apparent dose[30]. Measurements made by Ramani et al[30], found this phenomenon to have a negligible effect on the dose if a wait period of 60 seconds was observed after each read out before the next measurement was made.

2.4.2 Long Term Response/Response with Accumulated Dose

The response of MOSFETs is known to decrease with accumulated dose[30, 33]. The threshold voltage of a MOSFET detector is affected by the trapping of holes in the Silicon dioxide which lead to a reduction in the electrical field in the gate oxide[34]. This influences the electron-hole recombination and charge yield. Fewer holes escape electron-hole recombination leading to fewer holes being trapped at the p-type Silicon/Silicon dioxide interface[35].

Cheung et al[33], found that the decrease in response of CMRP MOSFETs followed a low second order polynomial. This response was reproducible and the rate of decrease was found to be related to the effective energy of radiation. For 6 MV linac radiation a decrease of 0.13% per Gy was observed, with a decrease of 0.19% per Gy for 250 kVp radiation and a decrease of 0.33% per Gy for 100 kVp radiation. Kron et al[34], found a linear decrease in the response of CMRP MOSFET detectors of approximately 3% per threshold voltage change of 1 Volt at 4 MV linac radiation.

2.4.3 Linearity

Ramaseshan et al[32], found the response of microMOSFET detectors manufactured by Thompson and Nielson to be linear between 0.05 Gy and 5 Gy. Cheung et al[33], measured CMRP MOSFET detectors over a wider range and found their response to be linear between 0 Gy and 30 Gy, an important factor given that in brachytherapy the dose per fraction can range from 6-12 Gy for prostate treatments[36].

2.4.4 Dose Rate Response

MOSFET detectors have been found to show no variation in response across a range of dose rates. Fagerstrom et al[37], measured the dose rate response of the Dose Verification System (Sicel Technologies, NC, USA) and found no variation in response across dose rates between 3.7 $mGys^{-1}$ and 14 $mGys^{-1}$. Similarly, Halvorsen[38], measured the dose rate response of the OneDose system (Sicel Technologies, IA, USA) and found no variation across dose rates between 13.3 $mGys^{-1}$ and 79.9 $mGys^{-1}$. Ramaeshan et al[32], measured the dose rate response of microMOSFET detectors (Thompson and Nielsen, Ottawa, Canada) and found no variation across dose rates between 16.7 $mGys^{-1}$ and 100 $mGys^{-1}$. Dose rates used in brachytherapy typically range from 2.5 $mGys^{-1}$ up to 125 $mGys^{-1}$ (for a 10 Ci Ir-192 source at 10 mm and a 5 Ci Ir-192 source at 50 mm[39]).

2.4.5 Energy Response

The response of MOSFET detectors is related to the effective atomic number of the material from which the detector is made, including the sensitive oxide layers, substrate material and detector housing[33]. At low photon energies, below 100 kVp, the photo electric effect results in the emission of excess photo electrons from the detector packaging which contribute to the dose measured[32]. The response is also dependent on the dynamics of recombination of the electron-hole pairs in the silicon dioxide[34]. As photon energy decreases the recombination effects increase leading to reduced sensitivity.

Cheung et al[33], measured the response of CMRP MOSFET detectors to varying photon energies and found the response was a maximum at 30 kVp of 3.2 times the response at 6 MV, whereas Kron et al[34], found the response was a maximum at 35 kVp of 7.1 times the response at 6 MV. Kron et al [34], also measured the response of Thomson and Nielsen MOSFET detectors and found a maximum response at 50 kVp of 3 times the response at 6 MV. The maximum response occurring at a higher energy for the Thomson and Nielsen MOSFETs is due to a thicker layer of packing around the MOSFET chip sensor. The Thomson and Nielsen MOSFETs had a 2 mm thick epoxy covering while the CMRP MOSFETs had no epoxy covering. The epoxy covering acted as an additional filter for the low-energy part of the spectra[34], resulting in the maximum over response occurring at a higher effective energy.

2.4.6 Temperature Response

All MOSFET devices have an inherent thermal error which can shift the threshold voltage as a function of temperature[40, 41]. Cheung et al[40], found that the response of a CMRP MOSFET detector varied by only 1.5% when irradiated over a range of temperatures from 15°C to 40°C. This is in agreement with the findings of Rmaseshan et al[32], who also measured the response of Thompson and Nielsen MOSFET detectors and found no measurable variations across temperatures ranging from 20°C to 40°C. However, Cheung et al[40], also found that if the

MOSFET detector undergoes a large temperature change after its initial threshold voltage read out and before the final voltage readout, there could be a variation of up to 10% compared to measurements made when the initial and final voltage read out are made at the same temperature. Cheung et al[40], also found that the threshold voltage of a CMRP MOSFET detector decreased with increasing temperature in the absence of dose. A decrease of 50 mV was observed when the detectors temperature was increased from 20°C to 45°C.

In Chapter 4 of this thesis we describe the measurements made to characterise the MOSkin detectors used for this project

2.5 Clinical Intra-Operative Brachytherapy (IOBT)

2.5.1 History

In 1901, only five years after the discovery of radioactivity, a case of cutaneous lupus was treated with a small amount of radium[42]. This is considered the birth of brachytherapy. Two years later, in 1903 Alexander Graham Bell suggested that 'there is no reason why a tiny fragment of radium sealed in a tiny glass tube should not be inserted into the very heart of the cancer', which can be credited as the first reference to interstitial brachytherapy[42]. An early instance of Intra-Operative brachytherapy occurred in 1929 when Sir Henry Souttar inserted radium needles into a brain tumour via a hole in the skull flap[43].

2.5.2 Modern Intra-Operative Brachytherapy

The modern version of Intra-Operative brachytherapy began in the 1980s. While remote afterloading devices had been in clinical use since the 1960s they had primarily been used for the treatment of outpatients, operating theatres had not been designed with adequate shielding for the use of HDR sources during surgery[44]. The first applicators used in HDR IOBT consisted of plastic needles anchored in superflab which was flexible enough to access and treat most surfaces[45]. This basic design of the applicator has not changed in the last 30 years. The HAM applicator[46], Figure 2.7, consists of an array of catheters embedded in a flexible pad of silicone rubber. Many radiotherapy departments custom make their own flexible Intra-Operative templates (FIT), using catheters and silicone[47, 48] or catheters and stomahesive[49]. One such example is the applicators constructed from catheters and foam, rigid Derlin or silicone by Martinz-Monge et al[50] at the Ohio State University's James Cancer Hospital.

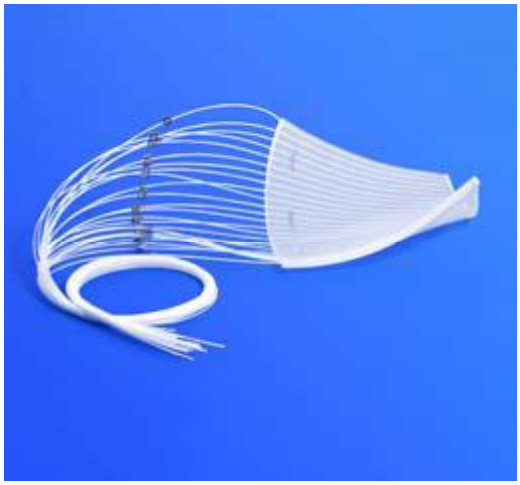

Figure 2.7 Photograph of a HAM applicator used in IOBT treatments.

2.5.3 Issues with Intra-Operative Brachytherapy

The main reason for choosing Intra-Operative radiation therapy over other treatment techniques is so that a large dose of radiation can be delivered directly to the tumour volume or tumour bed (if the tumour has been excised with close or positive margins) which cannot be achieved with other techniques. The circumstances of the radiation delivery, during surgery in an operating room, mean that CT imaging for treatment planning is typically not possible. The treatment plan used may be a library plan that is not specific to the patient. This introduces variations between the assumed geometry and the actual geometry of the treatment plan, which adds uncertainties. The position of the catheters within the applicator may only be accurate to within 1 mm, adding to geometrical uncertainty. Also, there may be some curvature in the applicator as a result of where it is placed for treatment which cannot be accounted for accurately and leads to uncertainty.

In Chapter 5 we describe measurements using TLD rods and MOSkin detectors with an IOBT applicator to compare their suitability for this brachytherapy technique.

2.6 Conclusions

It is clear from the literature that the response of TLDs and MOSFETs will vary due to a range of physical properties and irradiation conditions. In the chapters that follow, the characteristics for TLD rods and MOSkin detectors that were made available for this project, were measured under conditions that represent typical brachytherapy applications. The intention is to use the results of these measurements to either estimate the uncertainty in the dosimeter readings, or investigate the use of correction factors that can be applied when the detector is used in non-reference conditions. The measurement of a backscatter correction factor for IOBT is described to provide a specific example of the application of the correction factors and uncertainty estimates.

3 Characterisation of Thermoluminescent Dosimeters

3.1 Introduction

The TLD rods were characterised in order to make a comparison with the dosimetric characteristics of the MOSkin detectors. Also to assign a value of uncertainty to the TLD rod measurements made using the IOBT applicator. The measurements of the TLD rod dosimetric characteristics were carried out prior to the measurements with the MOSkin detectors. This was done to refine the methodology given the MOSkins have a limited useful lifetime, which is a function of accumulated dose, meaning repeated measurements with the MOSkins were not practical. The dosimetric characteristics of the TLD rods measured were sensitivity, linearity, dose rate response, angular response, energy response and temperature response. Some characteristics were measured even though the TLD rods were unlikely to exhibit a response, for example temperature response. These were measured anyway to develop and confirm the methodology prior to the MOSkin measurements. All measurements were carried out at the Peter MacCallum Cancer Centre.

3.2 Materials

3.2.1 TLD rods

Eighteen TLD rods (type TLD-100, Harshaw, USA) were used in this project. Each rod had dimensions of 6 mm × 1 mm × 1 mm, giving a total dosimetric volume of 6 mm^3 per detector. With the exception of individual TLD rod sensitivity, the dosimetric characteristics of the TLD rods were determined for the batch of TLD rods as a whole.

3.2.1.1 Read Out and Annealing Process

TLD readout was performed at the Peter MacCallum Cancer Centre using an automated TLD reader with hot nitrogen heating (Harshaw 5500). The read out process took place between 24 and 72 hours post irradiation. This time window was sufficient to allow the electron traps with short half lives to completely empty without loss of signal information. The read out process involved three stages – 'preheating', 'acquiring' and 'annealing'. The 'preheating' stage lasts for 15 seconds and heats the TLD rods to a temperature of 129°C. The 'acquiring' stage lasts for 20 seconds and heats the TLD rods to a temperature of 270°C. The 'annealing' stage lasts for 15 seconds and heats the TLD rods to a temperature of 316°C. The data was collected during the acquiring stage.

The annealing stage of the readout process did not heat the TLD rods to a temperature sufficient to empty all electron traps, further annealing was required before the TLD rods could be irradiated again. This further annealing was carried out using a dedicated annealing oven (SEM, TLD4, South Australia). This annealing process involved heating the TLD rods at 400°C for one hour and then at 100°C for two hours.

3.2.2 Linac

Two linacs were used at the Peter MacCallum Cancer Centre. A Varian 600c Linac, (Varian, Palo Alto, CA), was used for 6 MV beam energy measurements and a Varian iX Linac, (Varian, Palo

Alto, CA), was used for energy response measurements using 6 MV and 18 MV beam energies. For all measurements carried out on the linacs, gantry and collimator rotations of 0^{o} were used with 100 mm × 100 mm field sizes and 1000 mm source to surface distance, (SSD).

3.2.3 Ir-192 source

In this project a Nucletron microSelectron V2 Ir-192 source, (Nucletron, Veenendaal, The Netherlands), at the Peter MacCallum Cancer Centre was used. The Ir-192 source was in the form of a thin steel encapsulated pellet measuring a total of 0.9 mm in diameter and 4.5 mm in length. The actual source measured 0.65 mm in diameter and 3.6 mm in length. A cross section of the source pellet is shown in Figure 3.1.

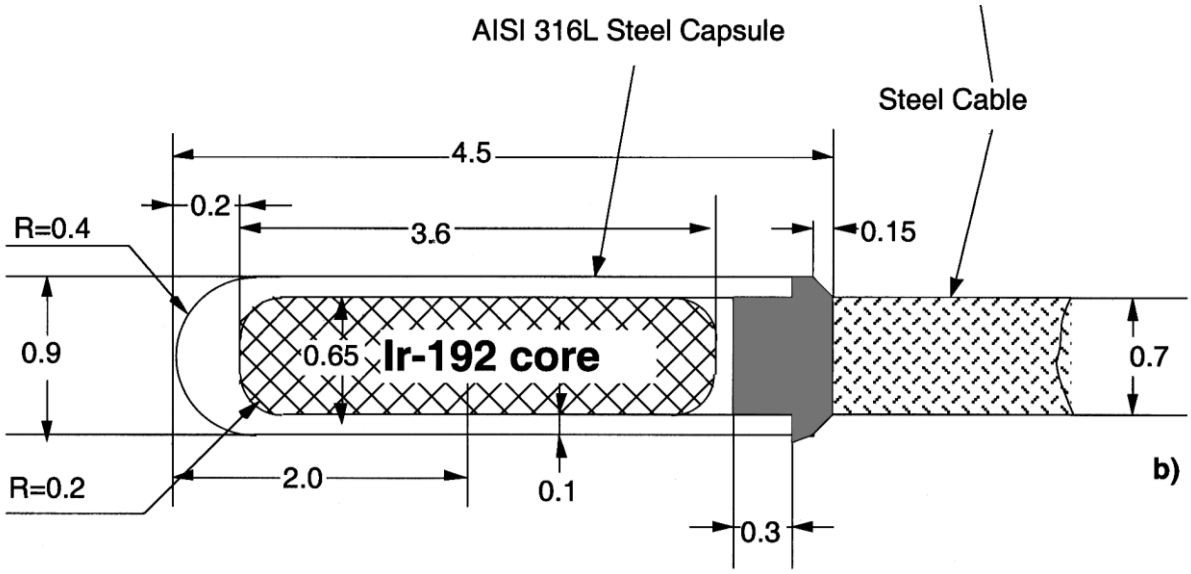

Figure 3.1 The design of the Nucletron microSelectron V2 Ir-192 source showing source and encapsulation dimensions[39].

The dose distribution around the Nucletron microSelectron source has been described by Daskalov et al[39], who used Monte Carlo photon transport simulation to calculate the complete 2-D dose rate distribution over the 1-70 mm distance range. It is this description that was used in the brachytherapy treatment planning system at the time this work was carried out. They described the dose rate per unit air-kerma strength in terms of x and y coordinates

with y representing the long axis of the pellet and x being perpendicular to the long axis. The dose rate per unit air-kerma strength drops off rapidly with distance from the pellet in both the x and y directions, leading to a high dose rate gradient in close proximity to the pellet. The dose rate per unit air-kerma strength is shown in Figure 3.2 for a line extending radially outwards (in the x direction) from the centre of the source.

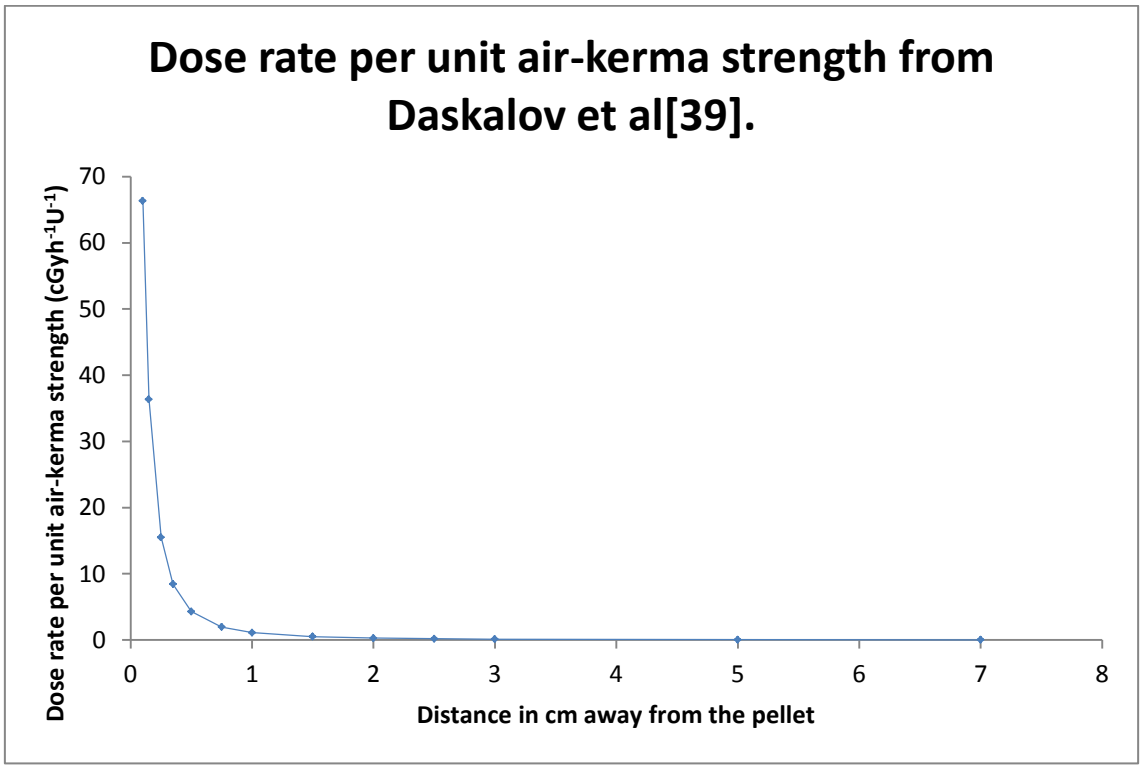

Figure 3.2 Dose rate per unit air-kerma strength for the line y = 0[39].

Figure 3.3 shows the bare spectrum from an Ir-192 source[51] and Figure 3.4 shows the spectrum from a micro-Selectron source[51]. The encapsulation around the micro-Selectron source removes some of the lower energy components of the spectrum.

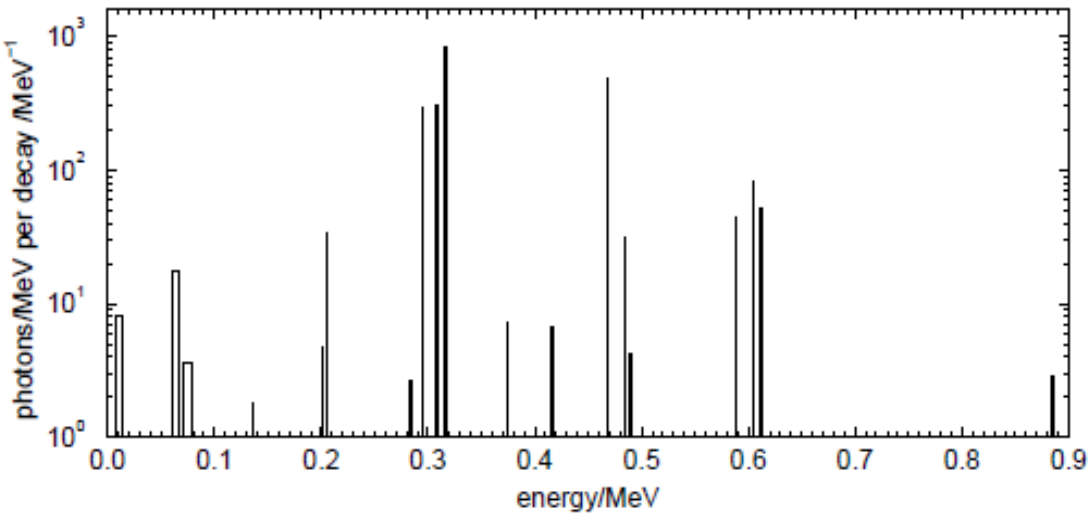

Figure 3.3 The bare spectrum from an Ir-192 source[51].

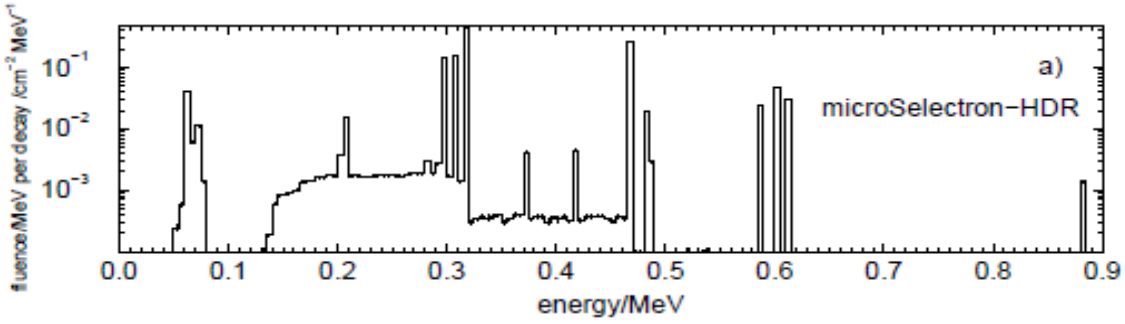

Figure 3.4 The spectrum from a microSelectron Ir-192 source[51]

3.2.4 Deep and Superficial X-Ray Machine

For energy dependence measurements, a deep and superficial x-ray unit was used (Pantak Therapax MXT225), at the Peter MacCallum Cancer Centre. All measurements with this machine were made using a 100 mm diameter cone with an SSD of 300 mm. Six beam qualities described by their half value layer (HVL), were used. The beam qualities were converted from HVL to equivalent energy using Equation 3.1.

$$HVL = \frac{\ln 2}{\mu} \qquad \text{Equation 3.1.}$$

Where μ is the linear attenuation coefficient

Values of μ were obtained for aluminium and copper from Khan[10]. Table 3.1 lists the beam qualities used in terms of their HVL and the calculated effective energy.

HVL	Beam Quality (Effective Energy keV)
0.35 mm Al	15.7
0.75 mm Al	19.1
1 mm Al	21.2
2 mm Al	28.4
4 mm Al	38.3
0.5 mm Cu	59.9
1 mm Cu	80.3
2 mm Cu	108.8

Table 3.1 Beam qualities used on the Pantak Therapax X-Ray machine as calculated using Equation 3.1.

3.2.5 Ionisation Chamber

Three ionization chambers were used in this project. A Farmer type ionisation chamber (NE 2571, 0.6 cm^3 NE Technologies Ltd, Reading, UK), was used for measurements made on the 6 MV linac and is the chamber routinely used in the calibration of the Peter MacCallum Cancer Centre linacs using the TRS 398 protocol[52]. A PTW Type 30010 (PTW Freiburg, Germany) ionisation chamber was used for measurements with the HDR Ir-192 source. This chamber had been purchased specifically for brachytherapy research projects and had been calibrated at the Australian Radiation Protection and Nuclear Safety Agency (ARPANSA), laboratory in a Co-60 and a kilovoltage x-ray beam so that an air kerma chamber calibration coefficient ($N_{K,ARP}$) for use with Ir-192 could be derived using the TRS 1274 formalism[53, 54]. An Exradin A10 (Standard Imaging Inc., WI, USA) parallel plate ionisation chamber was used for measurements

made with the deep and superficial x-ray unit, this chamber was routinely used in the calibration of the deep and superficial x-ray units and has a relatively flat energy response over the energy range of interest.

3.2.6 Phantoms

Two phantoms employed by Peter MacCallum Cancer Centre were used in determining the TLD rod characteristics. An existing 100 mm radius cylindrical PMMA (Polymethyl Methacrylate) phantom was used with the Ir-192 source, and a solid water slab phantom was used with the linac.

The cylindrical PMMA water phantom had a diameter of 200 mm and a depth of 300 mm. It contained a central channel in which a specially designed PMMA holder for the TLD rods or MOSkins could be inserted. It also had three equally spaced channels at radial distances of 50 mm in which catheters for the Ir-192 source could be inserted, see Figure 3.5. The cylinder was hollow with an access plug at the top allowing it to be filled with water.

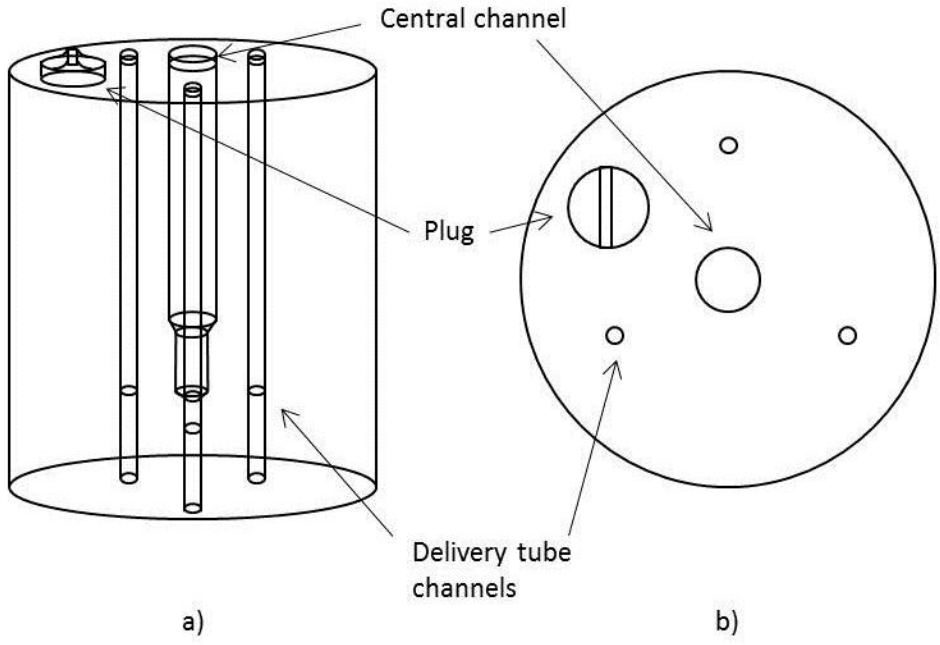

Figure 3.5 Diagram of the cylindrical PMMA water phantom used with the Ir-192 source showing central channel, delivery tube channels and plug a) side view b) top view.

The solid water slab phantom consisted of a 300 × 300 × 20 mm slab made up of three parts of Plastic Water® PW-3020 (CNMC Company, Inc, Nashville, TN, USA) and brown Standard Grade Solid Water®, (SGSW), Gammex 457 (Gammex, Inc, Middleton, WI, USA). The central piece of the slab was made from brown Standard Grade Solid Water®, this piece could be removed entirely and comprised a top and bottom half. On the inner side of each half there were 0.5 mm deep grooves where the TLD rods could sit and a larger cut out customised to the shape of the cylindrical ion chamber. This central piece was engineered such that when all three pieces of the slab were combined the TLD rods and ionisation chamber would be at the same source to surface distance. Figure 3.6 shows the three pieces together and separated and Figure 3.7 shows the positions of the TLD rods and ionisation chamber in relation to a photon beam from a linac.

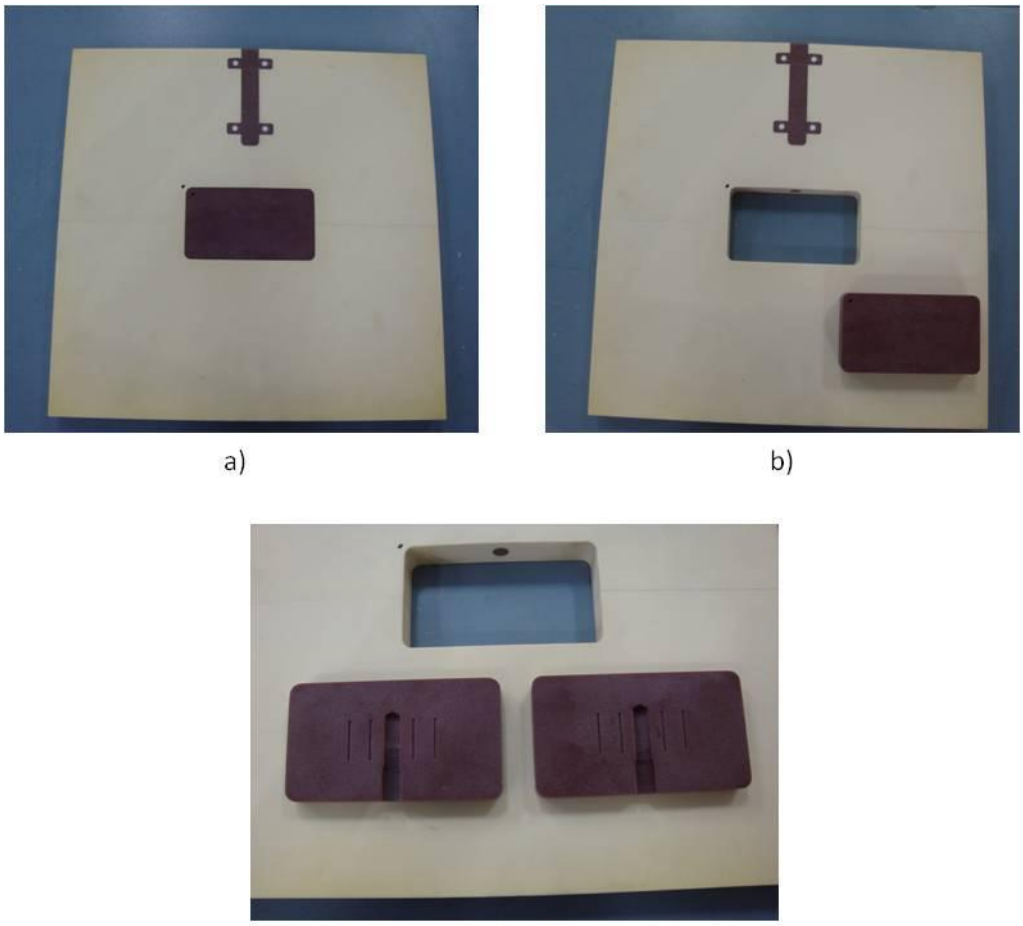

Figure 3.6 Photograph of the solid water slab phantom used for TLD rod and ion chamber measurements a) top view of all pieces fitted together b) top view with central piece removed c) inner sides of central piece.

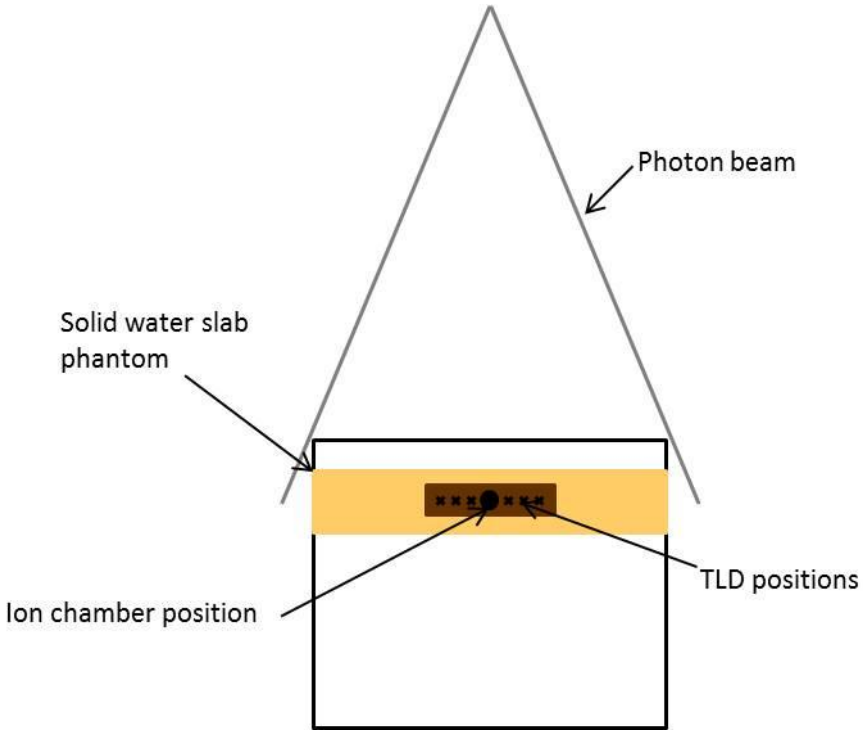

Figure 3.7 Diagram of the relative positions of the TLD rods and ionisation chamber when the solid water slab phantom is used in a linac beam.

3.3 Methods

3.3.1 Sensitivity

The thermoluminescent property of TLD 100 material is due to the presence of impurities within the LiF lattice structure. Ideally, all TLD rods in the same batch will give the same response, however, the impurities are not distributed completely evenly throughout the material which, in addition to slight size and mass differences, results in small variations in the response of each individual TLD rod[5]. These small variations result in small variations in the response to equal quantities of radiation. This variation in response is known as TLD sensitivity. The sensitivity of each individual TLD rod must be measured prior to any measurements being made.

The sensitivity is a measure of the response of one TLD rod in comparison to the average response of the batch of TLD rods to a uniform dose. Initially new TLD rods must be irradiated several times in order for their sensitivity to stabilise.

The sensitivity of the TLD rods was measured by exposing all 18 TLD rods to a uniform dose from a 6 MV linac. The TLD rods were arranged in a 3 mm thick PMMA holder which had a number of 1 mm deep channels. The PMMA holder was placed between slabs of PTW RW3 (PTW, Freiburg, Germany), 100 mm below the holder and 15 mm above. 50 Monitor Units were delivered to the TLD rods at a rate of 250 $MUmin^{-1}$, which at a depth of 15 mm equates to a delivered dose of 0.5 Gy.

Once read out, the readings for the individual TLD rods were divided by the average reading of all 18 TLD rods to give an individual TLD rod sensitivity for that irradiation. This process was repeated until the standard deviation of the last three individual sensitivities for all TLD rods was below 3.0%. At this point the sensitivity of the TLD rods was considered stabilised. The sensitivity of the TLD rods was determined at least once every three months during the period of experimental use.

3.3.2 Linearity

Ideally, there should be a linear relationship between a dosimeter response and the dose delivered over a range of doses. In which case the dose measured could be calculated by simply multiplying the reading by a constant. Not all radiation detectors respond this way and those that do may be linear only over a certain range, e.g. radiochromic film[6].

The linearity of the TLD rods was determined using the 6 MV linac. The TLD rods were arranged in the solid water slab phantom. The solid water slab phantom was then arranged between slabs of PTW RW3 such that the TLD rods were at a depth of 50 mm and there was 100 mm of PTW WR3 below the TLD rods to provide backscatter material. Doses of 0.5 Gy, 1 Gy, 2 Gy, 3 Gy, 4 Gy and 5 Gy were delivered to the TLD rods using a constant dose rate of 250 $MUmin^{-1}$. Three TLD rods were irradiated at each dose.

3.3.3 Angular Response

The entire TLD rod is the detection volume, as such the angular response of the detector is determined by the physical dimensions of the rod. The radial and azimuthal directions about the TLD rods are shown in Figure 3.8a and 3.8b. Figure 3.8c shows how the distance to the centre of the TLD rod will change with changing angle in the radial direction. For the radial direction the distance from the TLD rod surface to the centre of the rod will range from 0.500 mm to 0.707 mm. However, during the full rotation the distance along the central axis of the irradiating source to the centre of the TLD rod will be a constant 50 mm, it is only the distance through TLD material to the centre of the TLD rod that changes. As TLD 100 material is water equivalent the dose rate at the centre of the TLD rod will be constant for all radial angles. As such, a radial angular response of the TLD rod was not expected to be observed and was not measured.

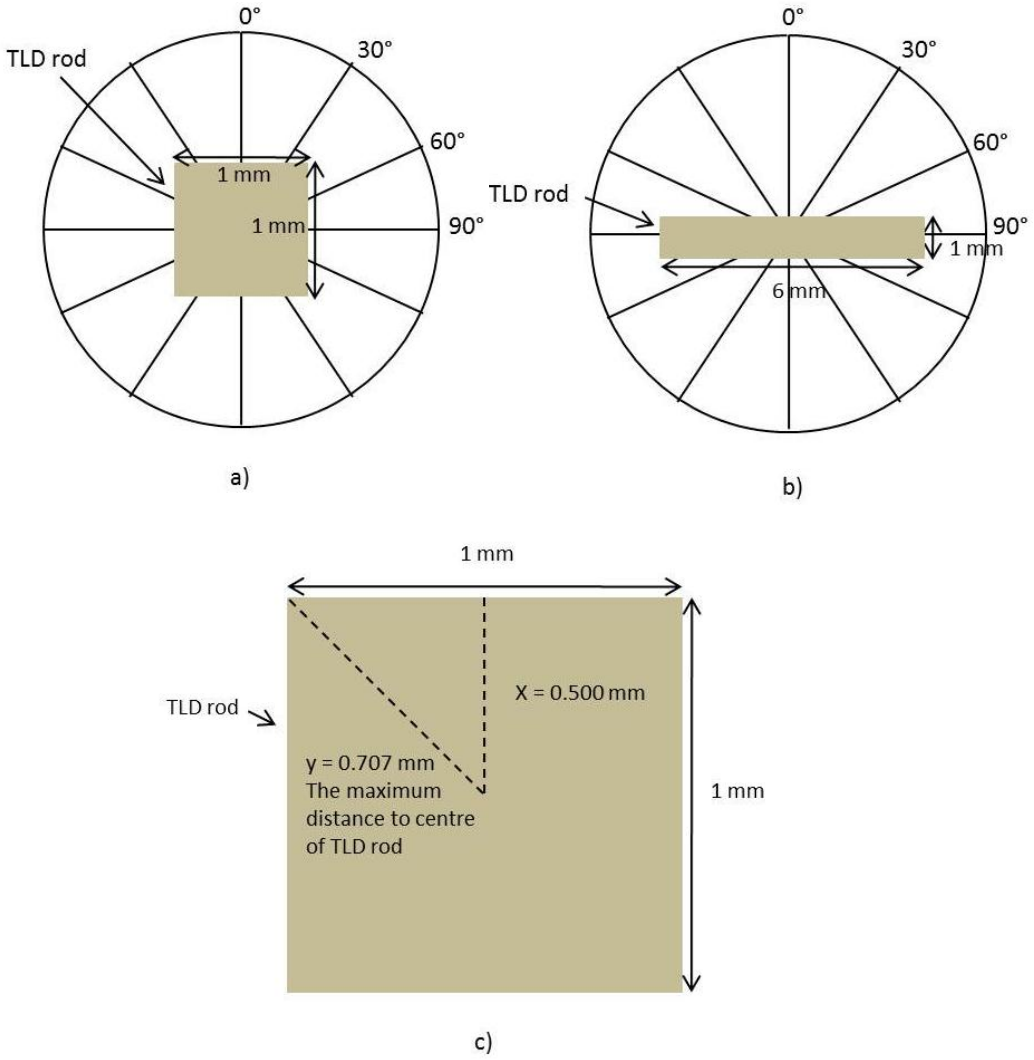

Figure 3.8 Diagram of a) the radial angular direction about a TLD rod b) the azimuthal angular direction about a TLD rod c) TLD rod cross section showing the maximum variation in distance to the centre of the TLD rod in the radial angular direction.

In the azimuthal direction the dose to the TLD rod can be calculated by assuming the TLD rod is made up of six sections of 1 mm^3 volume each, as shown in Figure 3.9 as sections A-F. If the Ir-192 source is assumed to be at a constant distance from the centre of the TLD rod, the dose to each individual section can be calculated using dose rate per unit air kerma strength data from Daskalov et al[39]. The dose to the entire TLD rod is then calculated by summing the dose to each section A-F. Figure 3.10 shows theoretically how the dose to the TLD rod will vary with changing azimuthal angle for different source to detector distances.

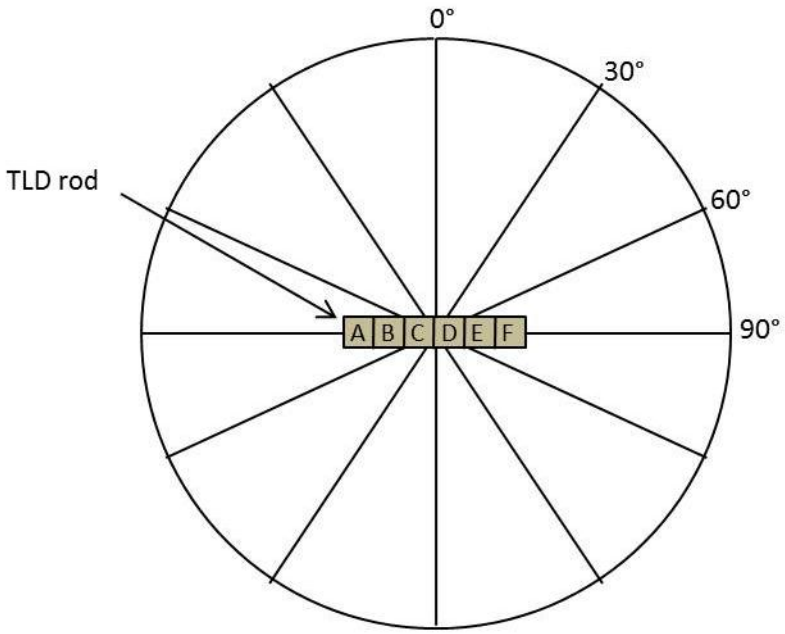

Figure 3.9 Diagram of the TLD rod when considered to be made up of six sections A-F, each 1 mm^3 in volume. The long axis of the Ir-192 source will be parallel to the circumference of the circle of specified radius.

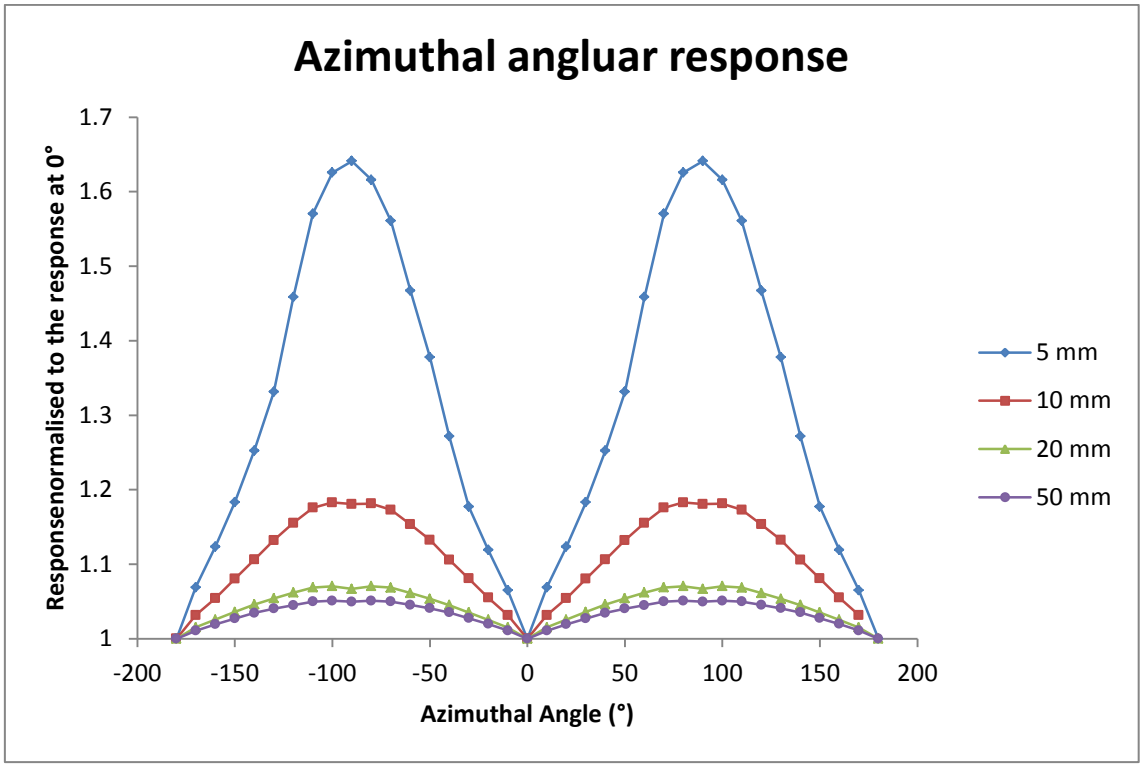

Figure 3.10 The theoretical variation in azimuthal response with varying radius of a TLD rod used in this project calculated from dose rate per unit air kerma strength from the tables developed by Daskalov et al[39], for Ir-192 radiation in water.

It can be seen that the greater the source to centre of the TLD rod distance the less the variation in dose, which is a result of the inverse square drop off of the source strength. At radial distances of 5 mm, 10 mm, 20 mm and 50 mm, the TLD rod will theoretically over respond by 64.10%, 18.30%, 7.05% and 5.09% respectively. The azimuthal angular response of the TLD rods was measured to both confirm this calculation and to validate the methodology prior to the MOSkin measurements.

The azimuthal angular response of the TLD rods was measured using the cylindrical PMMA water phantom and the Ir-192 source. The TLD rod PMMA holder is designed to contain three TLD rods end to end, however, the use of spacers allowed one TLD rod to be irradiated in the middle position at one time.

The azimuthal angular response of the TLD rods was measured by keeping the PMMA TLD rod holder in a fixed orientation in the central channel and varying the position of the Ir-192

source in one of the 50 mm radius channels. The orientation of the TLD rods in the PMMA holder was such that the radiation angle of incidence was diagonal across the long axis of the TLD rod and would change with each source position in the catheter. The changing distance between the Ir-192 source and the TLD rod was corrected using dose rate per unit air kerma strength data from tables developed by Daskalov et al[39]. Source positions within the catheter could be chosen at discrete 2.5 mm intervals, each of which is referred to as a source 'dwell position'. The range of azimuthal angles measured was achieved by stepping the source through every second dwell position for a length of -37.5mm to +30.0mm, a total length of 67.5 mm, which represented the length available within the phantom.

To determine the source dwell position that coincided with the perpendicular bisector of the TLD rod, the PTW Type 30010 ionisation chamber was placed in the central channel of the cylindrical water phantom and the source was stepped through a number of dwell positions. The dwell position that recorded the highest dose with the ion chamber was considered the perpendicular bisector of the detector. The three highest doses were recorded at dwell positions 11, 12 and 13, as shown in Figure 3.11. The measurement point along the long axis of the ion chamber was specified to be at a distance of 13 mm inside the tip of the chamber by the manufacturer[55]. The PMMA TLD rod holder for the cylindrical phantom was designed such that the centre of the middle TLD rod would match the position of the measurement point of the ionisation chamber when each were inserted in to the phantom, however, this would also be confirmed. A skewing of the azimuthal angular response results for the TLD rods in either positive or negative angular direction could indicate that the incorrect dwell position was chosen to coincide with the perpendicular bisector of the detector, which would lead to measurements being corrected for the wrong dose based on the assumed source to detector distance. The range of azimuthal angles measured was achieved by stepping the source through every second dwell position either side of positions 11 and 13 over the length of the

phantom. Measurements were made only at every second dwell position as each dwell position required a different TLD rod be placed in the holder which was a time consuming process.

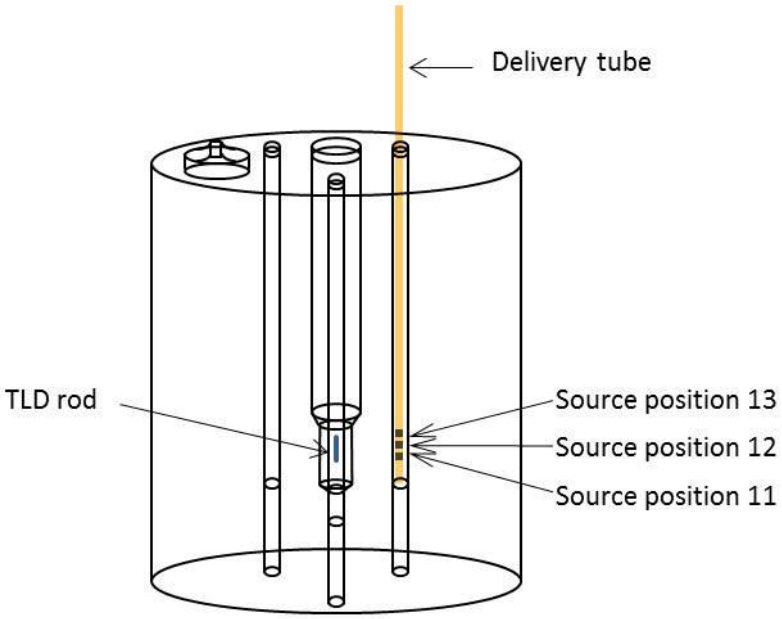

Figure 3.11 Diagram of the cylindrical PMMA phantom showing TLD rod position and source dwell positions that could correspond to the perpendicular bisector of the TLD rod.

3.3.4 Energy Response

TLDs are known to exhibit an over response to low energy x-rays compared to the response at 6 MV from a linac[18]. The energy response of the TLD rods was measured using the deep and superficial X-ray machine, a Cs-137 source and the 6 MV and 18 MV linac with the solid water slab phantom.

3.3.4.1 D/SXRT

In routine clinical practice, the monitor units for patient treatment using the Deep and Superficial X-ray unit at the Peter MacCallum Cancer Centre are calculated according to Equation 3.2.

$$\mathrm{MU} = \frac{\mathrm{SurfaceDose/Fx}}{\mathrm{ISL}\times\mathrm{BSF}\times\mathrm{CCF}} \times 100 \qquad \text{Equation 3.2.}$$

Where $ISL = \left(\frac{SSD}{SSD \pm x}\right)^2$ $Inverse\ Square\ Law$

$BSF = Back\ Scatter\ Factor$

$CCF = Cone\ Correction\ Factor$

$Fx = No.of\ Fractions$

Three TLD rods were placed in the grooves of the central piece of the solid water slab phantom (Figure 3.6c). The slab phantom was placed on top of 100 mm of PTW RW3 to provide backscatter, and the 100 mm diameter cone was directly touching the top of the solid water slab phantom, meaning the TLD rods were at a depth of 10 mm in SGSW. A dose of 1 Gy was delivered at each beam quality given in Table 3.1. The dose was confirmed using the Exradin A10 parallel plate ionisation chamber for the two lowest effective energies and the NE Farmer style 2571 ionisation chamber for the remaining effective energies.

3.3.4.2 Cs-137

The TLD rods were irradiated in a Nordion Gammacell 40 Irradiator (MDS Nodion, Ottowa, Ontario, Canada). The TLD rods were irradiated by two Cs-137 sources, one above and one below, at a dose rate of 0.6 Gymin^{-1}. The Cs-137 sources were supplied with a calibration certificate and hence the dose rate at mid plane was determined by applying a correction for decay.

3.3.4.3 MV

For the 6 MV and 18 MV linac measurements the TLD rods were irradiated using the solid water slab phantom (Figure 3.6) and additional slabs of PTW RW3. The TLD rods were placed in the grooves of the central piece of the solid water slab phantom. Slabs of PTW RW3 were

placed on top such that the TLD rods were at a depth of 50 mm (40 mm PTW RW3 + 10 mm SGSW), with 100 mm of PTW RW3 placed below the solid water slab phantom. A dose of 1 Gy was delivered at each effective energy with the NE Farmer style 2571 ionisation chamber used to confirm the dose.

3.3.5 Dose Rate Response

The response of a detector can be affected by the rate at which the dose is delivered. TLDs are known to be dose rate independent up to 10^8 Gys^{-1}[5], however, as the dose rate response of the MOSkin detectors is unknown the dose rate response of the TLD rods was examined for experimental design purposes.

The dose rate response of the TLD rods was measured by irradiating the TLD rods through different depths of PTW RW3 slabs. The same dose was delivered to the surface of the slabs for each measurement meaning the dose delivered to the TLD rods decreased according to percentage depth dose measurements determined from ionisation chamber measurements made previously on the same linac. Measurements were made at depths of 15 mm, 30 mm, 50 mm, 80 mm and 100 mm. 100 MU's were delivered to the surface for each measurement which was equivalent to doses of 1.0 Gy, 0.94 Gy, 0.86 Gy, 0.74 Gy and 0.66 Gy respectively. The dose at each depth was confirmed using the NE Farmer style 2571 ion chamber. The dose rate at each depth was calculated as 41.66 $mGys^{-1}$, 39.30 $mGys^{-1}$, 35.87 $mGys^{-1}$, 30.84 $mGys^{-1}$ and 27.69 $mGys^{-1}$ respectively. For each measurement depth there was at least 100 mm of PTW RW3 slabs below the TLD rods to provide adequate backscatter material. All measurements were normalised to a dose of 1 Gy.

3.3.6 Temperature Response

Theoretically TLDs will not display a temperature response as they are not real time detectors and heating is required during the read out process. However, the TLD rods were examined for

a temperature response in order to develop the methodology prior to the MOSkin measurements.

The temperature response of the TLD rods was measured using the cylindrical PMMA water phantom and the Ir-192 source. The cylindrical PMMA water phantom was filled with hot water, approximately 34^{o}C, and wrapped in a 'Bair Hugger' warming blanket. The purpose of the warming blanket was to minimise heat loss to the surrounding air while measurements were being made. The cap to the cylindrical water phantom was removed and a digital thermometer probe was inserted into the water to monitor the temperature, see Figure 3.12.

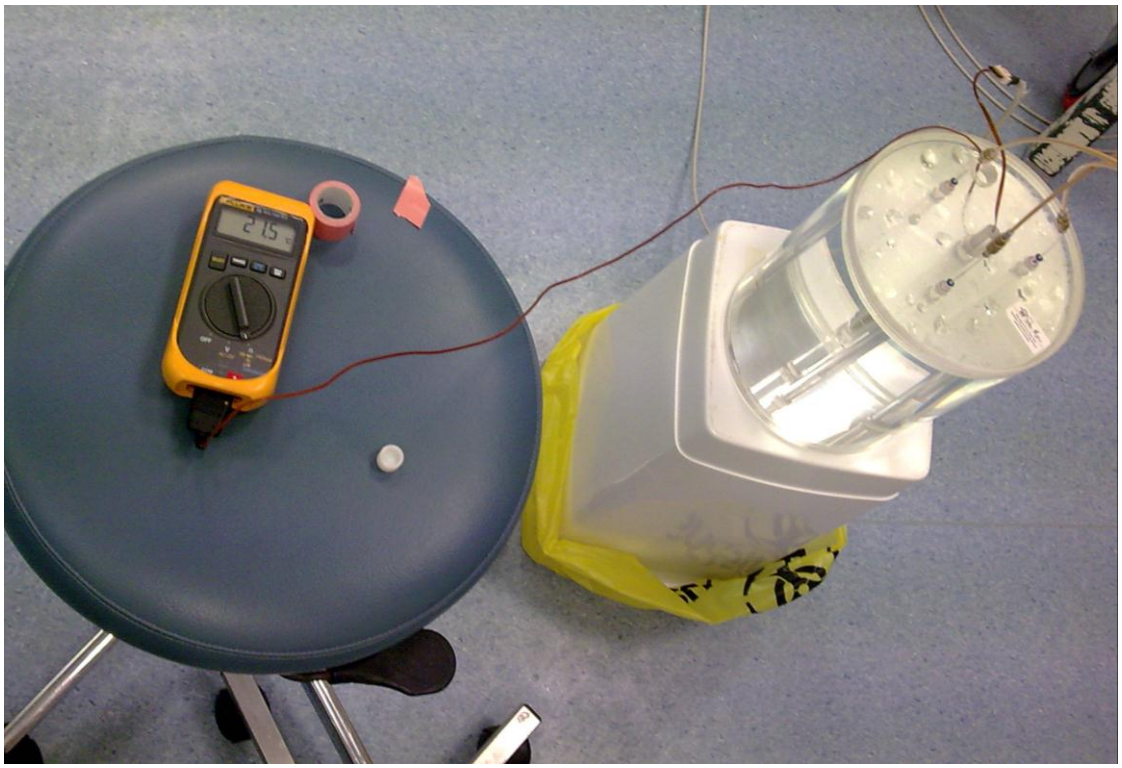

Figure 3.12 Photograph of the cylindrical PMMA water phantom with the digital thermometer inserted via the plug hole at the top.

Three TLD rods were inserted into the PMMA TLD holder placed inside the phantom. The Ir-192 source was then used to deliver a dose of 1 Gy to the TLD rods. The cylindrical water phantom was then emptied of the hot water and filled with room temperature water, approximately 22^{o}C. Three TLD rods were again irradiated with a dose of 1 Gy at this lower temperature without use of the warming blanket.

3.4 Results

3.4.1 Sensitivity

Individual sensitivities for the 18 TLD rods were obtained four times during the course of the characterisation process. All raw TLD rod measurements were corrected for individual TLD rod sensitivity using Equation 3.3.

$$Corrected\ Measurement = \frac{Raw\ TLD\ rod\ measurment}{Individual\ TLD\ rod\ sensitivity} \qquad \text{Equation 3.3.}$$

Due to the identical appearance of each TLD rod and the accidental reordering of the TLD rods, a comparison between consecutive sensitivity calculations for the same TLD rod could not be made. However, the sensitivity, or calibration factor, for each measurement with a TLD rod was known and applied accordingly.

3.4.2 Linearity

The response of the TLD rods was linear with dose in the range of 0.5 Gy to 5 Gy, within 2.8%, as shown in Figure 3.13. Each point represents the average of three measurements with the error bars being the standard deviation of the mean of the three measurements normalised to the average measurement at a dose of 1 Gy summed in quadrature with the standard deviation of the mean of the relevant sensitivity measurements. The average normalised standard deviation was 2.8%. A linear equation was fit to the data and is also shown in Figure 3.13. The equation described a linear response with a gradient of 1.11.

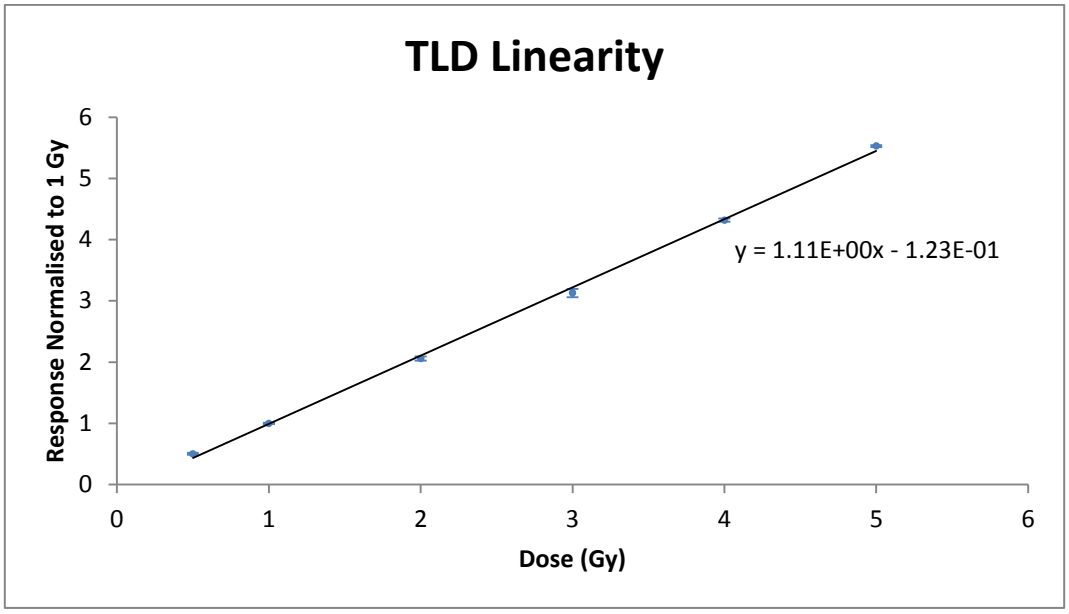

Figure 3.13 Linear response of the TLD rods with dose, error bars are the standard deviation of the mean of the three measurements at each dose normalised to the response at 1 Gy summed in quadrature with the standard deviation of the mean of the relevant sensitivity. The average size of the error bars was 2.8%.

3.4.3 Angular Response

The azimuthal angular response of the TLD rods was measured by varying the dwell position of the Ir-192 source while keeping the position of the TLD rod constant in the centre of the phantom. The TLD rod measurements were first corrected for dose response for the varying source to detector distances using dose rate per unit air kerma strength data obtained from Daskalov et al[39]. The source to detector distance at 0° was 50 mm. There was found to be no significant response in the TLD rods with azimuthal angle over the range of angles measured, this is shown in Figure 3.14. As only one TLD rod measurement was taken at each angle the error bars of 1.1% represent the standard deviation of the mean of the relevant sensitivity measurements.

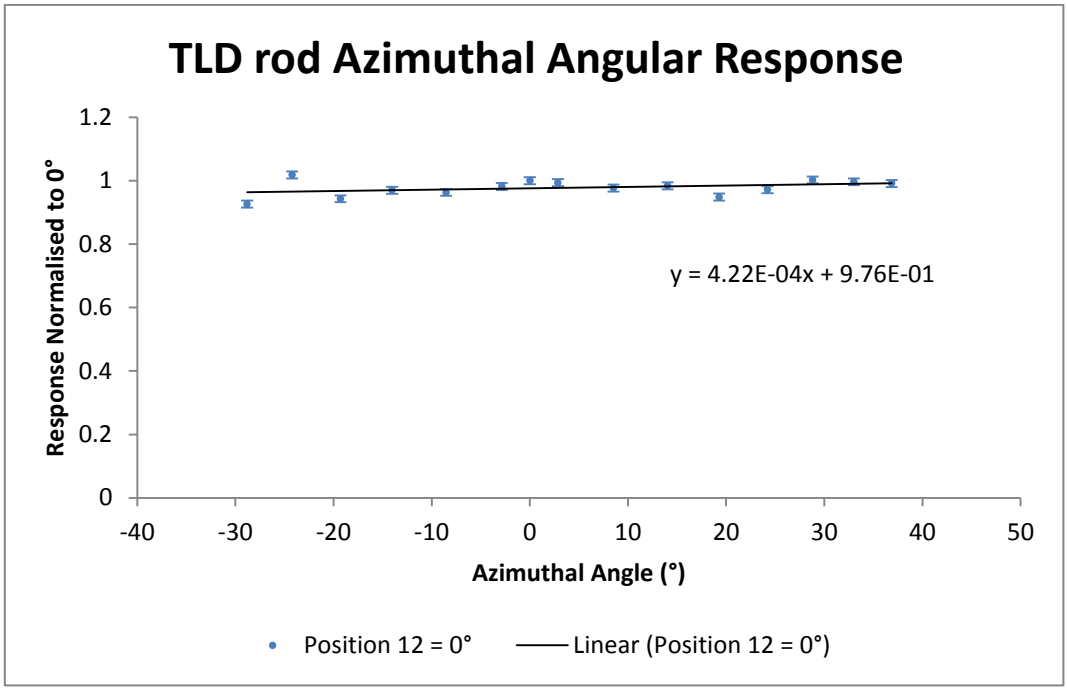

Figure 3.14 The azimuthal angular response of the TLD rods, error bars are the standard deviation of the mean of the relevant sensitivity measurements which was 1.1%.

A linear equation was fit to the measurement points producing a line with a very low positive gradient of 0.00422 per degree. As the gradient was not absolutely zero the measurements were also corrected for source to detector distances for the two cases assuming dwell position 11 and dwell position 13 coincided with the perpendicular bisector of the TLD rod, these are shown in Figure 3.15.

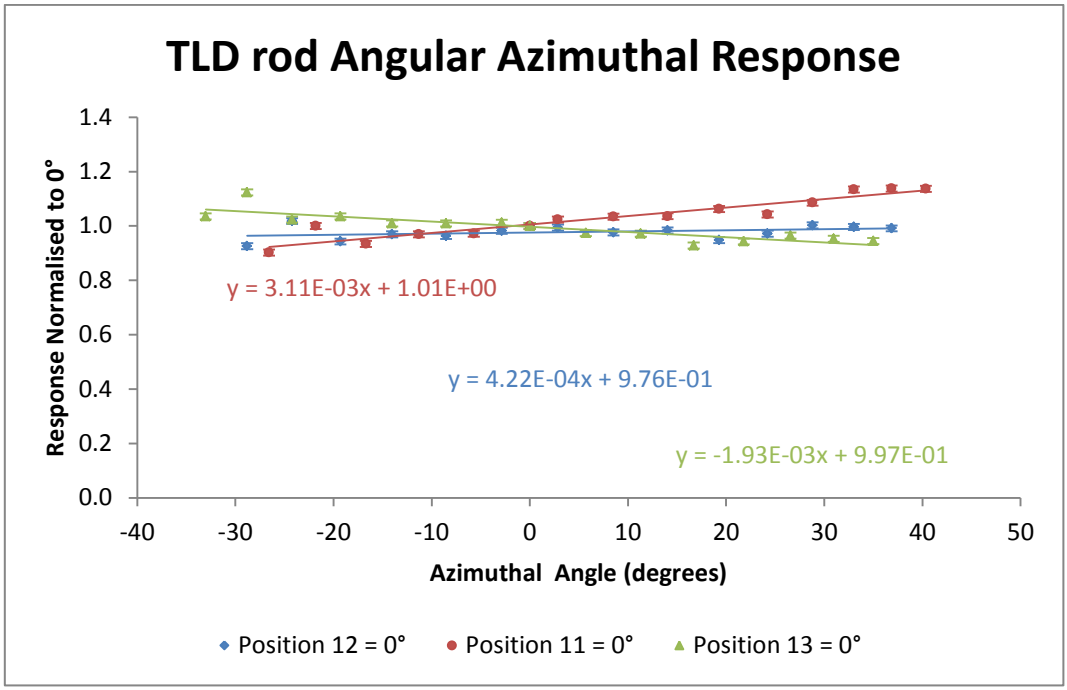

Figure 3.15 TLD rod azimuthal angular response calculated for the cases when dwell position 11, 12 and 13 are the perpendicular bisector of the detector, error bars are the standard deviation of the mean for the relevant sensitivity measurements which was 1.1%.

For position 11 coinciding with the perpendicular bisector of the TLD rod a linear equation with a larger positivie gradient was produced, of 0.00311 per degree was produced, and for position 13 coinciding with the perpendicular bisector of the TLD rod a linear equation with a larger negative gradient of -0.00193 per degree was produced. It is possible that the perpendicular bisector of the TLD rod could correspond to a position between dwell positions. To test this, the dwell position corresponding to 0° was plotted against the gradient of the linear line of best fit produced. A linear equation was then applied to these three points and the dwell position corresponding to a theoretical gradient value of 0 was calculated to be 12.67, this is shown in Figure 3.16.

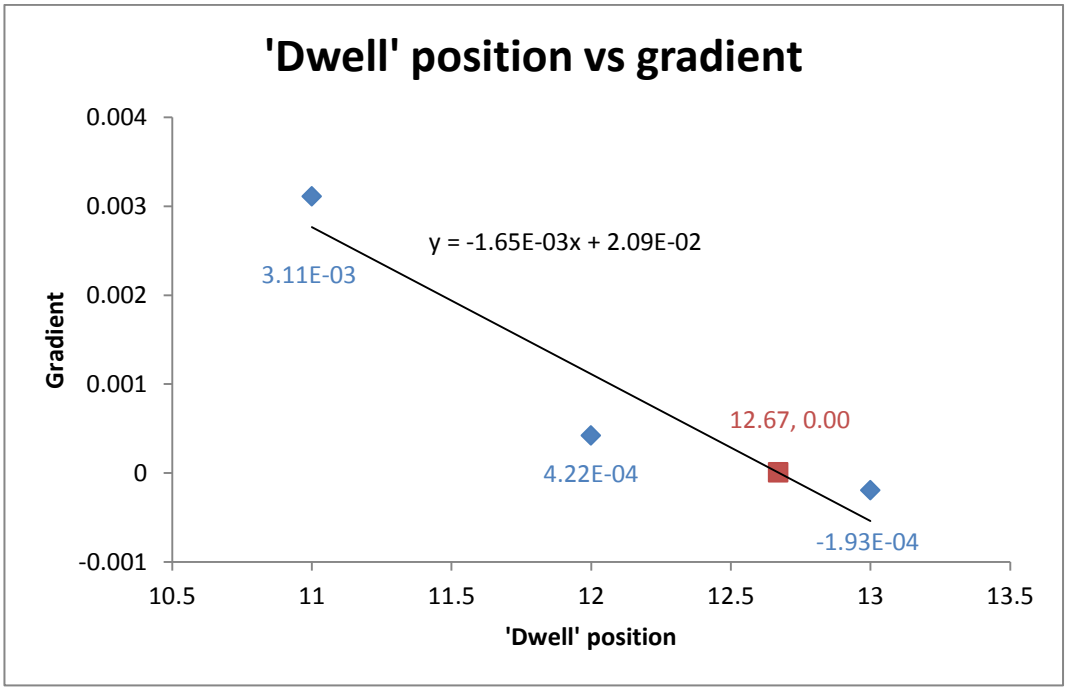

Figure 3.16 The gradient of the line of best fit plotted against dwell position for the cases when dwell position 11, 12 and 13 are considered to coincide with the perpendicular bisector of the detector, also shown is linear equation of best fit.

The TLD rod measurements were then corrected for dose for the case when dwell position 12.67 coincided with the perpendicular bisector of the TLD rod, these are shown in Figure 3.17. A linear equation with a smaller negative gradient of -0.0000128 per degree was produced, again the error bars represent the standard deviation of the mean of the relevant sensitivity measurements 1.1%, indicating that the true perpendicular bisector of the TLD rod most likely lies between dwell position 12 and dwell position 13. The maximum over response of 3.3% occurred at -24.9° and the maximum under response of 5.9% occurred at -29.4°. While the response did vary more than the magnitude of the uncertainty, there was no trend to the response with angle indicating the response was constant across the range of angles measured. The standard deviation of the mean of all measurements was 2.3%.

The transit time of the Ir-192 source could also cause the results to be skewed showing an increase in response observed for negative angles. The Ir-192 source travels out of the HDR unit and along the guide tubes at a speed of 500 mms^{-1}. The total length of catheter that is

inside the phantom is 100 mm, which would take the source 0.2 seconds to traverse. For measurements made when the source is at the furthest dwell position inside the phantom, the extra dose received during the time when the source is entering and exiting the phantom can be added to the dose received at that dwell position. A conservative estimate of this extra dose can be calculated by assuming that the source is at an average distance from the TLD rod for the entire 0.4 seconds. This equates to an extra 1.3 mGy of dose received which would skew the results for negative angles.

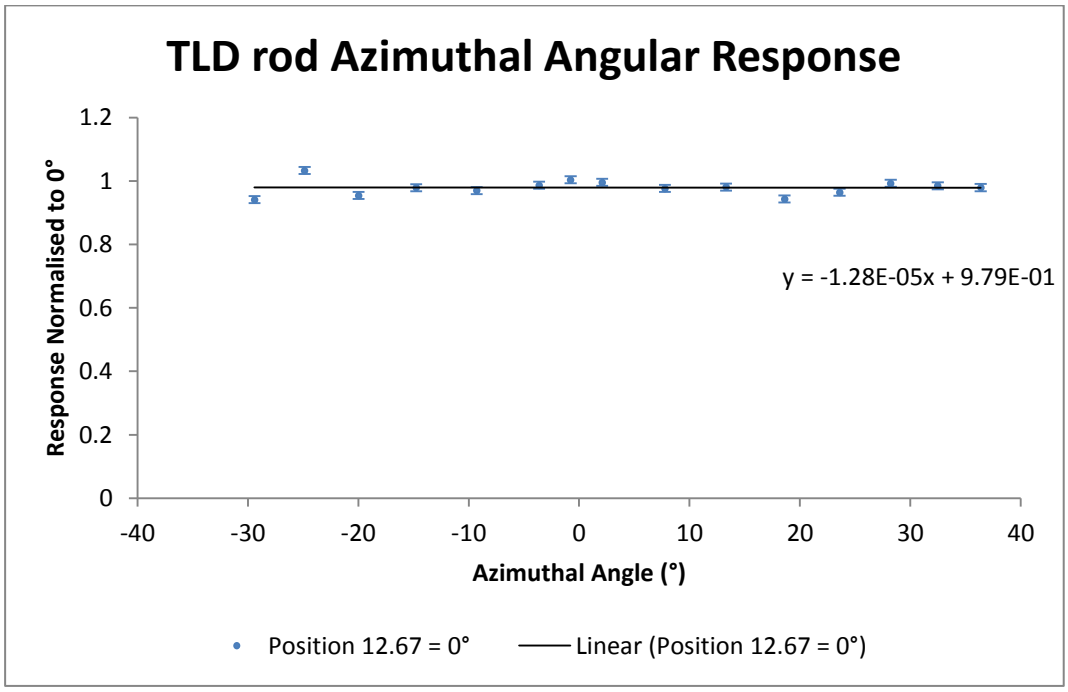

Figure 3.17 TLD rod azimuthal angular response corrected for position 12.67 corresponding to the perpendicular bisector of the TLD rod, error bars are the standard deviation of the mean of the relevant sensitivity which was 1.1%.

3.4.4 Energy Response

The TLD rod measurements were first corrected for individual sensitivity then normalised to the response at 6 MV, this is shown in Figure 3.18. The error bars represent the standard deviation of the mean of the three measurements at each point summed in quadrature with the standard deviation of the mean of the relevant sensitivity. The average size of the error bars was 1.2%. The response of the TLD rods showed an increase for lower energies with a

maximum over response compared to the response at 6 MV of 51.2% at 40 keV. Kron et al[34], derived an equation to describe the variation of detector response R with energy E, this is shown in Equation 3.4.

$$R(E) = \left\{1 - e^{-\alpha_1(E-E_1)}\right\}\left[1 + \frac{\alpha_2}{(E-E_2)^3}\right] \qquad \text{Equation 3.4.}$$

Where α_1 *is a fitting parameter which determines the importance of exponential fall-off towards low energies*

α_2 *is a fitting parameter which determines the importance of inverse cubic fall-off towards higher energies*

E_1 *and* E_2 *are fitting parameters that allow for an energy shift for the two components*

This equation was used to determine a curve of best fit for the measurements. The values for α_1, α_2, E_1, and E_2 were determined using MATLAB. The values determined were,

$$\alpha_{1=} 2.47 \times 10^{-2} \qquad E_1 = 4.66 \times 10^{0}$$

$$\alpha_2 = 8.97 \times 10^{5} \qquad E_2 = -4.20 \times 10^{1}$$

The resulting curve is also shown in Figure 3.18. From this fit we were able to determine that the maximum over response compared to the response at 6 MV of 58.5% occurred at 29 keV. From this equation the response of the TLD rod at 397 kV, the average energy of an Ir-192 source, was calculated to be 1.1% higher than the response at 6 MV.

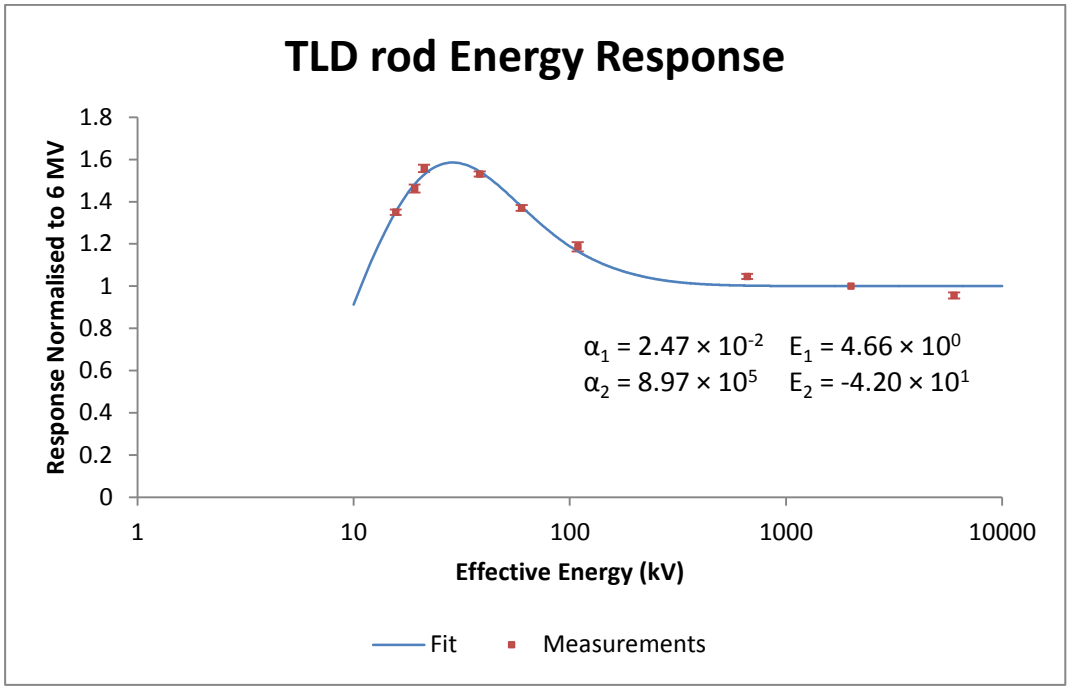

Figure 3.18 TLD rod energy response plotted as a function of effective energy, error bars are the standard deviation of the mean of the measurements at each energy summed in quadrature with the standard deviation of the mean sensitivity. The average error bar size was 1.2%. Also shown is a line representing Equation 3.4 and values for the parameters of the equation.

3.4.5 Dose Rate Response

The TLD rod measurements taken at different depths in solid water were normalised to a dose of 1 Gy using previously generated depth dose measurements made with the NE Farmer style 2571 ionisation chamber. The normalised measurements are shown in Figure 3.19. The error bars represent the standard deviation of the mean of the three measurements at that dose rate, summed in quadrature with the standard deviation of the mean of the relevant sensitivity measurements. The average error bar size was 1.5%. The TLD rod response varied by between -1.2% to 2.6% over the range of dose rates measured. While the variation in the response is larger than the uncertainty for 1 standard deviation, it is within 2 standard deviations, and there is no trend with dose rate, indicating that there is no variation in response over the dose rates measured.

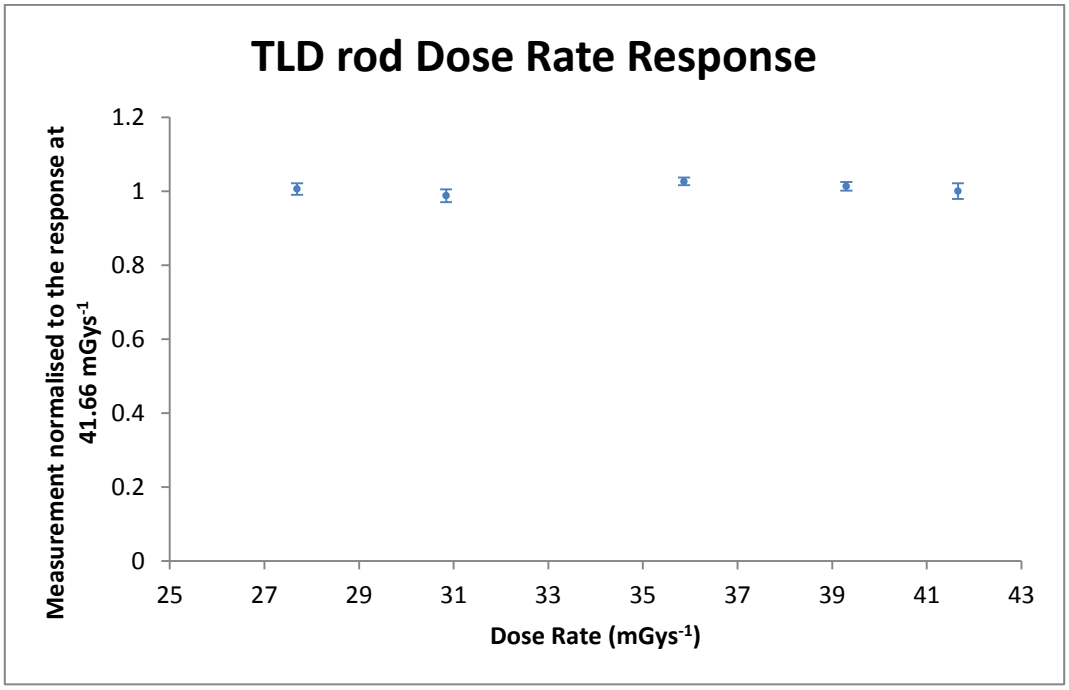

Figure 3.19 TLD rod dose rate response measurements, error bars are the standard deviation of the mean of the three measurements summed in quadrature with the relevant standard deviation of the mean sensitivity. The average error bar size was 1.5%.

3.4.6 Temperature Response

Measurements were made by irradiating three TLD rods each at two different temperatures. The first temperature of 34°C is comparable to normal body temperature. The second temperature of 22°C is comparable to normal room temperature in the theatre where the measurements were made.

Three TLD rods were irradiated at each temperature. The average of the measurements at each temperature is shown in Figure 3.20. The error bars represent the standard deviation of the mean of the three averaged measurements summed in quadrature with the standard deviation of the relevant sensitivity measurements. At 22^{o}C the error bars are 4.2% and at 34^{o}C the error bars are 4.9%. The difference in response between measurements made at the two temperatures is approximately 4.3%, indicating that there is no measureable difference in the response of the TLD rods over this range of temperatures. These TLD rod measurements

were not corrected for dose due to variations in source detector distance, which could add an uncertainty of between 0.7% and 1.2%, which could explain the relatively large error bars.

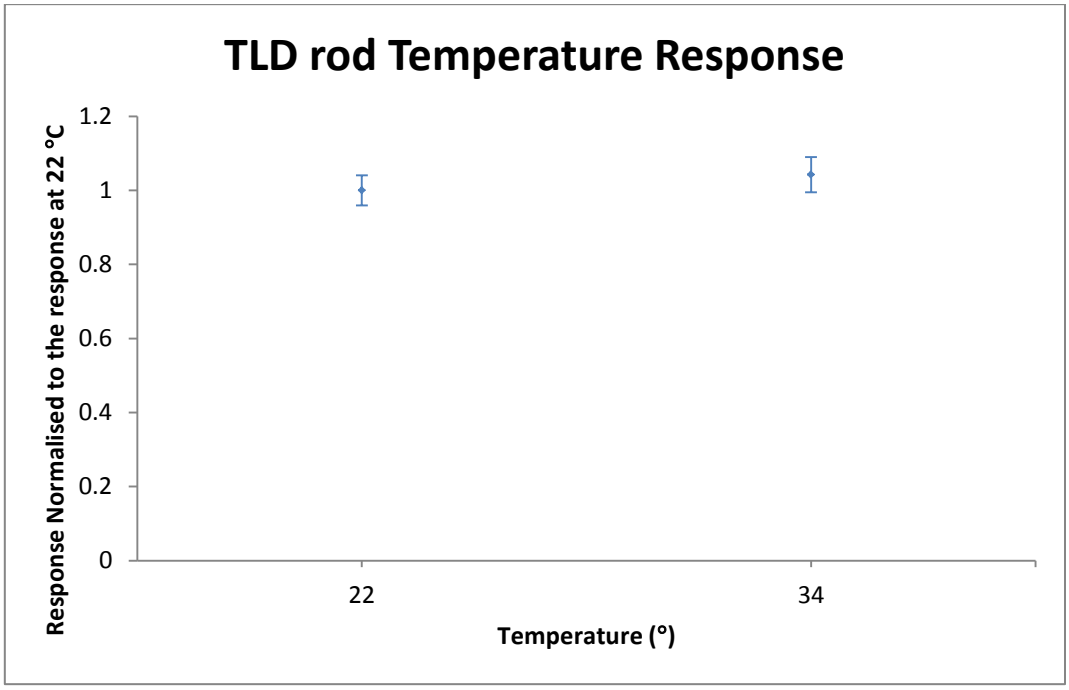

Figure 3.20 TLD rod temperature response measurements made at 22°C and 34°C, error bars are the standard deviation of the mean measurements for each temperature summed in quadrature with the relevant standard deviation of the mean stability. The error bars are 4.2% for 22°C and 4.9% for 34°C.

3.5 Discussion

3.5.1 Sensitivity

Due to the accidental reordering of the TLD rods a comparison of sensitivity over a long period of time for each individual TLD rod could not be made. However, prior to each set of measurements the relevant sensitivity of all TLD rod measurements was known and was applied to all results.

3.5.2 Linearity

The TLD rods displayed linearity with dose in the range of 0.5 Gy to 5 Gy. This is consistent with previous findings that state the useful range for measurements is between 0.001 Gy and 10 Gy[5]. Supralinearity was not observed.

3.5.3 Angular Response

TLDs are volume detectors and as such their geometrical shape is expected to determine if they will exhibit an angular response. Over the range of angles measured in the azimuthal direction the response varied by a maximum of 9.2%. The range of angles measured was between -29.4^{o} and 36.4^{o}. It is possible that we would observe a larger variation in response outside of these angles, theoretically the maximum over response of the TLD rod will occur at ± 90^{o} and will be greatest at the shortest distance from the Ir-192 source. The initial increase in response for positive angles suggests that extra dose from source transit time has a negligible effect on the results.

3.5.4 Energy Response

An equation to describe the response of dosimeters to variations in radiation energy indicated a maximum over response compared to the response at 6 MV of 58.5% at 29 keV. This is consistent with previous findings which indicate an over response between 30% and 70% for LiF: Mg,Ti[5, 18, 34].

The average energy in air from an Ir-192 source is 397 keV[53], and from the equation it was calculated that the TLD rods will over respond by 1.1%, relative to 6 MV photons, to x-rays of this energy. In clinical use the TLD rods would be irradiated through a depth of tissue. The effective energy of the spectrum of radiation from an Ir-192 source decreases with increasing depth in water. For brachytherapy dosimetry it is possible that the TLD rod could be placed on the surface of the patient's skin at a distance from the radioactive source that could vary from a few millimetres to several centimetres. The effective energy from Ir-192 source is 337 keV at 10 mm depth and 258 keV at 50 mm depth[21], which would change the response of the TLD rods, relative to 6 MV, by 1.6% and 3.1% respectively. According to the equation of best fit, as the average energy of the spectrum decreases the over response of the TLD rods will increase until the effective energy of 29 keV is reached, at which point the over response will begin to decrease.

3.5.5 Dose Rate Dose Response

The measurements showed that the response of the TLD rods between dose rates of 27 $mGys^{-1}$ and 42 $mGys^{-1}$ was constant, and while this does not cover the range of dose rates typical in brachytherapy (2 - 120 $mGys^{-1}$), it is consistent with previous findings stating that LiF:Mg,Ti TLD materials are dose rate independent up to 10^8 $mGys^{-1}$[5].

3.5.6 Temperature Response

As expected, no variation in the response of the TLD rods was observed over the range of temperatures measured. Indicating that the response will not be affected by the body temperature of a patient should they be placed inside a body cavity or on the skin surface of a patient.

3.5.7 Summary of Results

TLD rod		
Dosimetric Characteristic	**Standard Uncertainty**	**Explanation**
Sensitivity	Individual value assigned to each raw measurement	A correction factor should be applied to all raw measurements
Linearity	2.8%	The average of the standard deviation of the mean from the six doses measured
Azimuthal Angular Response	4.6%	The average variation of measurements over the range -29.4° to +36.4°
Energy Response	Polynomial fit to calculate the response at any energy 1.2%	A correction factor can be applied if the angle is known The average of the standard deviation of the mean from the nine energies measured
Dose Rate Response	1.8%	The average of the standard deviation of the mean from the five dose rates measured
Temperature Response	4.6%	The average of the standard deviation of the mean from the two temperatures
Total Uncertainty	**6.2%**	**(1 SD)**

Table 3.2 Summary of the measured TLD rod dosimetric characteristics and standard uncertainties.

3.5.8 Suitability for Brachytherapy Dosimetry Measurements

The characteristics of TLD rods making them suitable for brachytherapy dosimetry are as follows – they have a small physical size, are approximately tissue equivalent (due to similarity of effective atomic number), have a linear response with dose over the range relevant to radiation therapy fractions, are dose rate independent over a wide range, they display little angular dependence, are independent of moderate temperature variations and can store the dose for long periods of time. Whilst they may be suitable for measurements in high dose gradients the disadvantages of TLD rods in relation to brachytherapy dosimetry are as follows

– they require a careful annealing process post irradiation, they cannot be marked in any way and must always be kept clean, if they become contaminated this contamination will be burnt in during the annealing process and they will no longer be useful, they are incapable of giving a dose reading in real time and they are sensitive to changes to radiation energy.

3.6 Conclusion

The largest influence on the response of the TLD rod is the effective energy of the radiation. This can be corrected for if the effective energy of radiation is known but could lead to a large added uncertainty if the radiation energy is below 100 keV and is unknown. The lengthy annealing process post irradiation and the continuous careful handling are disadvantages but these are made up for by the reliability and consistency of the TLD rod as a radiation dosimeter.

4 Characterisation of MOSkin detectors

4.1 Introduction

The dosimetric characteristics of MOSkins were measured to assess their suitability for measurements of dose for brachytherapy applications. The dosimetric characteristics measured were stability, accumulated dose response, linearity, dose rate response, angular response, energy response and temperature response. All experimental work was carried out at the Peter MacCallum Cancer Centre.

4.2 Materials

4.2.1 MOSkin Detectors

Twenty MOSkin detectors, in two batches of ten, were obtained from the Centre for Medical Radiation Physics, CMRP, University of Wollongong, UoW, NSW, Australia. The MOSkin is a variation on the MOSFET dosimeter. The MOSkin consists of a long thin ribbon with dimensions of 330 mm × 3 mm × 0.4 mm, as shown in Figure 4.1. The size of the MOSFET chip is 0.6 mm × 0.8 mm × 0.35 mm[56] with a gate oxide thickness of 0.55 µm[13]. The chip is located under a build up layer of a specified thickness of kapton (a polyimide film that retains its physical properties over a wide range of temperatures[57]). The thickness of the kapton layer is such that the MOSkin has a water equivalent depth of detection of 70 µm. While each MOSkin is individually constructed, each dosimetric response was measured on a minimum of two MOSkins then extrapolated to the batch.

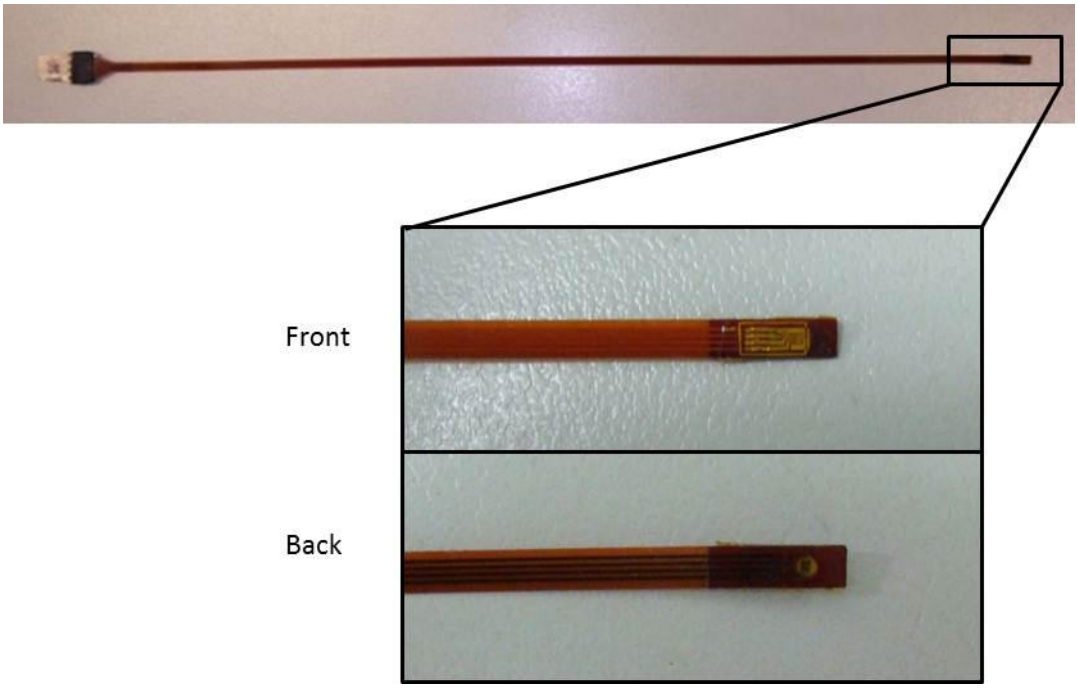

Figure 4.1 Photograph of the MOSkin detector with a close up of the MOSFET chip as seen from the font of the detector and the back of the detector.

4.2.1.1 MOSkin Measurement Read Out Process

MOSkin measurements were made using the Clinical Semiconductor Dosimetry Systems reader, CSDS, shown in Figure 4.2. Each individual MOSkin is connected to the reader via a cable. The reader is capable of connecting up to five individual MOSkins at once. Connection to the reader applies a bias voltage of 3-16 volts to each MOSkin. A measurement is made by recording the threshold voltage pre irradiation then again post irradiation, the radiation dose received is proportional to the change in threshold voltage.

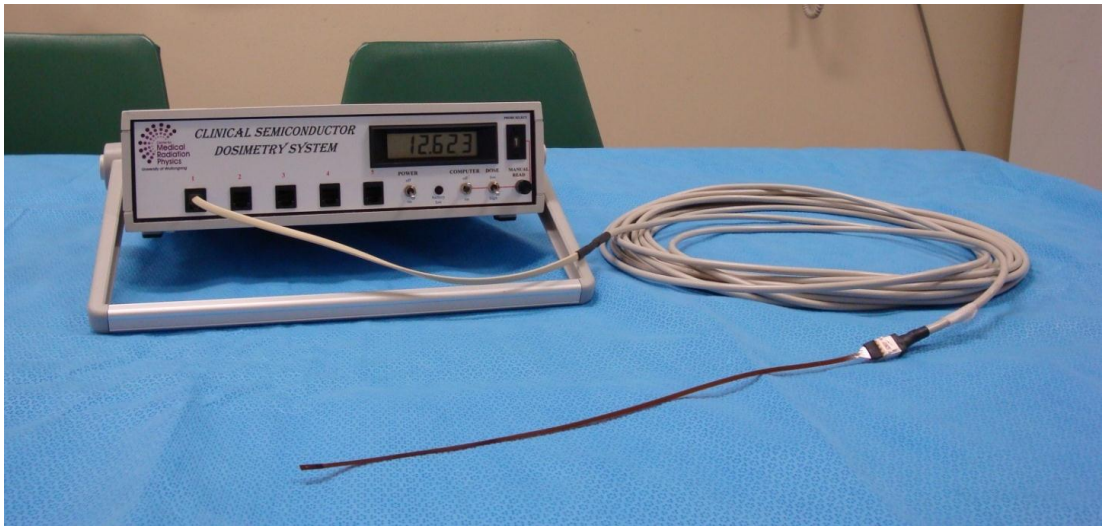

Figure 4.2 Photograph of the Clinical Semiconductor Dosimetry System reader attached to one MOSkin.

4.3 Methods

The MOSkin characterisation was completed after the TLD rod characterisation. The measurements were done in this order to refine the experimental design prior to using the MOSkins, namely, to avoid taking unnecessary measurements with the MOSkins as they have a useful lifetime which is a function of accumulated dose.

4.3.1 Taking a MOSkin Measurement

Each time a measurement was made, the MOSkins were connected to the bias voltage for at least 15 minutes, unless stated otherwise. The threshold voltage was read by selecting the correct channel on the CSDS and then pressing the 'Read' button once. The threshold voltage was read immediately prior to each irradiation, then read again 60 seconds post irradiation to minimise the effect of 'creep up', *see Section 2.4.1.1.*

4.3.2 Accumulated Dose Response

MOSFET detectors are known to display a decrease in response with total dose accumulated by the detector[33, 34]. The accumulated dose response of the MOSkins was measured in two ways. The first was by repeated irradiation using the Varian 600c 6 MV linac. Two MOSkins were placed at a depth of 50 mm in PTW RW3 (PTW Freiburn, Germany) solid water as shown in Figure 4.3. The detectors were placed on top of 10 mm superflab (an in house manufactured bolus material made from water, glycerine and gelatine) to cushion the MOSkins from the weight of the overlaying PTW RW3 slabs. 100 mm of PTW RW3 slabs were placed below the superflab for backscatter. Doses of 116 MU (1 Gy at 50 mm depth) were delivered to the MOSkins repeatedly, and the change in threshold voltage as a function of dose was recorded for the entire usable lifetime of the detector. The usable lifetime of the detector was expired when the threshold voltage was no longer readable and the CSDS read 'nA'.

The rate of change of response with accumulated dose of MOSFETs is known to be energy dependent[33]. Measuring the accumulated dose response for the lifetime of the detector

using the Ir-192 source was not practical due to the excessively long time it would take to deliver 1 Gy repeatedly for the lifetime of the detector, given our limited access to the HDR Ir-192 source. As such the second method for measuring the accumulated dose response made use of an existing sequence of measurements made using the Ir-192 source. These measurements were made with the initial purpose of measuring the radial angular response. A single MOSkin was placed inside the PMMA holder inside the cylindrical water phantom, (see Section 3.2.6). The MOSkin was irradiated three times using the HDR Ir-192 source, then the PMMA holder was then rotated through 30^{o} and irradiated another three times. This process continued until the PMMA holder had been rotated through a full 360^{o} and the front of the MOSkin was again directly facing the Ir-192 source. The measurements at 0^{o} and 360^{o} were recorded as a function of total dose.

4.3.3 Stability

Statistical fluctuations lead to variations in the threshold voltage, meaning two identical doses of radiation may not result in two identical changes in threshold voltage.

The stability of the MOSkins was measured in two ways. The first method involved irradiating ten MOSkins on the Varian 600c 6 MV linac (Varian, Palo Alto, CA). The MOSkins were placed on top of 10 mm of superflab which was placed on top of 100 mm of PTW RW3. On top of the MOSkins was 50 mm of PTW RW3. The layer of superflab was used below the MOSkins to prevent damage to the detectors. Two MOSkins were irradiated at once, as shown in Figure 4.3.

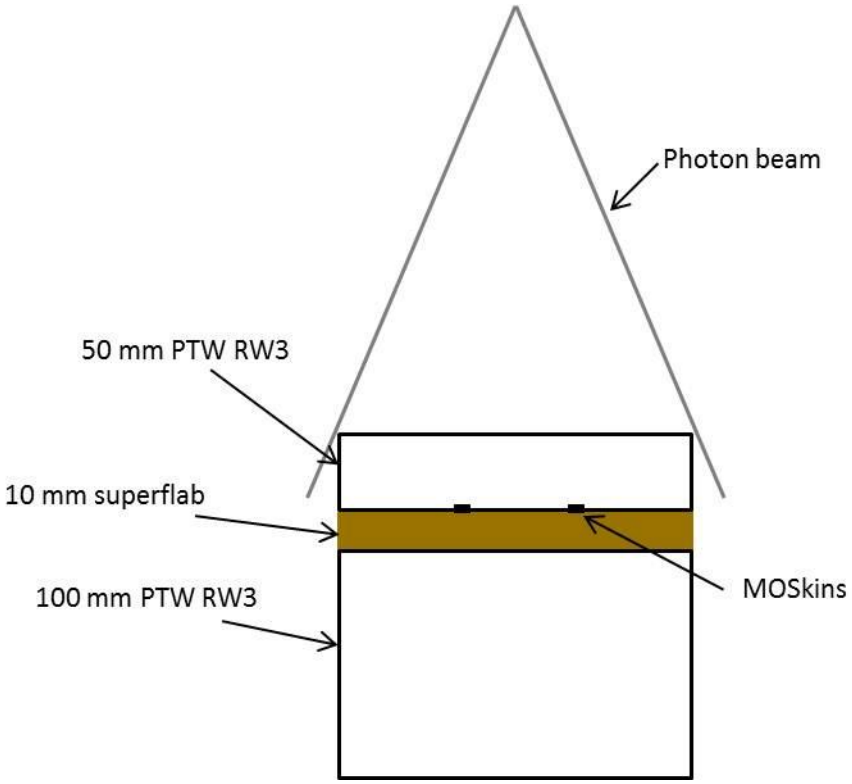

Figure 4.3 Diagram of set up for MOSkin accumulated dose response and stability measurements using the 6 MV linac.

A dose of 60 MU's, (SSD 1000 mm, field size 100 mm × 100 mm), which at a depth of 50 mm equates to a dose of 0.5 Gy, was delivered to the MOSkins a total of five times and the response of each MOSkin was recorded as a function of dose. All 10 MOSkins had no prior dose history and had been connected to the bias supply for less than 15 minutes at the time the first measurement was made.

The second method involved connecting a single MOSkin to the CSDS and taking a threshold reading every 60 seconds, for a total of 15 minutes, without irradiating the MOSkin. The threshold voltage was recorded as a function of time. The prior dose history of the MOSkin was approximately 20 Gy of accumulated dose and the MOSkin was connected to the bias supply immediately before the first threshold reading was made.

4.3.4 Linearity

Ideally, there should be a linear relationship between the dose delivered and the response of a detector over a range of doses. For the MOSkins, this translates to increases in dose being directly proportional to increases in threshold voltage changes.

The linearity of the MOSkins was measured using the 6 MV linac and the solid water slab phantom. The solid water slab phantom consisted of a 20 mm thick slab which had a removable section in the middle and into which the NE Farmer 2571 ionisation chamber could be inserted, (see Section 3.2.6). Two MOSkins were placed at a depth of 50 mm in PTW RW3 on top of 10 mm of superflab. The solid water slab phantom was used so that the NE Farmer 2571 ionisation chamber could be placed directly below the MOSkins, as shown in Figure 4.4.

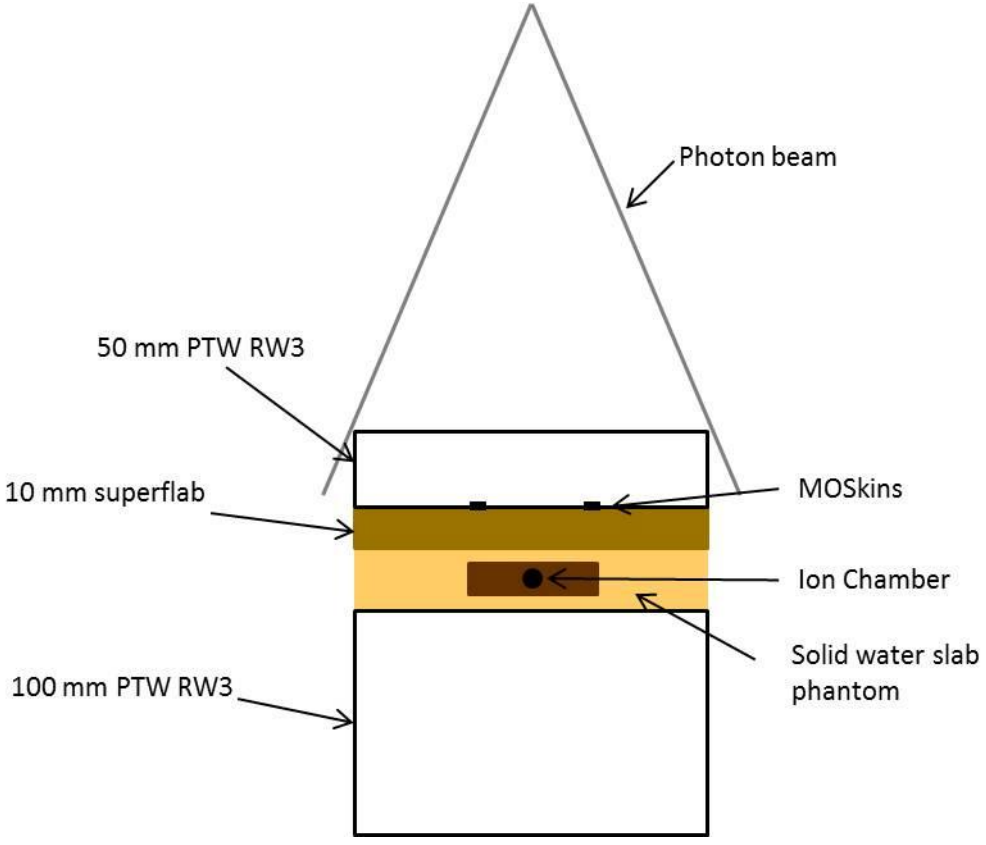

Figure 4.4 Diagram of set up for MOSkin linearity measurements using the 6 MV linac and solid water slab phantom.

The solid water slab phantom was placed directly below the layer of superflab with the ionisation chamber inserted. This put the centre of the ionisation chamber at a distance of 20 mm below the MOSkins. Below the solid water slab phantom was another 100 mm of PTW RW3. The dose delivered to the MOSkins and ion chamber was calculated using percentage depth dose measurements determined from ionisation chamber measurements made previously on the same linac. Doses of 0.5 Gy, 1 Gy, 2 Gy and 5 Gy were delivered to the MOSkins at a dose rate of 250 $MUmin^{-1}$. The ionisation chamber was used to confirm the delivered dose. The response of the MOSkins was recorded as a function of dose.

4.3.5 Angular Response

Unlike the TLD rods, where the sensitive volume of the detector is the entire physical size of the detector, the sensitive detection volume of the MOSkin is contained within a MOSFET silicon chip located at one end of the MOSkin ribbon. The MOSFET chip on the MOSkins has dimensions of 0.6 mm × 0.8 mm × 0.35 mm and within this the gate oxide was 0.55 µm thick. With such a small detection volume it is likely that the radiation angle of incidence will have a measureable effect on the response of the detector.

The angular response of the MOSkins was measured using the cylindrical PMMA water phantom and the Ir-192 source. The angular response was measured in both the radial and azimuthal direction, as indicated in Figure 4.5.

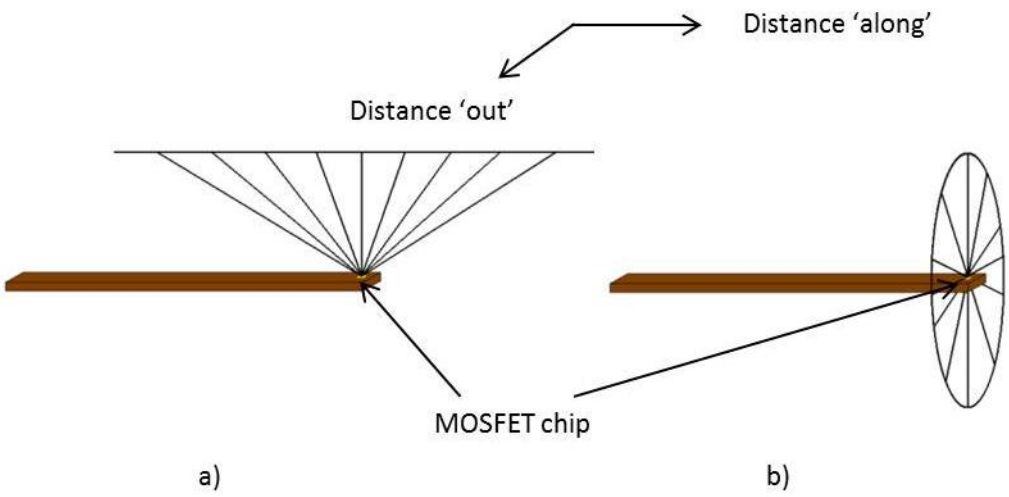

Figure 4.5 Diagram of a) azimuthal and b) radial angular directions around the MOSkin in reference to the position of the MOSFET chip on the ribbon.

4.3.5.1 Radial Angular Response

The radial angular response was measured by sending the Ir-192 source to a single dwell position and rotating the PMMA MOSkin holder around the central axis of the phantom in 30° increments. To determine the source dwell position that would coincide with the perpendicular bisector of the MOSkin, and hence, deliver the highest dose, an ion chamber was placed in the central channel of the cylindrical water phantom and the source was stepped through a number of 'dwell positions'. A 'dwell position' refers to a source position in the catheter. The source position that coincided with the maximum ion chamber reading was assumed to be the perpendicular bisector of the MOSkin for the measurements. The MOSkin was rotated through a full 360° in 30° steps and the response of the MOSkin was recorded as a function of radial angle.

4.3.5.2 Azimuthal Angular Response

The azimuthal angular response was also measured using the cylindrical water phantom and the Ir-192 source. The radial orientation of the MOSkin in the PMMA holder was kept fixed in the central channel and the position of the Ir-192 source in one of the 50 mm radius channels

was varied. Each source dwell position in the catheter created a different radiation angle of incidence to the MOSkin and a different source to detector difference. Corrections for the changing source to detector distance were made by correcting each measurement for dose using the known geometry of the set up and dose rate per unit air kerma strength data from tables developed by Daskalov et al[39]. All dwell positions within the catheter were at a distance of 50 mm out (perpendicular to the source axis, in the x direction) so only the distance along the source axis (in the y direction) changed. Daskalov et al[39], gives the dose rate per unit air kerma strength factors for a number of distances in the y direction corresponding to x = 50 mm. Where an exact position was not covered in the table, the factor was estimated from a polynomial fit of the surrounding points. An assumption was made that the MOSFET chip detection volume perfectly coincided with the ion chamber measurement point and all distance corrections were made on this basis. To investigate the effect of an error on this assumption the distance corrections were repeated but with dwell position offsets of ± 2.5 mm (one dwell position) along the y-axis.

4.3.6 Energy Response

MOSFETs are known to exhibit a variation in response to changing radiation energy[32, 33, 34, 58, 59]. The energy response of the MOSkins was measured using the deep and superficial X-ray unit (Pantak Therapax X-ray unit Model MXT225) and the 6 MV and 18 MV linac (Varian iX linac). The beam qualities measured using the deep and superficial X-ray unit were 15.7 keV, 19.1 keV, 21.2 keV, 28.4 keV, 38.3 keV, 59.9 keV, 80.3 keV and 108.8 keV. These beam qualities were calculated based on the filtration used in the beam using the method described in Section 3.2.4. Monitor units delivered using the deep and superficial X-ray unit were calculated using the method described in Section 3.3.4.1. Measurements were made at the surface and at a depth of 10 mm in brown Standard Grade Solid Water® Gammex 457, (SGSW), (Gammex, Inc, Middleton, WI, USA) with at least 100 mm of PTW RW3 below for scatter material, see Figure

4.6. Unlike the TLD measurements, a response using the Cs-137 source could not be measured as the Cs-137 unit is not physically capable of containing a detector with a cable attached.

Figure 4.6 Photograph of the set up of the energy response measurements using the deep and superficial X-Ray unit.

Doses of 0.5 Gy or 0.75 Gy were delivered to the MOSkins at each beam quality. All measurements were then normalised to doses of 1 Gy. For the 6 MV and 18 MV linac measurements the MOSkins were irradiated at a depth of 50 mm in PTW RW3 on top of 10 mm of superflab with another 100 mm of PTW RW3 below to provide adequate backscatter material, as shown in Figure 4.7.

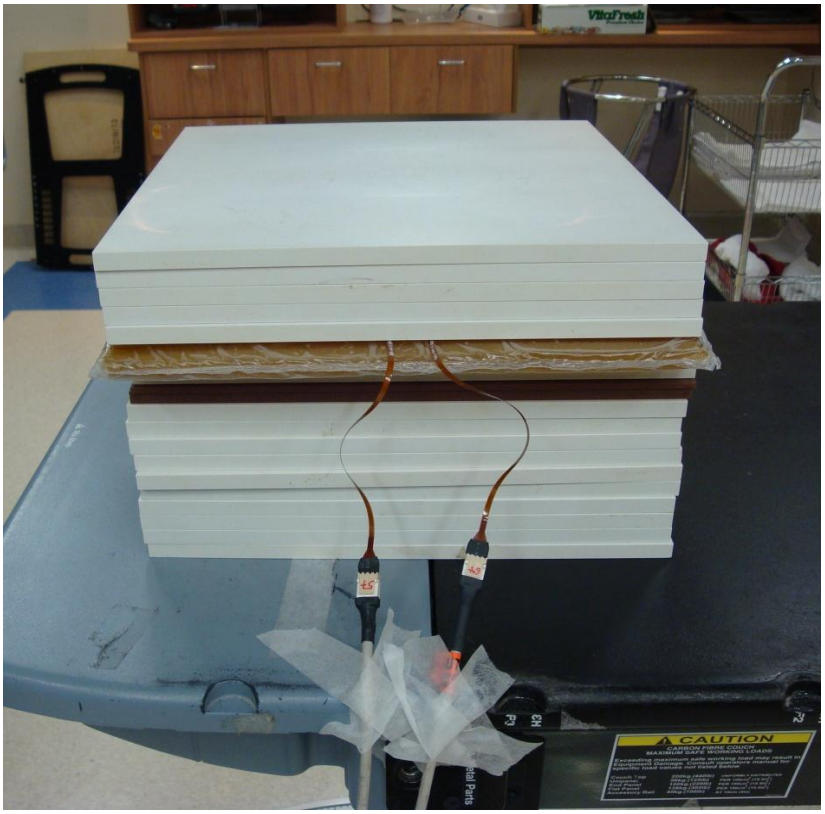

Figure 4.7 Photograph of the set up for the energy response measurements using the 6 MV and 18 MV linac.

A dose of 1 Gy was delivered at each beam quality. The response of the MOSkins at each beam quality was recorded as a function of effective energy.

4.3.7 Dose Rate Response

The response of a detector can be affected by the rate at which the dose is delivered. The dose rate response of the MOSkins was measured in two ways, using the 6 MV linac and using the Ir-192 source.

Using the 6 MV linac, measurements were made by irradiating the MOSkins through different depths of white solid water. The MOSkins were placed on top of 10 mm of superflab material with 100 mm of PTW RW3 below to provide back scatter material. The irradiation depth was changed by placing different thicknesses of PTW RW3 water above the MOSkins. The source to surface distance remained 1000 mm for all measurements. Measurements were made at depths of 10 mm, 15 mm, 30 mm, 50 mm, 80 mm and 100 mm. 100 MUs were delivered for

each measurement which was equivalent to doses of 0.99Gy, 1.0 Gy, 0.94 Gy, 0.86 Gy, 0.74 Gy and 0.66 Gy. The dose rate at each depth was 41.45 $mGys^{-1}$, 41.67 $mGys^{-1}$, 39.30 $mGys^{-1}$, 35.87 $mGys^{-1}$, 30.84 $mGys^{-1}$ and 27.69 $mGys^{-1}$ respectively. These dose rates were calculated from the percentage depth dose measurements made previously on the linac used at the Peter MacCallum Cancer Centre. The response of the MOSkin was recorded as a function of dose rate.

The second method to measure the dose rate response of the MOSkins used the Ir-192 source and an Intra-Operative Brachytherapy (IOBT), applicator. The IOBT Applicator consisted of a series of six catheters sandwiched between layers of water equivalent wafers. The six catheters were aligned parallel to each other with a 10 mm gap between each one. The IOBT applicator will be discussed in greater detail in Section 5.2.

The MOSkins were placed on top of 10 mm of superflab material with 50 mm of PTW RW3 below. A variable amount of white solid water was placed between the MOSkins and the IOBT applicator. Above the applicator was placed another 30 mm of PTW RW3 to provide backscatter. Wadded paper towels were used either side of the applicator to prevent the applicator being compressed, as shown in Figure 4.8.

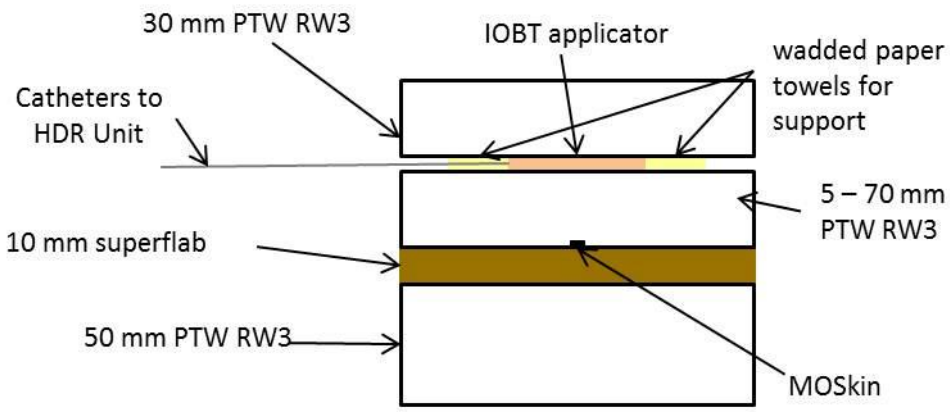

Figure 4.8 Diagram of the set up for the dose rate response measurements using the HDR Ir-192 source and IOBT applicator.

For each depth the treatment plan was altered such that 0.5 Gy was delivered to the MOSkins. Measurements were made at six different depths in PTW RW3. These depths are shown in Table 4.1 along with the effective energy of the Ir-192 spectrum at this depth and the dose rate that was a result of the source strength at the time of the measurements and treatment durations. The effective energy of the spectrum at each depth was calculated using Monte Carlo modelling carried out by D. Cutajar (obtained through personal correspondence).

Depth in Solid Water (mm)	Effective Energy of the Ir-192 spectrum (keV)	Dose Rate at depth in solid water ($mGys^{-1}$)
5	351.5	69.44
10	320.1	37.87
20	290.5	14.45
30	266.0	7.18
50	230.3	2.72
70	206.1	1.37

Table 4.1 Table of the depths used for dose rate measurements using the Ir -192 source and the IOBT applicator and the effective energy of the Ir-192 spectrum at each depth.

For each depth the measurements were corrected for the energy response and the response of the MOSkin was recorded as a function of dose rate.

4.3.8 Temperature Response

The MOSFET chip used on the MOSkin is a semiconductor device and is subject to inherent thermal response, which can shift the threshold voltage[40]. For the purpose of in-vivo dosimetry the detector can be placed on the surface of the patient's skin, or inside the patient's body. In both situations the detector will be exposed to temperatures higher than those in normal laboratory conditions meaning for in vivo measurements the temperature response must be determined.

The temperature response of the MOSkins was measured using the cylindrical water phantom and the Ir-192 source. Measurements were taken with four separate MOSkins. The cylindrical water phantom was filled with room temperature water, approximately 22°C, the cap to the cylindrical water phantom was removed and a digital thermometer probe was inserted into the water to monitor the temperature. A single MOSkin was then inserted into the phantom using the PMMA holder. The MOSkin was left inside the phantom for 120 seconds prior to irradiation so thermal equilibrium could be reached. Two measurements were taken with each of the four MOSkins. The room temperature water was then removed and the cylindrical phantom was then filled with hot water, approximately 38°C, and wrapped in a 'Bair Hugger' warming blanket to minimise loss of heat. Again each MOSkin was placed inside the phantom for at least 120 seconds prior to irradiation so thermal equilibrium could be reached and two measurements were taken with each of the four MOSkins. A dose of 0.5 Gy was delivered to the MOSkins for each measurement and the response of the MOSkins was recorded as a function of temperature.

4.3.9 dual MOSkin Detectors

Towards the end of the experimental work a number of 'dual MOSkin' detectors were obtained from CMRP, UoW, NSW, Australia. These dual MOSkins consisted of two individual MOSkin detectors connected face to face with each detector being connected to the CSDS via its own cable. The 'dual MOSkin' is reported to allow for angular-independent measurements as it compensates for the naturally asymmetrical structure of the MOSFET chip relative to the beam direction[60]. This is achieved by averaging the measurements from each individual MOSkin. The 'dual MOSkin' is shown in Figure 4.9.

Figure 4.9 Photograph of a 'dual' MOSkin detector.

4.3.9.1 Angular Response

The response of the dual MOSkin was measured in both the radial and azimuthal angular directions using the same methods as used for the single MOSkins (see Section 4.3.5). As the 'dual MOSkin' was thicker than an individual MOSkin a second PMMA MOSkin holder was produced to accommodate them.

Each individual MOSkin from a 'dual MOSkin' was connected to the bias voltage for at least 15 minutes prior to taking the first measurement each time they were used. The threshold voltage was read by selecting the correct channel on the CSDS and then pressing the 'Read' button once. The threshold voltage was read immediately prior to each irradiation, then read again 60 seconds post irradiation.

4.4 Results

4.4.1 Accumulated Dose Response

A dose of 1 Gy was repeatedly delivered to two MOSkins using the 6 MV linac for the lifetime of each MOSkin, until the CSDS read 'nA'. Figure 4.10 shows the response of the two MOSkins normalised to the initial response of each MOSkin. The usable lifetime of the two MOSkins measured were both found to be approximately 70 Gy for 6 MV radiation. As such, 55 Gy was assumed to be a conservative estimate of the usable lifetime, since it may vary for Ir-192 radiation, for all MOSkin and dual MOSkin detectors used in this project.

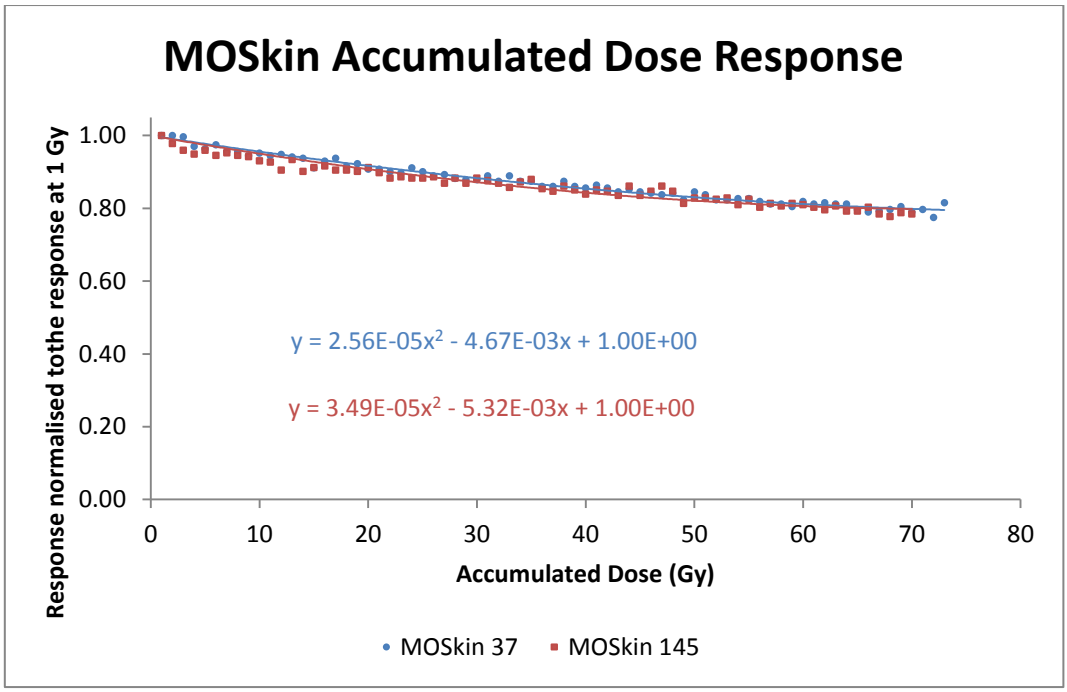

Figure 4.10 The normalised accumulated dose response of MOSkin 37 and MOSkin 145 as measured on the 6 MV linac. Also shown are 2nd order polynomial equations of best fit.

A line of best fit applied to the data (where x is the accumulated dose in Gy and y the normalised response), with a set intercept of *x=0, y=1*, revealed a slightly non linear decrease in the response in the form of a low second order polynomial for both MOSkins, this is also shown in Figure 4.10. An average of the normalised measurements for each MOSkin were also plotted against accumulated dose, this is shown in Figure Figure 4.11.

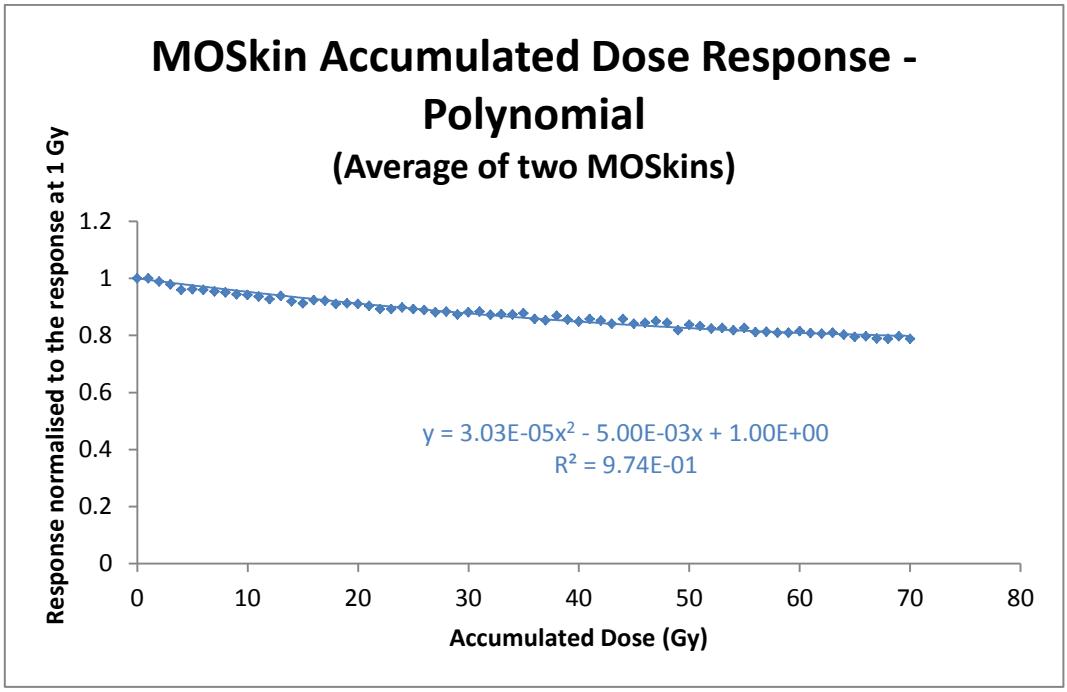

Figure 4.11 The average normalised accumulated dose response of MOSkin 37 and MOSkin 145 as measured on the 6 MV linac , also shown is a 2nd order polynomial equation of best fit.

The line of best fit that is obtained from averaging the measurements from two MOSkins is shown in Equation 4.1.

$$\text{Response} = 3.03 \times 10^{-5}\text{x}^2 - 5.00 \times 10^{-3}\text{x} + 1.00 \qquad \text{Equation 4.1.}$$

$$Where\ x\ is\ the\ dose\ in\ Gray$$

Figure 4.12 shows the average measurements with a linear equation of best fit applied, with a set intercept of *x=0, y=1*. The linear equation of best fit obtained is shown in Equation 4.2.

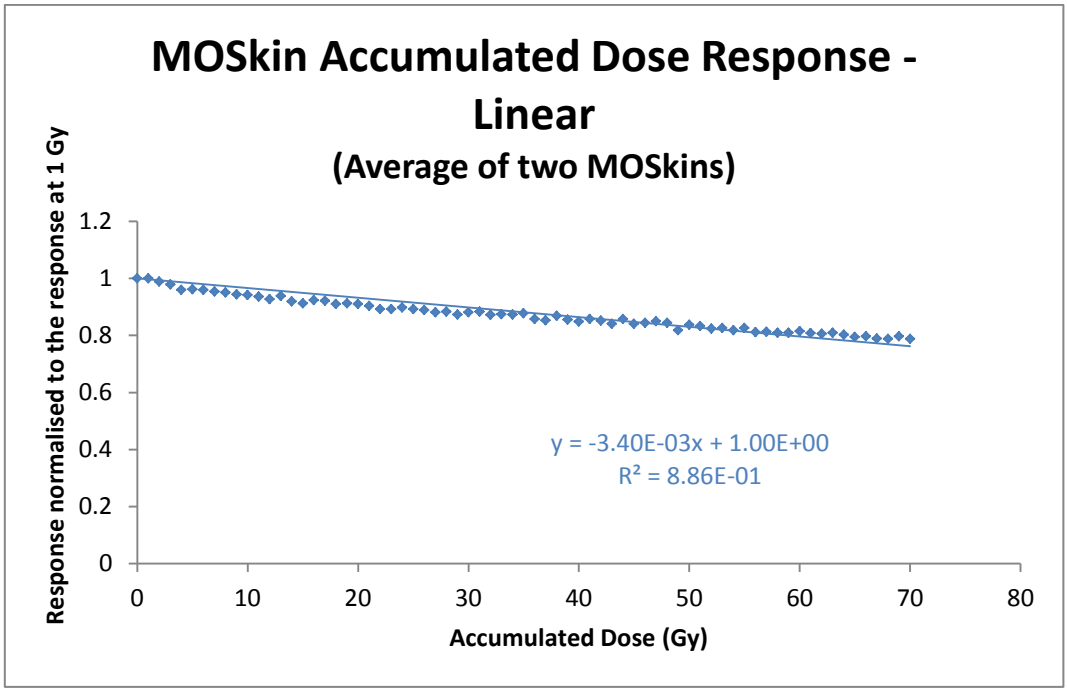

Figure 4.12 The average normalised accumulated dose response of MOSkin 37 and MOSkin 145 as measured on the 6 MV linac, also shown is a linear equation of best fit.

$$Response = 3.40 \times 10^{-3}x + 1.00 \qquad \text{Equation 4.2.}$$

$$Where\ x\ is\ the\ dose\ in\ Gray$$

The accumulated dose response for Ir-192 radiation was also estimated by using measurements made initially to calculate the radial angular response of the detector. The initial and final measurements from three MOSkins were used and are shown in Figure 4.13.

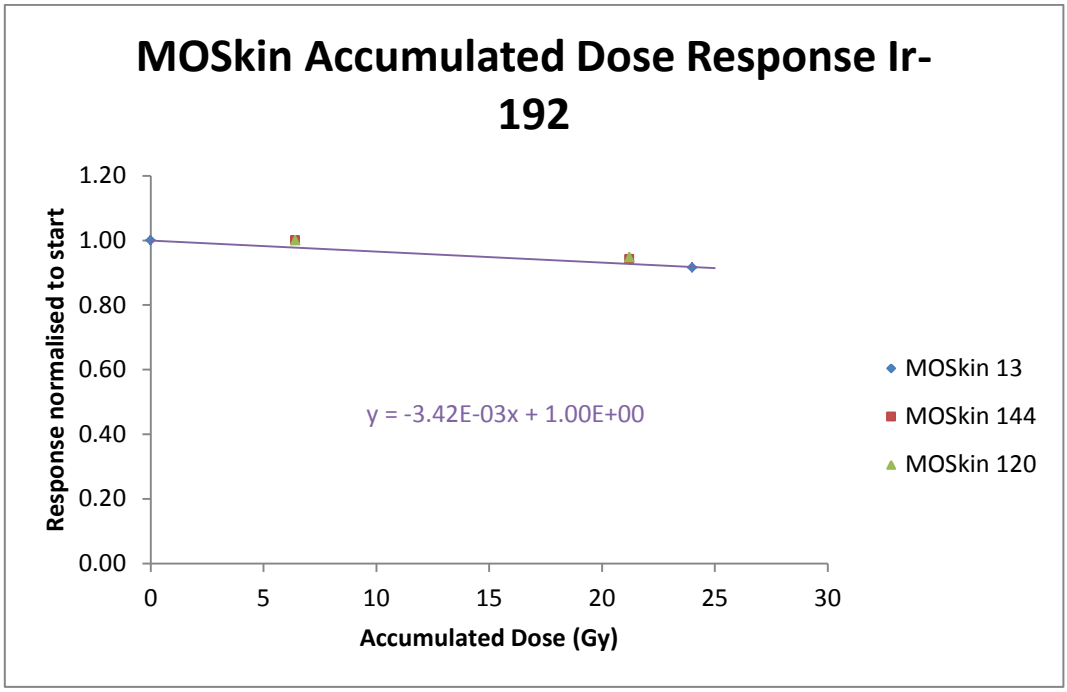

Figure 4.13 The accumulated dose response measurements normalised to the initial response as measured using the Ir-192 source, also shown is a linear equation of best fit.

The results for the three MOSkins were averaged and a linear line of best fit was applied to the points with a set intercept of *x=0, y=1*. The equation of this line is shown in Equation 4.3 and indicates a decrease of 0.342% per Gy.

$$Response = -3.42 \times 10^{-3} x + 1.00 \qquad \text{Equation 4.3}$$

$$Where\ x\ is\ the\ dose\ in\ Gray$$

When a linear fit is applied, the accumulated dose response of both 6 MV and Ir-192 radiation is 0.34% per Gy. However, as the polynomial fit produces a higher R^2 value, the polynomial response equation will be used to correct all raw measurements made with the Ir-192 source. All raw measurements made with the MOSkins discussed in the following sections were corrected for accumulated dose response, the correction factors used where in the form of Equation 4.4 and Equation 4.5.

6 MV Radiation

$$Accumulated\ Dose\ Corrected\ Response = \frac{Measurement}{\{1.00+(3.03\times10^{-5}\times x^2)-(5.00\times10^{-3}\times x)\}}$$

$$Where\ x\ is\ the\ dose\ in\ Gray$$ Equation 4.4.

Ir-192 Radiation

$$Accumulated\ Dose\ Corrected\ Response = \frac{Measurement}{\{1-(3.42\times10^{-3}\times x)\}}$$ Equation 4.5.

$$Where\ x\ is\ the\ dose\ in\ Gray$$

4.4.2 Stability

Ten MOSkins were irradiated five times each with a constant dose of 0.5 Gy, the raw measurements were then corrected for accumulated dose response using Equation 4.4. The standard deviation of the mean was calculated for the measurements from each MOSkin. The average value obtained from the 10 MOSkins was 0.9%. The average standard deviation obtained from the 10 MOSkins was 1.9% (1 SD).

The threshold voltage was also read from the CSDS over a period of fifteen minutes in the absence of any applied dose, the measurements are shown in Figure 4.14. The average change in threshold voltage recorded was 1.9 mV with a standard deviation of 1.1 mV.

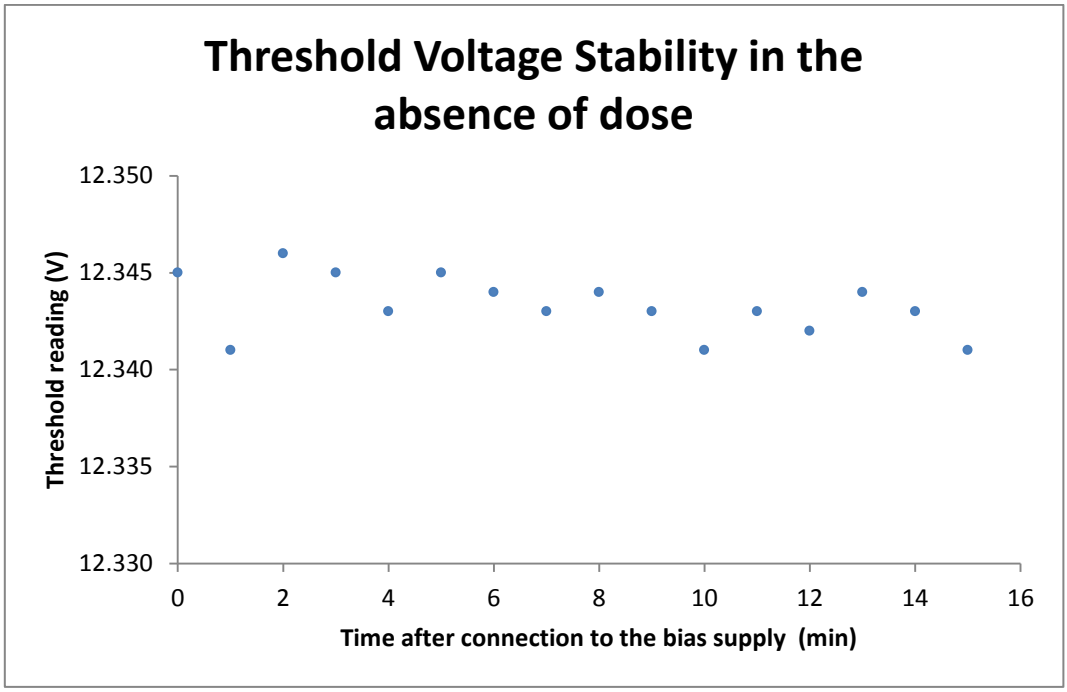

Figure 4.14 MOSkin threshold voltage stability measured in the absence of dose as a function of time connected to the bias supply.

4.4.3 Linearity

The MOSkin measurements were linear with dose in the range of 0.5 Gy to 5 Gy, as shown in Figure 4.15. Each point represents the average of three measurements normalised to the response at 1 Gy. The error bars represent the standard deviation of the mean of the three measurements summed in quadrature with the standard deviation of the mean of MOSkin stability. The average error bar size was 1.7 % and 1.4 % for MOSkins 14 and 15 respectively. A linear equation was fit to the data for each MOSkin, also shown in Figure 4.15.

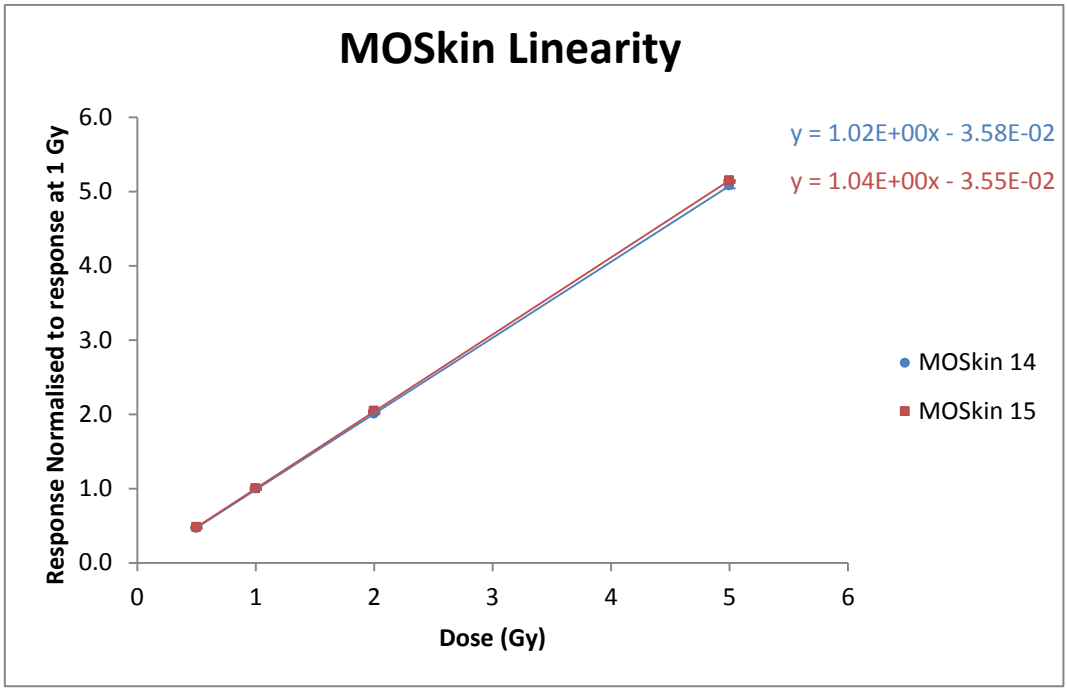

Figure 4.15 Linearity of the MOSkins with dose as measured using the 6 MV linac, the error bars represent the standard deviation of the mean measurements at each dose summed in quadrature with the standard deviation of the mean stability. The average error bar size is 1.7% and 1.4% for MOSkin 14 and 15 respectively.

Figure 4.16 shows the response of the MOSkins plotted as a function of voltage, indicating an average response of 373 mV per Gy.

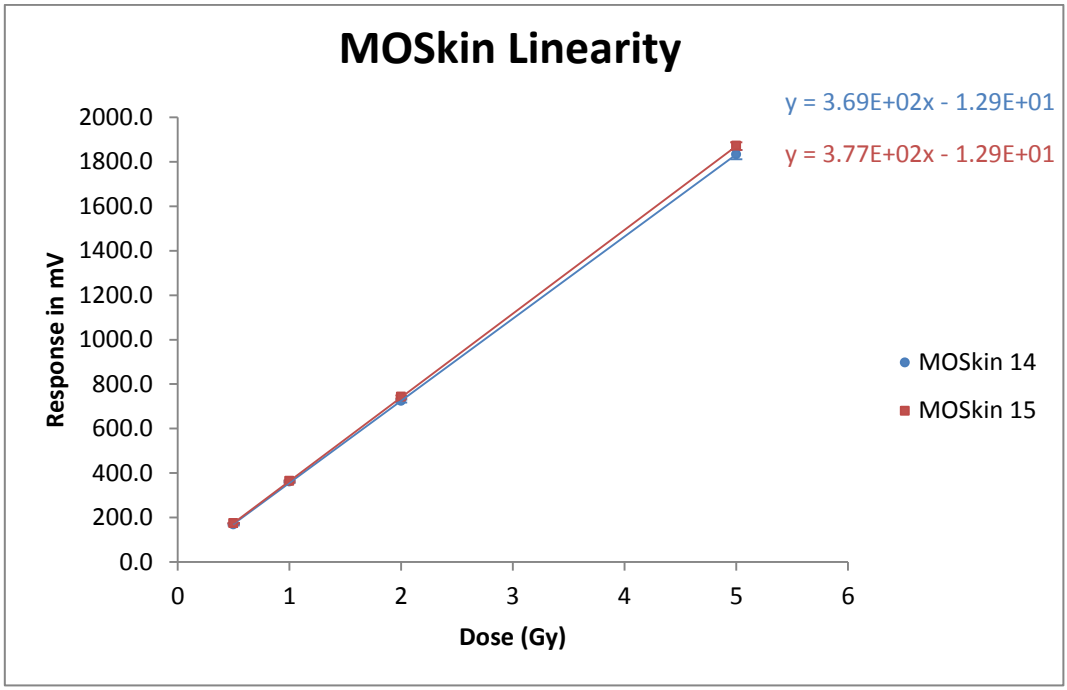

Figure 4.16 Linearity of the MOSkins as measured using the 6 MV linac plotted as a function of mV, the error bars represent the stand deviation of the mean measurements at each dose summed in quadrature with the standard deviation of the mean stability. The average error bar size is 8.6 mV and 7.4 mV for MOSkins 14 and 15 respectively.

4.4.4 Angular Response

The angular response of the MOSkins was measured in both the radial and azimuthal angular directions.

4.4.4.1 Radial Angular Response

In the radial direction three measurements were taken at each 30° interval for a full rotation. When the front of the MOSkin was facing the source it was defined to be at 0° rotation. The average of each set of three measurements was taken as the value for that angle. Figure 4.17 shows the accumulated dose response corrected radial angular response as a function of radial angle.

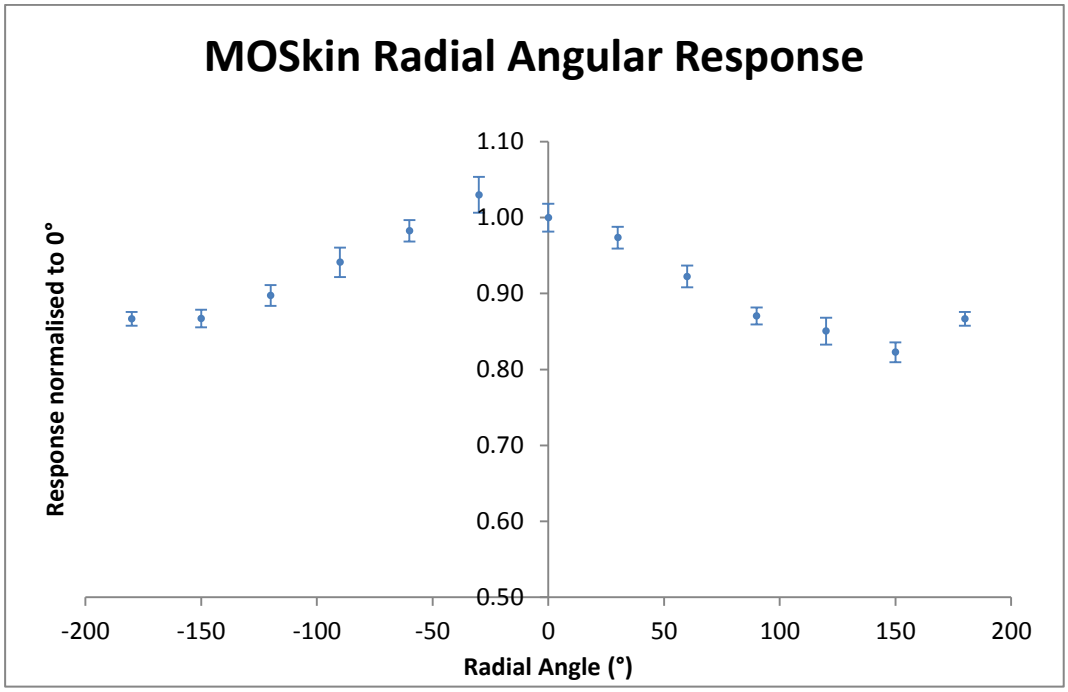

Figure 4.17 Radial angular response of the MOSkins as measured using the Ir-192 source, the error bars represent the standard deviation of the mean measurements at each angle summed in quadrature with the standard deviation of the mean stability. The average error bar size is 1.5%. Note the truncated vertical axis.

The maximum radial angular response occurs at -30° rather than at 0° as expected from the symmetrical design of the MOSkin. There are two possible explanations for this, one is a simple angular offset. The magnitude of the simple angular offset was calculated by fitting a polynomial equation to the measurement points then finding the angle at which the polynomial equation was a maximum. Using this method an angular offset of 20.1° was calculated however, while the resultant response was a maximum at 0° it did not have the required symmetry about 0°, also an offset of 20.1° is relatively large considering the size of the angular increments for measurements (30°), and therefore unlikely.

The second possible explanation is a simple spatial offset in the position of the slit in which the MOSkin sits inside the MOSkin holder, specifically an offset both in a direction away from the source and transverse to the source, as shown in Figure 4.18.

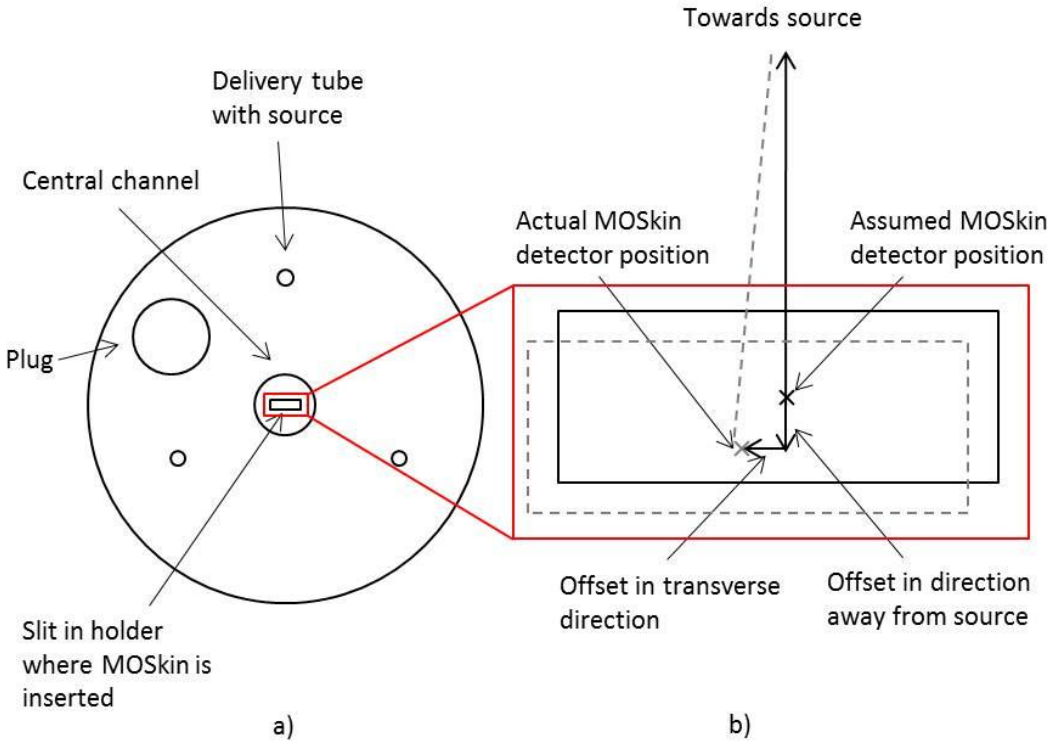

Figure 4.18 Diagram of a) top view of cylindrical PMMA phantom and b) close up of slit in MOSkin holder showing offset of position of MOSkin detector within slit (not to scale).

For the response at -30° to be greater than the response at 0° the offsets would have to be in the directions indicted in Figure 4.18b. The magnitude of the offsets required was calculated based on a least squares polynomial fit to the measurement points and also a least squares constraint on symmetry. A polynomial fit to dose rate per unit air kerma strength from Daskalov et al[39], was used to calculate the change in dose that would result from the changing source to MOSkin distance, the polynomial fit is displayed in Figure 4.19 and Equation 4.6.

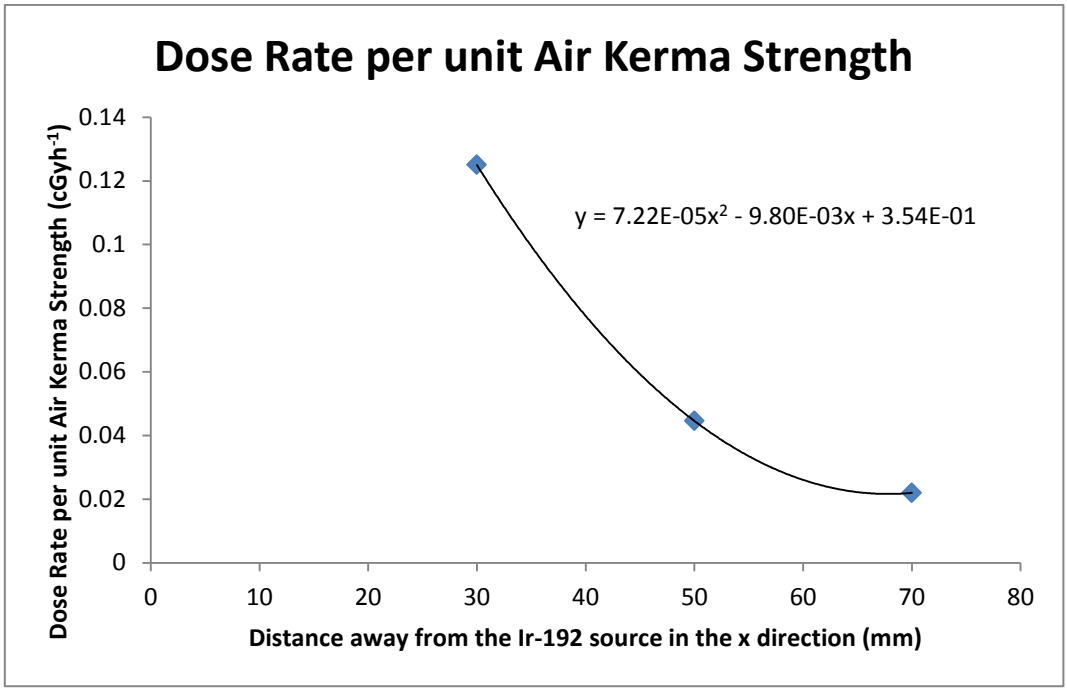

Figure 4.19 Plot of polynomial equation fit to points 30 mm, 50 mm and 70 mm from the source obtained from the Daskalov tables[39].

Polynomial Equation

$$Dose\ rate\ per\ unit\ air\ kerma\ strength = 7.22 \times 10^{-5}\ x^2 - 9.80 \times 10^{-3} x + 3.54 \times 10^{-1}$$

$$Where\ x\ is\ the\ distance\ away\ from\ the\ source\ in\ mm \qquad \text{Equation 4.6.}$$

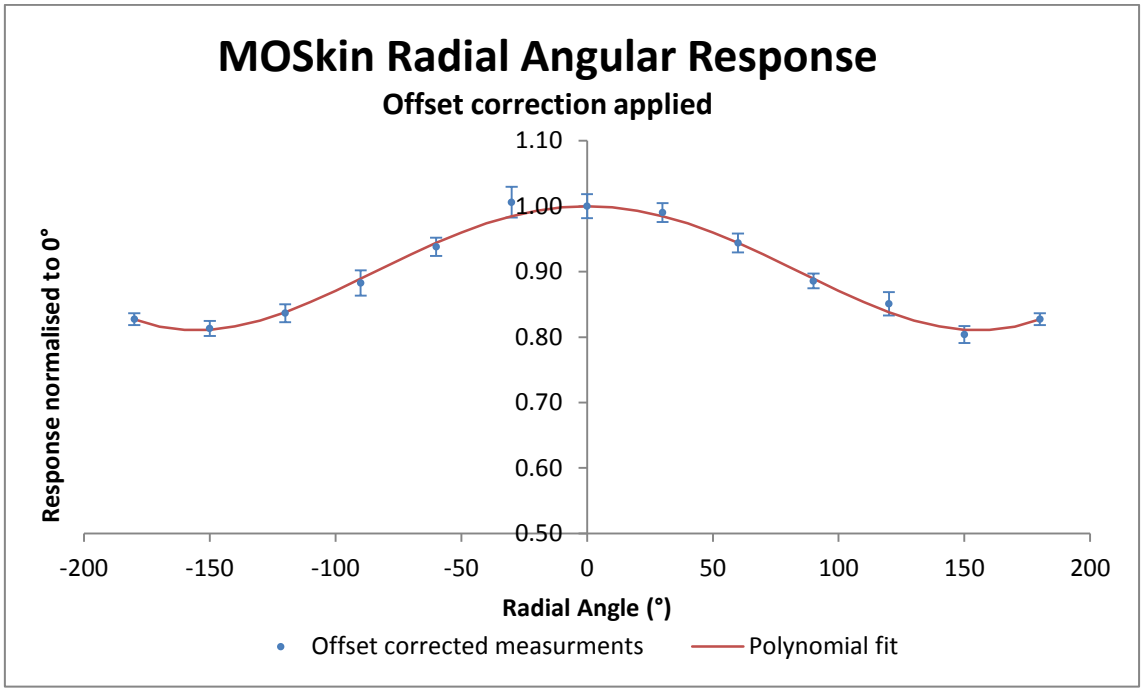

Figure 4.20 MOSkin radial angular response corrected for an offset of 0.4 mm in the direction away from the source and 0.7 mm transverse to the source. Average error bar size is 1.5%. Note the truncated vertical axis.

Equation 4.7 shows the fitted even polynomial equation which can be used to calculate the radial angular response at any angle. All offset corrected radial angular response measurements are consistent with this fit.

$$Response = -2.44 \times 10^{-15}x^6 + 4.42 \times 10^{-10}x^4 - 1.71 \times 10^{-5}x^2 + 1.00 \quad \text{Equation 4.7.}$$

$$Where\ x\ is\ the\ radial\ angle\ in\ degrees$$

The polynomial equation of fit predicts a maximum under response of 19.0% at ± 156°. The accuracy of the angle of incidence between source and detector will be different for each experimental set up, if a conservative degree of error of ± 5° is assumed, the uncertainty in the response of the MOSkin will be 2.1%.

4.4.4.2 Azimuthal Angular Response

The azimuthal angular response measurements were normalised for dose according to source detector distance using the tables described by Daskalov et al[39], then normalised to the response at 0°. Figure 4.21 shows the MOSkin response to azimuthal angular direction for the

initial choice of Ir-192 source position in the catheter. Each point represents the average of three measurements normalised to the response at 0°. The error bars represent the standard deviation of the mean of the three measurements normalised to the response at 0° summed in quadrature with the standard deviation of the mean of the stability. The average size of the error bars was 1.8%.

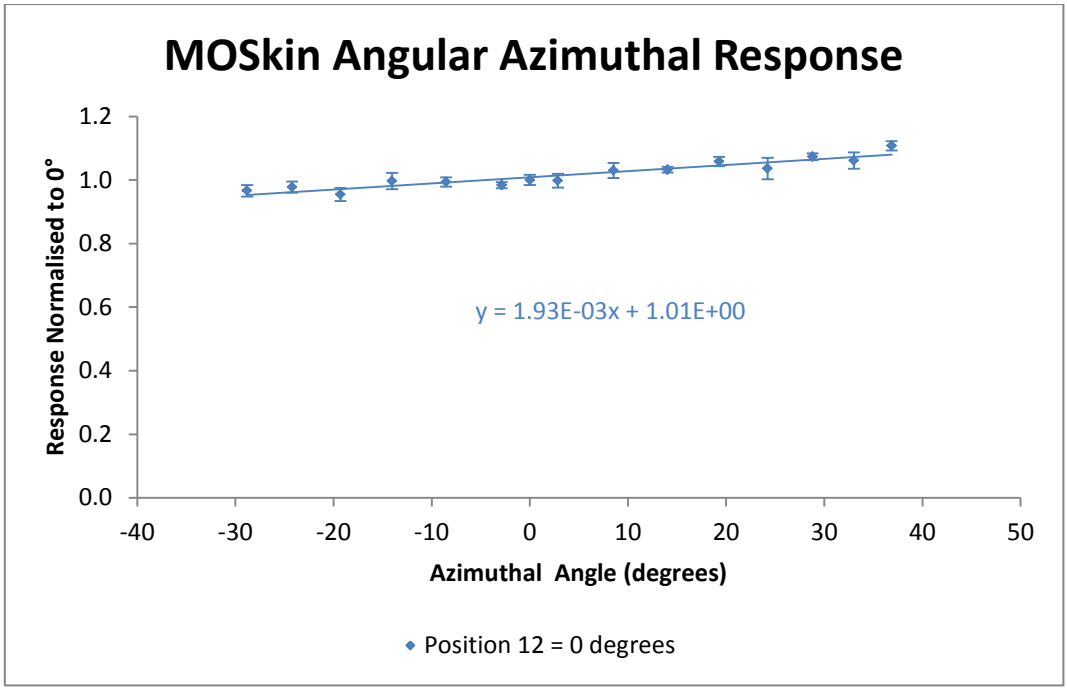

Figure 4.21 The azimuthal angular response of the MOSkins as measured using the cylindrical PMMA phantom and the Ir-192 source, the error bars represent the standard deviation of the mean of the measurements at each angle summed in quadrature with the standard deviation of the mean stability. The average size of the error bars was 1.8%. Also shown is a linear equation of best fit.

The response appears to increase towards increasing angles. A line of best fit produces a linear equation with a positive gradient. One possible explanation for this could be that the source position coinciding with the perpendicular bisector of the detector was chosen incorrectly. The two source positions immediately either side of the initial choice for the perpendicular bisector of the detector were also measured. Re-normalising the measurements for dose using the source to detector distances and data from the tables described by Daskalov et al[39], for each of these cases is shown in Figure 4.22. In Figure 4.22 the Ir-192 source positions in the catheter

are described in terms of 'dwell positions' as specified by the brachytherapy treatment planning system. Dwell position 12 corresponds to the initial choice of the position coinciding with the perpendicular bisector of the detector. Dwell position 11 corresponds to the source position immediately below position 12 in the catheter and dwell position 13 corresponds to the source position immediately above position 12 in the catheter. There is 2.5 mm between each source dwell position.

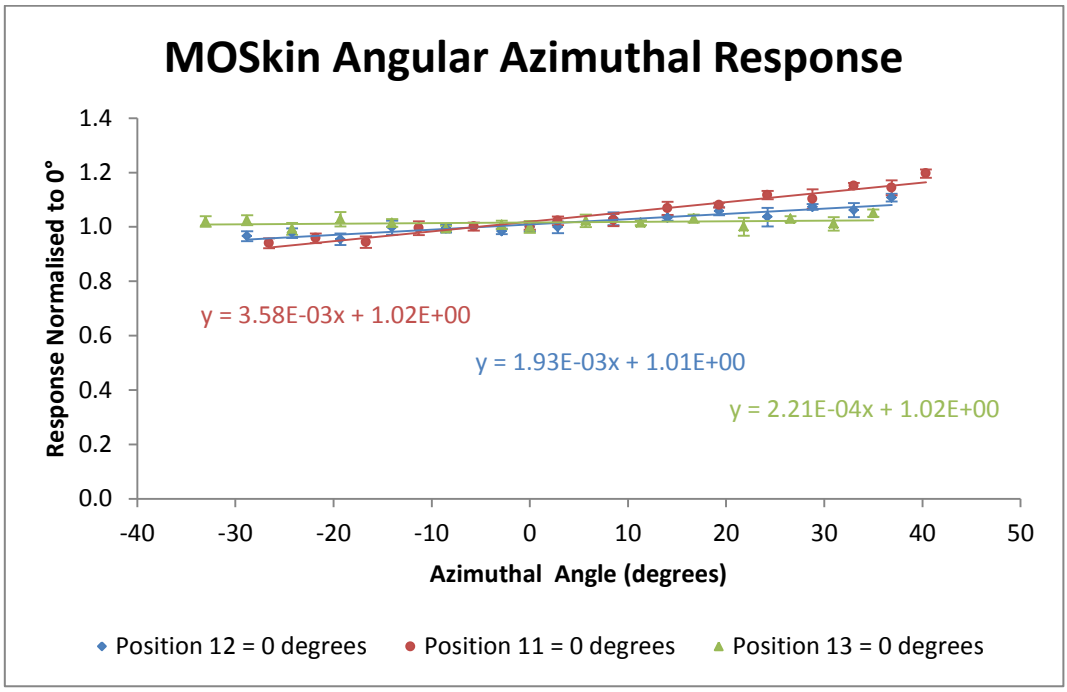

Figure 4.22 Azimuthal angular response of the MOSkins corrected for the cases where dwell position 11, position 12 and position 13 are considered to coincide with the perpendicular bisector of the detector, the error bars represent the standard deviation of the mean of the measurements at each angle summed in quadrature with the standard deviation of the mean stability. Also shown are linear equations of best fit.

From Figure 4.22 it can be seen that if the measurements are corrected for dose assuming dwell position 11 is considered the perpendicular bisector of the detector then a greater increase in response is seen for positive angles. If the measurements are corrected for dose assuming dwell position 13 is considered the perpendicular bisector of the detector then a smaller increase in response is seen for positive angles. Indicating that dwell position 13 is

closest to aligning will the true perpendicular bisector of the detector for the MOSkin inside the cylindrical phantom.

Normalised measurements taken with the ion chamber to determine the dwell position closest to the perpendicular bisector of the detector are shown in Figure 4.23. A second order polynomial equation has been fit to the points and is also shown.

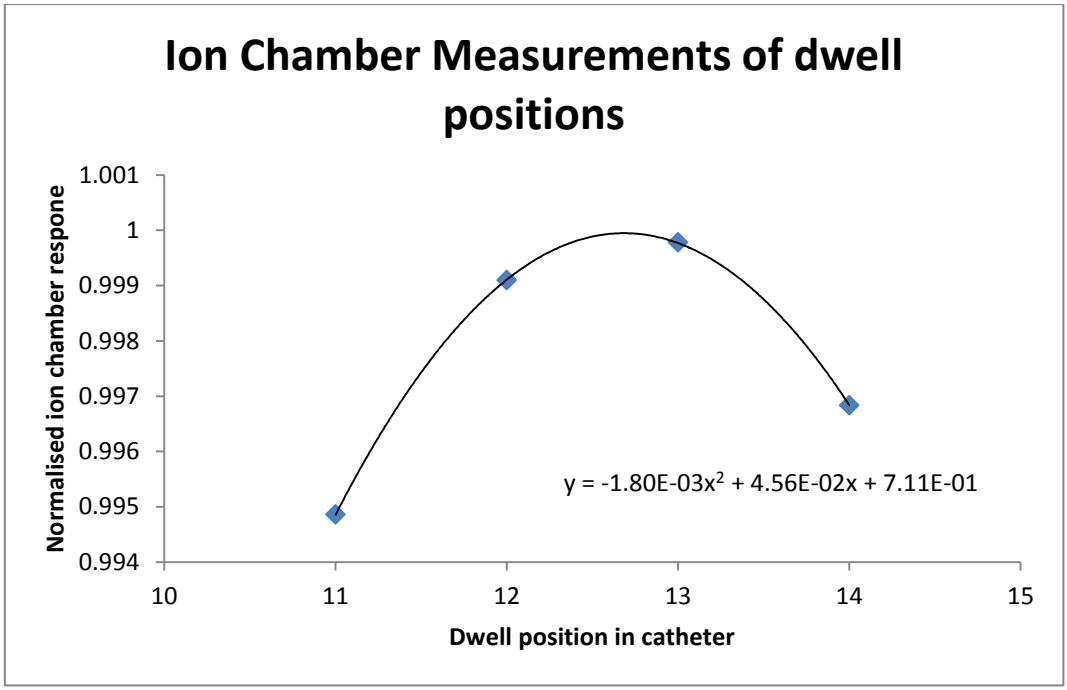

Figure 4.23 Ion chamber measurements made using the cylindrical PMMA phantom and the Ir-192 source plotted as a function of source dwell position. Also shown is a 2nd order polynomial equation of best fit.

According to the second order polynomial equation the maximum response of the ionisation chamber occurs between dwell position 12 and dwell position 13, at position 12.67. Figure 4.24 shows the azimuthal angular response measurements corrected for dose assuming that position 12.67 coincides with the perpendicular bisector of the detector.

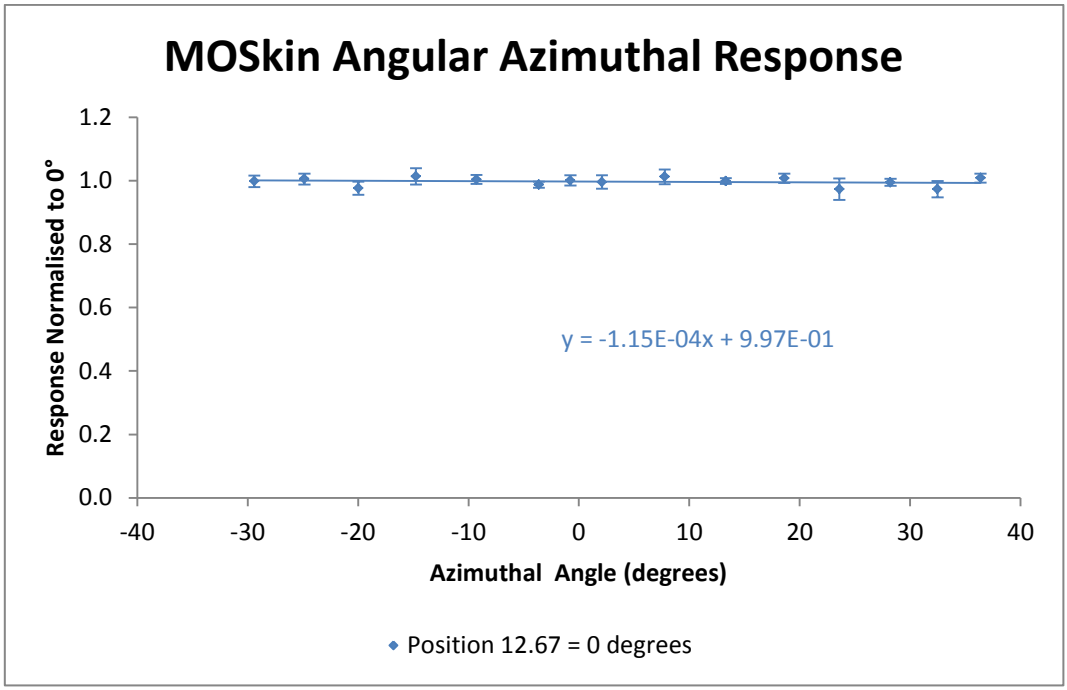

Figure 4.24 MOSkin azimuthal angular response measurements corrected for position 12.67 coinciding with the perpendicular bisector of the detector, the error bars represent the standard deviation of the mean of the measurements at each angle summed in quadrature with the standard deviation of the mean stability. The average size of the error bars was 1.8%. Also shown is a linear equation of best fit.

The maximum over response of 1.4% occurred at -14.8° and the maximum under response of 2.7% occurred at 23.6°. The average size of the error bars was 1.8%.

Another possible explanation for the increase in response seen for positive angles is that scatter radiation from the MOSkin ribbon is contributing to the dose and hence response. This would mean that for all source positions that are higher up in the catheter than the end tip of the MOSkin there would be additional scattered radiation contributing to the dose, as shown in Figure 4.25. This would also lead to an increase in response in positive angles.

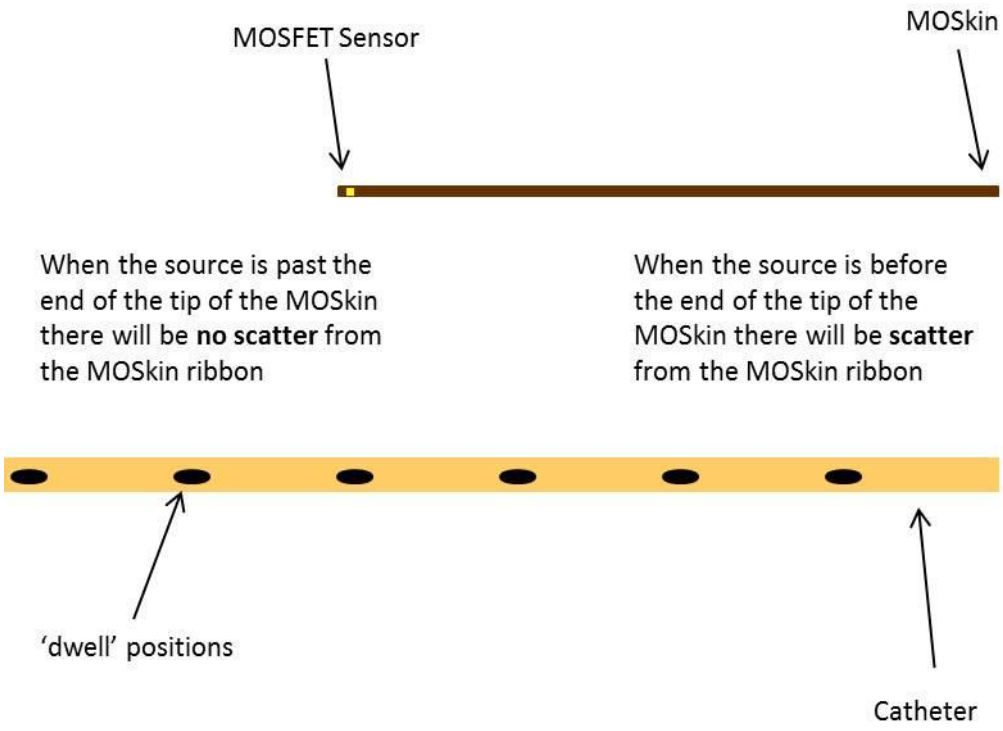

Figure 4.25 Diagram of MOSkin detector in relation to source positions in the catheter when using the cylindrical PMMA phantom and the Ir-192 source, in relevance to scatter from the MOSkin ribbon.

4.4.5 Energy Response

The energy response was determined by irradiating the MOSkins to a dose between 0.5 Gy and 1.0 Gy over the range of energies 15.7 keV to 18 MV. Responses normalised to the response at 6 MV are shown Figure 4.26. Each point represents the average of three measurements normalised to the response at 2000 keV. The error bars represent the standard deviation of the mean normalised to the response at 2000 keV summed in quadrature with the standard deviation of the mean stability, the average error bar size is 2.3%. The response showed an increase for lower energies with a maximum over response of 4.7 times the response relative to 6 MV at 20 keV. Also shown is an equation of best fit as described by Kron et al[34]. The equation takes the form of Equation 4.8.

$$Response = \{1 - e^{[-\alpha_1(E-E_1)]}\}[1 + \frac{\alpha_2}{(E-E_2)^3}]$$ Equation 4.8.

$Where\ \alpha_1\ and\ \alpha_2$ $are\ fitting\ parameters\ which\ determine\ the\ importance\ of\ exponential\ fall\ off\ towards\ low\ energies$

$E_1\ and\ E_2$ $allow\ for\ an\ energy\ shift\ for\ the\ two\ components$

The values obtained using MATLAB for the parameters were,

$\alpha_{1=} 4.57 \times 10^{-2}$ $E_1 = 2.98 \times 10^0$

$\alpha_2 = 2.15 \times 10^6$ $E_2 = -4.51 \times 10^1$

This equation indicates that the maximum over response of 4.74 times the response relative to 6 MV occurs at 19 keV. This equation can be used to calculate the response at any energy.

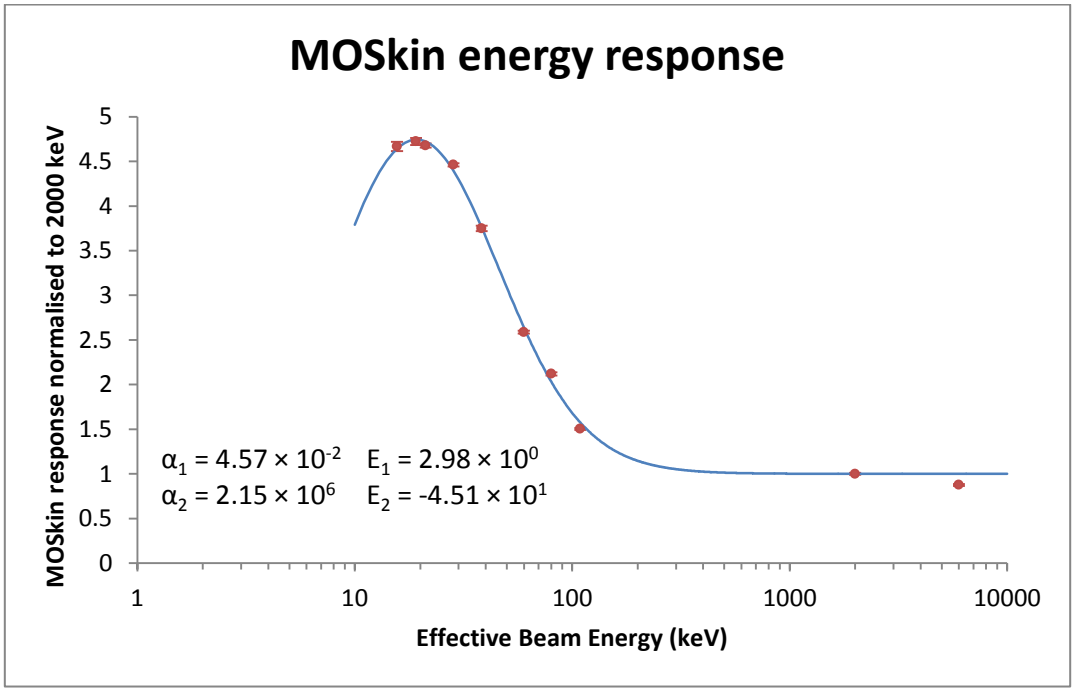

Figure 4.26 MOSkin energy response plotted as a function of effective energy, the error bars represent the standard deviation of the mean of the measurements at each energy summed in quadrature with the standard deviation of the mean stability. The average size of the error bars is 2.3%. Also shown is line representing Equation 4.8 and values for the parameters of the equation.

4.4.6 Dose Rate Response

The dose rate response was measured by irradiating 4 MOSkins using the 6 MV linac. Six different dose rates were achieved by irradiating the MOSkins at six different depths in PTW RW3. Each measurement was then normalised to a dose of 1 Gy. The measurements for the four MOSkins were then averaged for each dose rate, as shown in Figure 4.27. The error bars represent the average of the standard deviation of the mean for the three measurements summed in quadrature with the standard deviation of the mean stability. The average error bar size was 2.9 mV or 1.1%.

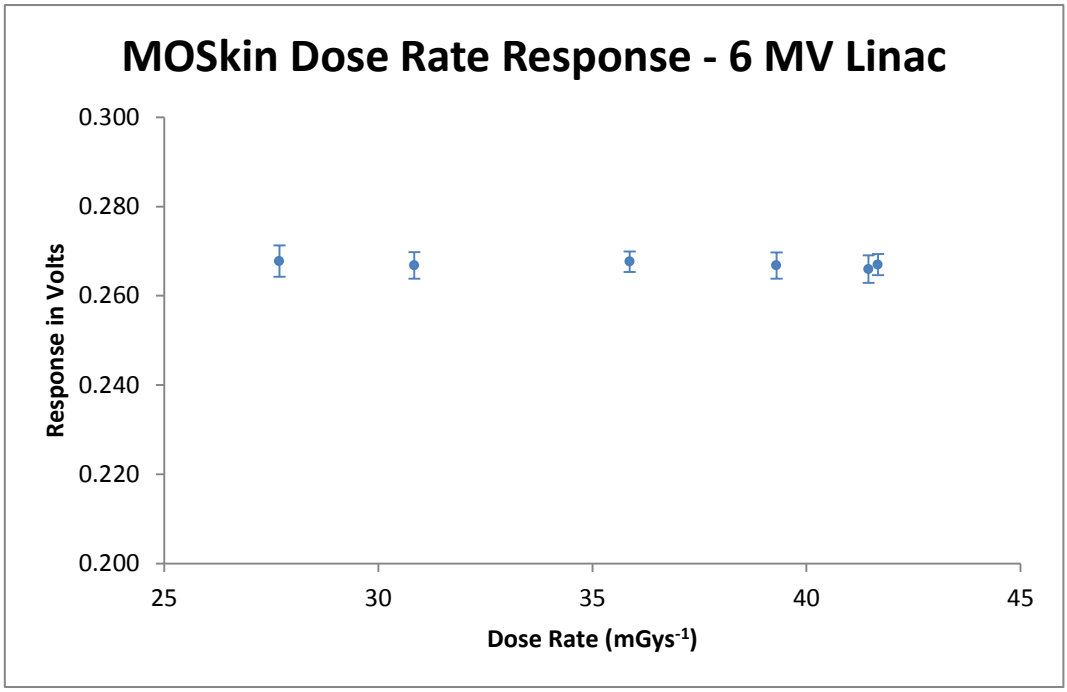

Figure 4.27 MOSkin dose rate response as measured using the 6 MV linac beam, the error bars represent the standard deviation of the mean of the measurements at each dose rate summed in quadrature with the standard deviation of the mean stability. The average size of the error bars was 1.1%.

The dose rate response of the MOSkins does not exceed the range defined by the error bars for this range of dose rates.

The dose rate response was also measured using the Ir-192 source and the IOBT applicator. Six different dose rates were achieved by irradiating the MOSkins through different depths of PTW RW3 using the Ir-192 source. As the effective energy of the spectrum from the Ir-192

source decreases with increased depth, the results were also corrected for energy response. The measurements from two MOSkins were then averaged for each dose rate, as shown in Figure 4.28. At short distances from the Ir-192 source there is a steep dose gradient. The uncertainty in the delivered dose that would result from an error of 0.1 mm in the source to detector distance was calculated using the data tables described by Daskalov et al[39]. This uncertainty was largest for the measurement position closest to the source (69.44 mGy^{-1}). The error bars in Figure 4.28 represent the average of the standard deviation of the mean for the three measurements summed in quadrature with the uncertainty in dose that would result from a ± 0.1 mm error in the source detector distance. The error bars range in size from 8.8 mV to 68.6 mV, or 3.3% to 20.8%, with an average error bar size of 20.2 mV or 6.6%. The average size of the error bars excluding dose rate 69.44 $mGys^{-1}$ was 3.8%.

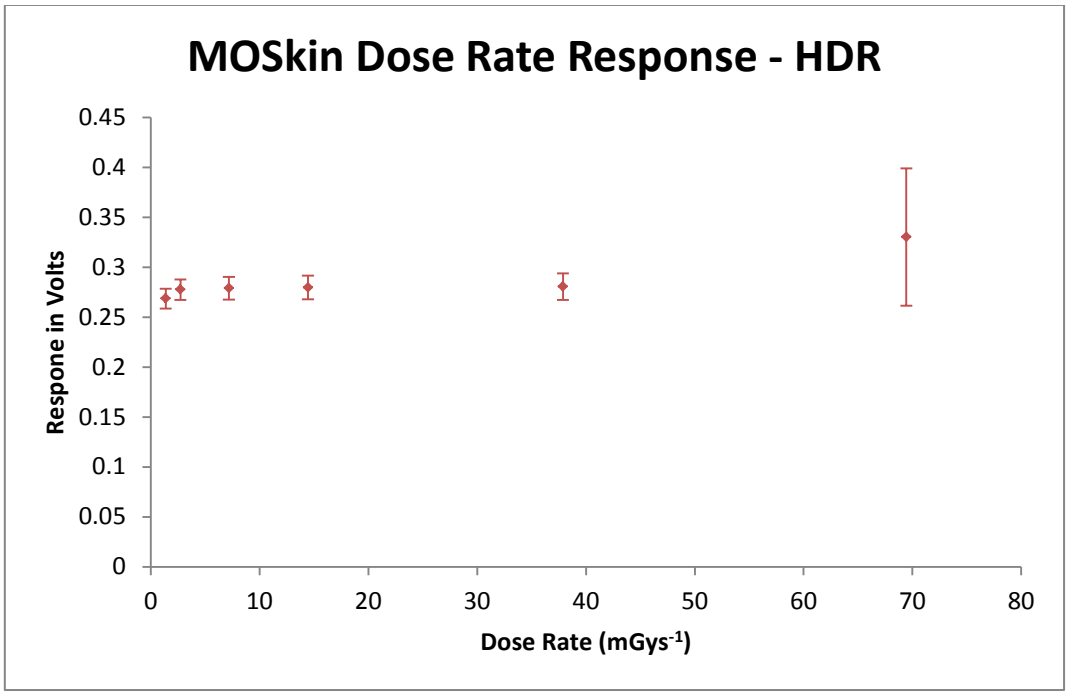

Figure 4.28 MOSkin dose rate response as measured using Ir-192, the error bars represent the standard deviation of the mean of the measurements at each dose rate summed in quadrature with the standard deviation of the mean stability and an uncertainty in dose from source to detector distance.

The dose rate response of the MOSkins does not exceed the range defined by the error bars for this range of dose rates.

4.4.7 Temperature Response

The temperature response was measured using four MOSkins at two temperatures. The first temperature of 38°C is comparable to normal body temperature and the second temperature of 22°C is comparable to ambient temperature in the operating theatre used at the Peter MacCallum Cancer Centre. Each MOSkin was put in the phantom 120 seconds prior to irradiation in order for thermal equilibrium to be reached. The results are shown in Figure 4.29.

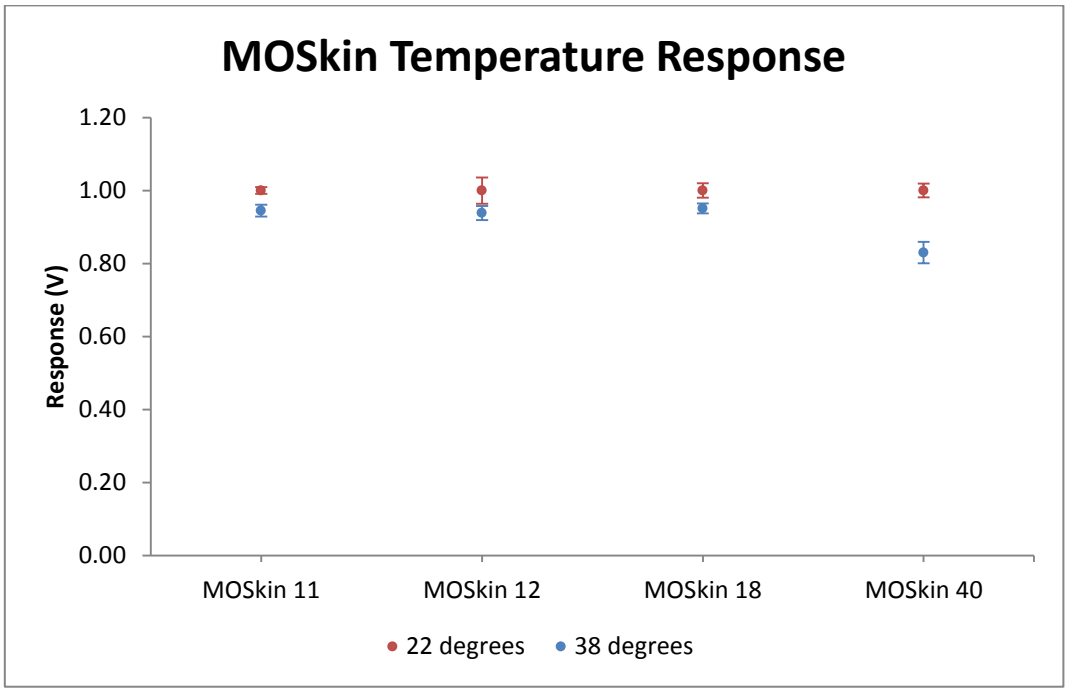

Figure 4.29 Temperature response of four MOSkin detectors measured at 22°C and 38°C, the error bars represent the standard deviation of the mean of the measurements at each temperature summed in quadrature with the standard deviation of the mean stability. The average size of the error bars was 2.1% for 22°C and 2.0% for 38°C.

The response of the MOSkins at 22°C is consistently higher than the response at 38°C. MOSkin 40 recorded the largest difference of 17.0% between the two temperatures. It should be noted that this MOSkin differed in design from all others by a lack of kapton layer above the MOSFET chip. The maximum variation in response of the other three MOSkins was 6.2%. The error bars represent the standard deviation of the mean of the two measurements normalised to the response at 22°C summed in quadrature with the standard deviation of the mean of the

stability. The average error bar size for 22°C was 2.1% and for 38°C was 2.0 %. The error bars do not account for the difference in response of the MOSkins at the two different temperatures indicating there is a relationship between response and temperature. Figure 4.30 shows the average response of MOSkin 11, 12 and 18 as a function of temperature. The error bars represent the average value of the error bars for MOSkins 11, 12 and 18 in Figure 4.29 (1.9%).

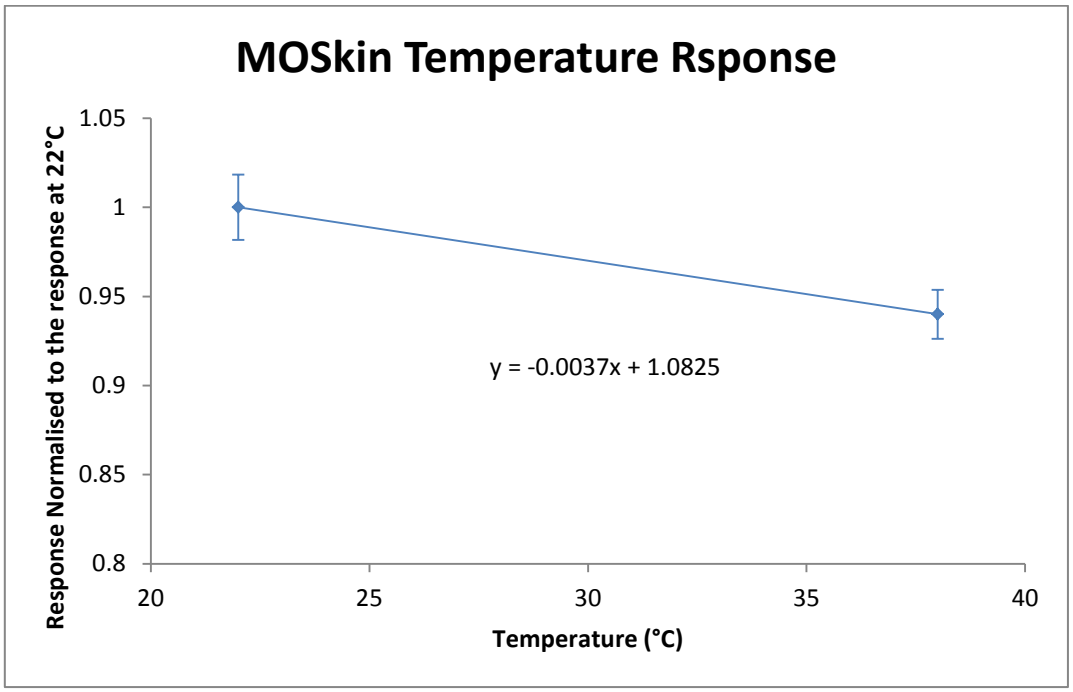

Figure 4.30 The average temperature response of MOSkins 11, 12 and 18 plotted as a function of temperature, the error bars represent the average error bar size for the three MOSkins as shown in Figure 4.27 (1.9%). Also shown is a linear equation of best fit.

Figure 4.30 indicates that between 22°C and 38°C the response of the MOSkin decreases by 0.37% per 1°C temperature increase. This translates to a 6.0% variation in response over a 16°C range.

4.4.8 dual MOSkin Angular Response

The angular response of the dual MOSkins was measured in both the radial and azimuthal direction. All measurements made with dual MOSkins were corrected for accumulated dose response using the same method used for the single MOSkins (see Section 4.4.1).

4.4.8.1 dual MOSkin Radial Angular Response

In the radial direction three measurements were made at each angular position. The three measurements were then averaged to give a single value for each angle. The maximum response of the dual MOSkin occurred at 0° so an offset in the position of the dual MOSkin slit inside the dual MOSkin holder was not considered.

The radial angular response of the dual MOSkin is shown in Figure 4.31. The error bars represent the standard deviation of the mean of the three measurements summed in quadrature with the standard deviation of the mean stability. The average error bar size was 1.6%.

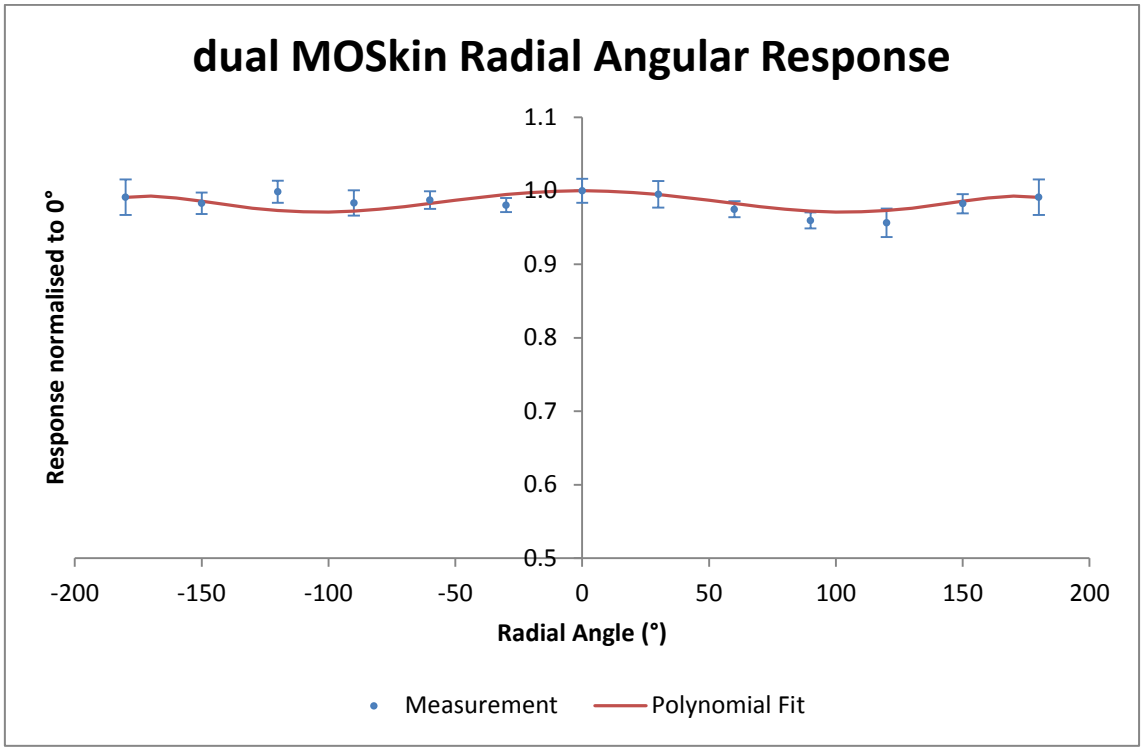

Figure 4.31 dual MOSkin radial angular response as measured using the cylindrical PMMA phantom and the Ir-192 source, the error bars represent the standard deviation of the mean of the measurements at each angle summed in quadrature with the standard deviation of the mean stability. The average size of the error bars was 1.6%. Also shown is a line representing Equation 4.10, the polynomial fit to the measurement points. Note the truncated vertical axis.

Also shown in Figure 4.31 is a line of best fit in the form of an even 6th order polynomial equation. This equation is shown by Equation 4.9 and can be used to calculate the angular response at any angle.

$$Response = -6.51 \times 10^{-15}x^6 + 3.93 \times 10^{-10}x^4 - 6.18 \times 10^{-6}x^2 + 1.00 \quad \text{Equation 4.9.}$$

$$Where\ x\ is\ the\ radial\ angle\ in\ degrees$$

According to the polynomial fit the maximum under response of 2.9% occurs at 104°. The variation in response for changing radial angles is reduced by a factor of 6 in comparison to the single MOSkin.

The accuracy of the angle of incidence between source and detector will be different for each experimental set up, if a conservative degree of error of ± 5° is assumed, the uncertainty in the response of the MOSkin will be 0.5%.

4.4.8.2 *dual MOSkin Azimuthal Angular Response*

The azimuthal angular response measurements were normalised for dose according to source detector distance using the tables described by Daskalov et al[39], then normalised to the response at 0°. Figure 4.32 shows the MOSkin response to azimuthal angular direction for the initial choice of Ir-192 source position in the catheter corresponding to the perpendicular bisector of the detector (dwell position 12). Each point represents the average of three measurements with the error bars representing the standard deviation of the mean of the three measurements summed in quadrature with the standard deviation of the mean stability.

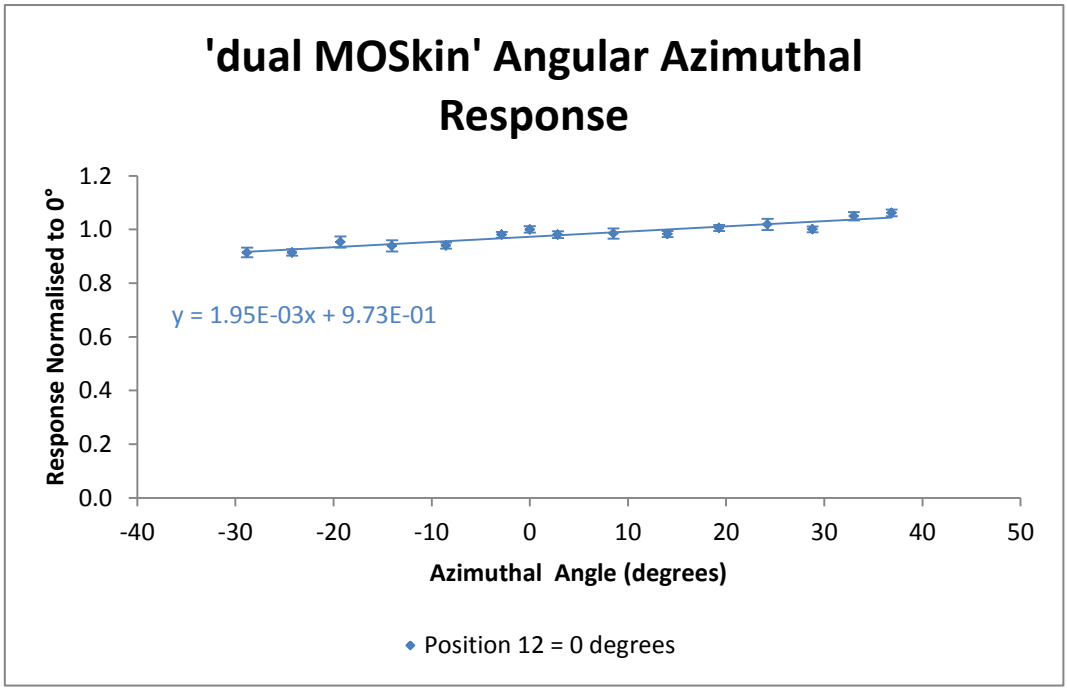

Figure 4.32 The azimuthal angular response of the dual MOSkins as measured using the cylindrical PMMA phantom and the Ir-192 source, the error bars represent the standard deviation of the mean of the measurements at each angle summed in quadrature with the standard deviation of the mean stability. The average size of the error bars is 1.5%. Also shown is a linear equation of best fit.

A line of best fit to the measurement points produces a linear equation with a positive gradient, similarly to the response of the single MOSkin for this choice of dwell position coinciding with the perpendicular bisector of the detector. Using the same method as for the single MOSkin (see Section 4.4.4), the measurements were also normalised for dose to the

cases where the dwell positions immediately either side of position 12 actually coincide with the perpendicular bisector of the detector, this is shown in Figure 4.33.

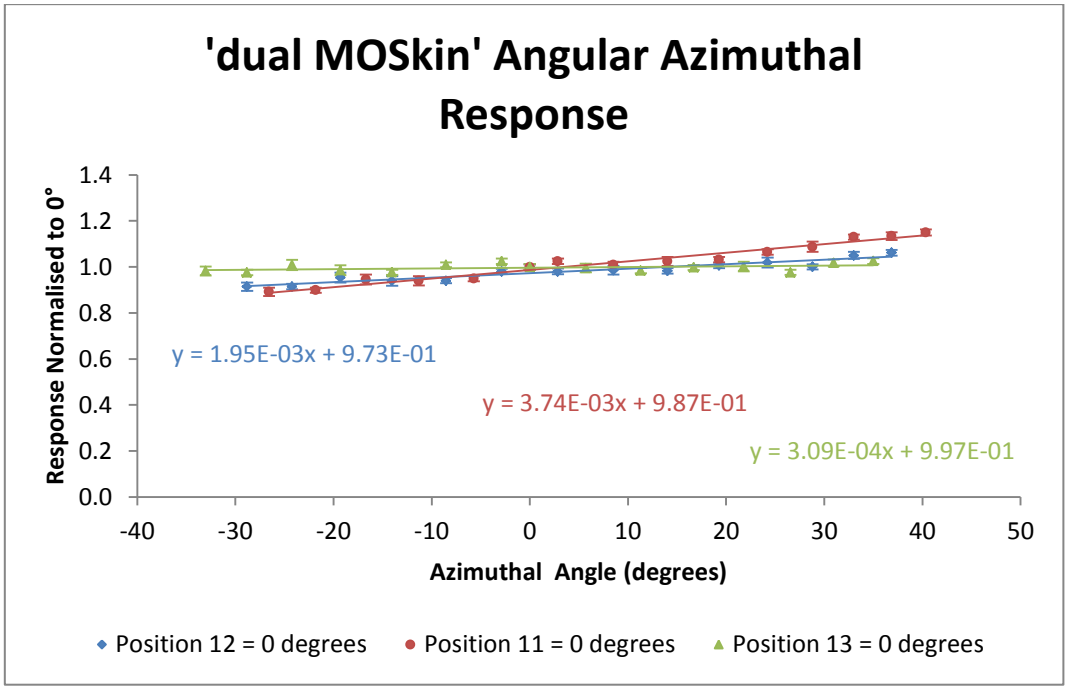

Figure 4.33 Azimuthal angular response of the dual MOSkins corrected for the cases where position 11, position 12 and position 13 are considered to coincide with the perpendicular bisector of the detector, the error bars represent the standard deviation of the mean of the measurements at each angle summed in quadrature with the standard deviation of the stability. Also shown are linear equations of best fit.

Figure 4.33 indicates that the measurements corrected for dose for the case where dwell position 13 coincides with the perpendicular bisector of the detector produces a line of best fit with the lowest gradient. According to the ion chamber measurements the position in the catheter that corresponded to the perpendicular bisector of the detector was 12.67 (between position 12 and 13), the results corrected for this case are shown in Figure 4.34.

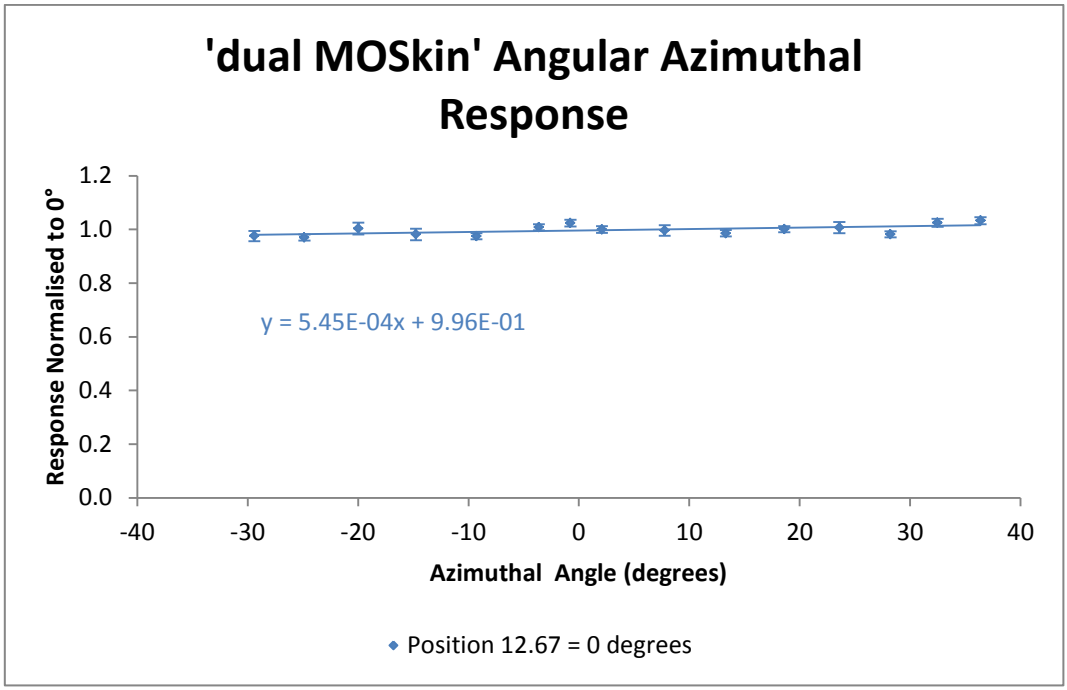

Figure 4.34 dual MOSkin azimuthal angular response measurements corrected for position 12.67 coinciding with the perpendicular bisector of the detector, the error bars represent the standard deviation of the mean of the measurements at each angle summed din quadrature with the standard deviation of the mean stability. The average size of the error bars is 1.5%. Also shown is a linear equation of best fit

The line of best fit produced for position 12.67 coinciding with the perpendicular bisector of the detector produces a larger gradient than for the case when position 13 coincides with the perpendicular bisector of the detector. This indicates that position 13 is the better choice for coinciding with the perpendicular bisector of the detector, which is a variation from the single MOSkin result. This variation may in part be due to the position of the MOSFET chip on the substrate being slightly different for each MOSkin. The distance from the end of the MOSkin ribbon to the centre of the MOSFET chip was determined for 10 single MOSkins (see Figure 4.35). The distance from the centre of the MOSFET chip to the end of the MOSkin ribbon ranged from 2.5 mm to 3.0 mm. The average distance was 2.75 ± 0.16 mm (1 SD). The physical difference between dwell position 12.67 and dwell position 13 is a distance of 0.83 mm, slightly more than the variation in the position of the detector on the ribbon.

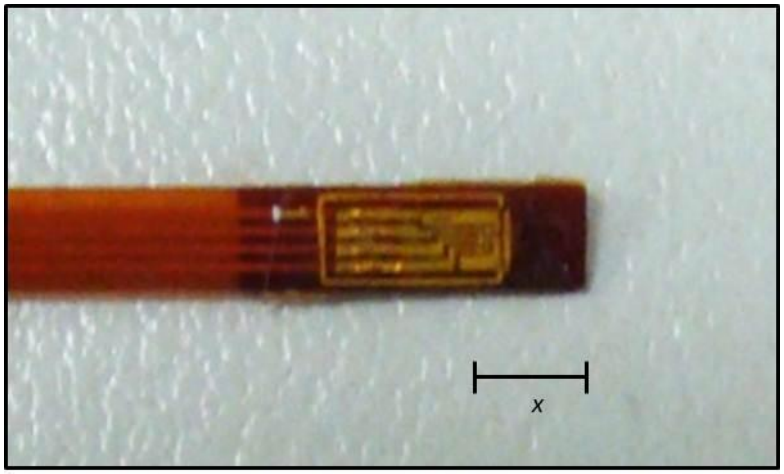

x, in (mm), is the distance from the centre of the MOSFET chip to the end of the MOSkin ribbon

Figure 4.35 Photograph of the MOSkin showing a close up of the MOSFET chip and the distance from the centre of the MOSFET chip to the end of the MOSkin ribbon.

Assuming dwell position 13 coincides with the perpendicular bisector of the detector, the maximum over response of 2.5% occurs at -2.9° and the maximum under response of 2.4% occurs at 26.6°. The average size of the error bars was 1.5%.

4.5 Discussion

4.5.1 Accumulated Dose Response

The response of the MOSkins to accumulated dose for 6 MV radiation indicated a low second order polynomial relationship. This is similar to the findings of Cheung et al[33], who also observed a decreasing response in the form of a low second order polynomial equation when examining an older style MOSFET detector also produced by the CMRP at the UoW. Cheung et al[33], also found that the accumulated dose response was related to the energy of the radiation used. They found that the ratios of the approximate gradients of the accumulated dose response related to the ratios of the energy response of the MOSFET detector. They measured the accumulated dose response for three beam energies and found that the greater the effective energy of the radiation, the smaller the decrease in response to accumulated dose. If the MOSkins used in this project were to behave similarly the gradient of the accumulated dose response with Ir-192 radiation should be steeper than for 6 MV radiation. For 6 MV radiation a decrease in response of approximately 0.340% per Gy was observed and for Ir-192 a decrease in response of approximately 0.342% was observed. These values are very similar, indicating negligible difference in response to accumulated dose between 6 MV radiation and Ir-192 radiation. The magnitude of the response is also greater than that observed by Cheung et al, who measured a decrease in response of 0.0013% per Gy for 6 MV radiation and 0.002% for 250 keV radiation[33]. The MOSFETs used by Cheung et al were manufactured by the CMRP, UoW, but they were not the same model/style of MOSFET as used in this project.

4.5.2 Stability

The threshold voltage varied by an average of 1.9 ± 1.1 mV (1 SD) in the absence of dose. For a dose of 1 Gy, which involves a threshold voltage change of approximately 373 mV this translates to an uncertainty of 1.3%, but for a dose of 0.25 Gy which involves a voltage change

of approximately 96 mV this translates to an uncertainty of 5.3% which cannot be considered negligible. The standard deviation of the mean of repeated readings in the presence of dose were found to vary by 0.9%, which is higher than for other MOSFET devices produced by the same manufacturer for which a standard deviation of 0.4% was reported[60]. However, it is in agreement with other MOSFET devices produced by other manufacturers for which a 1.0-2.0% (1 SD) variation in response for reproducibility has been reported[30, 32]. It has been suggested that the greater variability in our measurements, in comparison to other UoW MOSFET devices, could be the due to our CSDS reader as all readers are individually assembled (personal correspondence, D. Cutajar, UoW).

4.5.3 Linearity

The MOSkins were found to be linear with dose between 0.5 Gy and 5 Gy, which is consistent with previous findings of other MOSFET devices[32, 33, 60]. While this does not cover the entire range of typical single fraction doses in brachytherapy (potentially up to 12 Gy per fraction[36]), it does cover all subsequent measurements made for this project. Measurements with doses higher than 5 Gy were not made due to the limited life of the MOSkins and finite number provided for this project.

4.5.4 Angular Response

4.5.4.1 Radial Angular Response

In the radial direction the response of the MOSkins, with a simple spatial offset correction applied, displayed a decreasing response with angle as the angle moved away from 0^{o} in both directions. This is consistent with the physical shape of the MOSkin detector having a 'font' and a 'back', see Figure 4.1. With the spatial offset correction, the maximum response of the detector occurred at 0° and the maximum under response of 19.0% of the detector occurred at ± 156°. The uncertainty due to an error in angle of ± 5° is 2.1%.

4.5.4.2 Azimuthal Angular Response

In the azimuthal direction the angular response was measured over the range of angles -29.4^{o} to +36.4^{o}. All measurements were found to be within -2.7% to 1.4% of the 0^{o} measurement, which is similar with the findings of Kwan et al[13] who tested the azimuthal angular response of another MOSkin device also manufactured by the CMRP, UoW, and found all measurements to be within ± 2.0%. One possible explanation for the initial increase in response seen for positive angles is the incorrect choice of source dwell position coinciding with the perpendicular bisector of the detector. By re normalising the measurements to dose assuming a position between dwell positions coincides with the perpendicular bisector of the detector the increase in response seen for increasing angle was minimised. Another possible explanation for the increase in response seen for positive angles is that scattered radiation from the 'ribbon' of the MOSkin is contributing to the dose. The range of angles measured in the azimuthal direction was much smaller than measured in the radial direction. A larger response would be expected for larger angles, particularly for + 90^{o} where the radiation would be incident on the connection end of the MOSkin. Such measurements were not carried out due to the limitations of the physical design of the phantom.

4.5.5 Energy Response

The MOSkins display an increased response for low energy x-rays, indicating that the response of the MOSkin will increase as a function of depth in water for Ir-192 radiation. The maximum over response of 4.7 times relative the response at 6 MV occurred at the effective energy of 19 keV. Previous examinations of other MOSFET devices have found the maximum over response to occur at higher energies. Kron et al[34], observed a maximum over response of 7 times the response at 6 MV at 35 kV and Cheung et al[33], observed a maximum over response of 3.2 times the response at 6 MV at 75 kV, both using older style MOSFETs also manufactured by the CMRP, UoW. The older style of MOSFETs in these two studies used the 'epoxy bubble' design

which gives the detectors a deeper equivalent detection depth. The epoxy bubble acts as a filter for low energy x-rays[34]. The increased sensitivity of the MOSkin to lower energy x-rays in comparison could be explained by the absence of this epoxy bubble.

4.5.6 Dose Rate Response

No significant variation in response (<0.4%) was observed across the range of dose rates measured using 6 MV radiation, which is consistent with previous findings using other MOSFET detectors[32, 37, 38]. While the response measured using Ir-192 radiation did show some variation (up to 44.3 mV or 17.4%), the uncertainty due to dose meant that all results were consistent within experimental uncertainty.

4.5.7 Temperature Response

The measurements indicated the response of the MOSkins decreased with increasing temperature. Between 22°C and 38°C the response varied by 6.0 %, which is larger than the variation in response reported by Ramaseshan et al[32], and Ramani et al[30], who both reported variations of between 0.5% and 3.0% over the temperature range 20°C to 40°C. The larger difference in response seen in MOSkin 40 may be explained by the lack of kapton covering on the MOSFET chip. This kapton covering provides a layer of insulation, when this insulation is removed the MOSFET chip is exposed to the full extent of the temperature variation. Cheung et al[40], found that a wait period of 60 seconds was adequate for CMRP, UoW, MOSFETs to reach thermal equilibrium when placed on a patient's skin. It is possible that in the absence of this insulating layer the wait time used of 120 seconds was not adequate for the MOSkin to reach thermal equilibrium. Cheung et al[33], also suggest that in vivo readings using MOSFETs be made after the MOSFET has been removed from the patient and returned to the same temperature as the threshold voltage reading to minimise the uncertainty due to temperature effects. The response of MOSkins to changes in temperature is an important consideration for in vivo dosimetry where the detectors could be placed directly on the

patient's skin or inside the patient's body, however, for our measurements with the IOBT applicator it was not relevant.

4.5.8 dual MOSkins

4.5.8.1 dual MOSkin Radial Angular Resposne

In the radial direction, the response of the dual MOSkin varied by a total of 2.9%. This is reduced by a factor of six from the variation than observed for the single MOSkin of 19.0%. The uncertainty due to an error in angle of ± 5° is 0.5%.

4.5.8.2 dual MOSkin Azimuthal Angular Response

In the azimuthal direction the variation in response of the 'dual MOSkin' was in fact larger than that observed for the single MOSkin. As stated earlier, the range of angles measured in the azimuthal direction was considerably smaller than that measured in the radial direction. It is possible that a smaller variation in response, compared to the single MOSkin, would be observed if a full 360° range of angles were measured, thus including angles that resulted in the MOSFET chip being perpendicular to the source.

4.5.9 Summary of Results

Single MOSkin		
Dosimetric Characteristic	**Standard Uncertainty**	**Explanation**
Accumulated Dose	0.340 % per Gy for 6 MV 0.342% per Gy for Ir-192	A correction factor should be applied to all raw measurements
Stability	0.9%	The average standard deviation of the mean from the ten MOSkins measured
Linearity	1.4%	The average standard deviation of the mean from the four dose measurements
Radial Angular Response	Polynomial fit to calculate the response at any angle 2.1%	A correction factor can be applied if the angle is known. The uncertainty that would result from an error of ± 5° in angle
Azimuthal Angular Response	2.1%	The average variation of measurements over the range -29.4° to +36.4°
Energy Response	Equation of fit to calculate the response at any energy 2.3 %	A correction factor can be applied if the energy is known The standard deviation of the mean measurements from the ten energies measured
Dose Rate Response	1.0 % 6MV 3.8 % Ir-192	The average standard deviation of the mean measurements from the six dose rates measured
Temperature Response	0.37% per degree increase from 22°C to 38°C 2.0%	A correction factor can be applied if the change in energy is known The average standard deviation of the mean measurements for the two temperatures measured
Total Uncertainty	**5.9%**	**(1 SD)**

Table 4.2 Summary of the measured MOSkin dosimetric characteristics and standard uncertainties.

dual MOSkin		
Dosimetric Characteristic	**Uncertainty**	**Comment**
Radial Angular Response	Polynomial fit to calculate the response at any angle 0.5%	Can be applied as a correction factor if the angle is known The average standard deviation of the mean measurements from all angles
Azimuthal Angular Response	2.5%	The average variation of measurements over the range -33.0° to +35.0°
Total Uncertainty from Angular Response	**2.6%**	**(1 SD)**

Table 4.3 Summary of the measured dual MOSkin dosimetric characteristics and standard uncertainties.

4.6 Conclusion

For the single MOSkin the factors that will contribute most to variation in response are the accumulated dose response, radial angular response and energy response. A correction can be made to account for each of these assuming the conditions under which the measurement was made are known. For the dual MOSkin, for the purpose of convenience, the radial angular response may be reduced to a single value for uncertainty rather than a value calculated for each individual angle.

5 Intra-Operative Brachytherapy Measurements

The work contained in this chapter is based on the following publication, 'Lack of backscatter factor measurements in HDR applications with MOSkins', Australas Phys Eng Sci Med, 2011, Vol.34, No.4 34:545–552 [61], Appendix A.

5.1 Introduction

Intra-Operative Brachytherapy, or IOBT, is brachytherapy of the tumour or tumour bed during surgery. The main advantage of IOBT is that the tumour or tumour bed is exposed during surgery so catheter placement can be more precise than methods where any image guidance is external and frequently post catheter insertion. One use of IOBT is in the treatment of locally advanced rectal tumours in conjunction with chemotherapy and EBRT. In these cases the tumour is first excised then an IOBT applicator is placed on the tumour bed. The dose of radiation is then delivered by stepping the radioactive source through a series of catheters in the applicator. The applicator is then removed and the surgery is completed.

With regard to treatment planning, two challenges have been identified with the IOBT treatments for rectal cancer at the Peter MacCallum Cancer Centre. The first is geometric identification of catheters relative to one another and the tumour bed. In other forms of brachytherapy, CT or orthogonal images are used to plan the treatment. As the catheters are placed and removed during the same surgery CT images are not practical as CT machines are generally located outside the sterile operating theatre. Additionally, reconstruction from orthogonal images is time consuming and not compatible with a small time gap between applicator placement and treatment delivery. Due to these constraints the best library plan, which is thought to best represent the in situ catheter geometry, is used. The second problem relates to a calculation approach made by the treatment planning system. The treatment

planning system Nucletron Plato Brachytherapy, (Version 14.3.2, Nucletron, Veenendaal, The Netherlands), algorithm assumes that the HDR Ir-192 source is completely surrounded by scatter material and calculates the dose accordingly. In reality this is not the case because while the patient's body provides scatter material below the applicator, above the applicator there is usually only air or a thin layer of wet gauze. This thin layer merely ensures the applicator remains in contact with the tumour bed and it would be impractical to apply a large amount of scattering bolus material in the sterile field. A lack of adequate scatter material above the applicator will lead to an over-estimation in delivered dose. The magnitude of this over-estimation in dose due to lack of backscatter was determined with TLD rods, MOSkins and dual MOSkins.

Current Treatment Planning Systems use a simplistic algorithm which assumes that all tissue is water equivalent with no heterogeneities. MOSkins are not tissue equivalent, so will not be correctly modelled by current Treatment Planning Systems. In the future Model Based Dosimetry Algorithms (MBDAs) may remove this limitation. MBDAs are currently under review by the American Association of Medical Physics (AAPM) with report TG-186 in progress.

5.2 Materials

The IOBT applicator was constructed at the Peter MacCallum Cancer Centre from Nucletron 6 French flexible plastic catheters and a water equivalent wafer material (Stomahesive, ConvaTec, Princeton, NJ, USA). The applicators are constructed from 100 mm × 100 mm × 2 mm wafer sheets. The catheters are spaced 10 mm apart starting 5 mm inside the wafer edge, with the tips of the catheters placed 3 mm inside the wafer edge. Two wafer sheets are placed below the catheters and one wafer is placed above the catheters. Once constructed the applicator has a total thickness of 7 mm.

The wafer sheets used to construct IOBT applicators at the Peter MacCallum Cancer Centre can be cut down from the maximum 100 mm × 100 mm to dimensions that are appropriate for individual treatments. The applicator used in this project had dimensions of 60 mm × 90 mm × 7 mm and contained six catheters, as shown in Figure 5.1.

a) b)

Figure 5.1 Photograph of the IOBT applicator used in this project a) top view, b) perspective view.

5.3 Methods

The dose delivered to the underside of the IOBT applicator was measured at five positions on the IOBT applicator, see Figure 5.2.

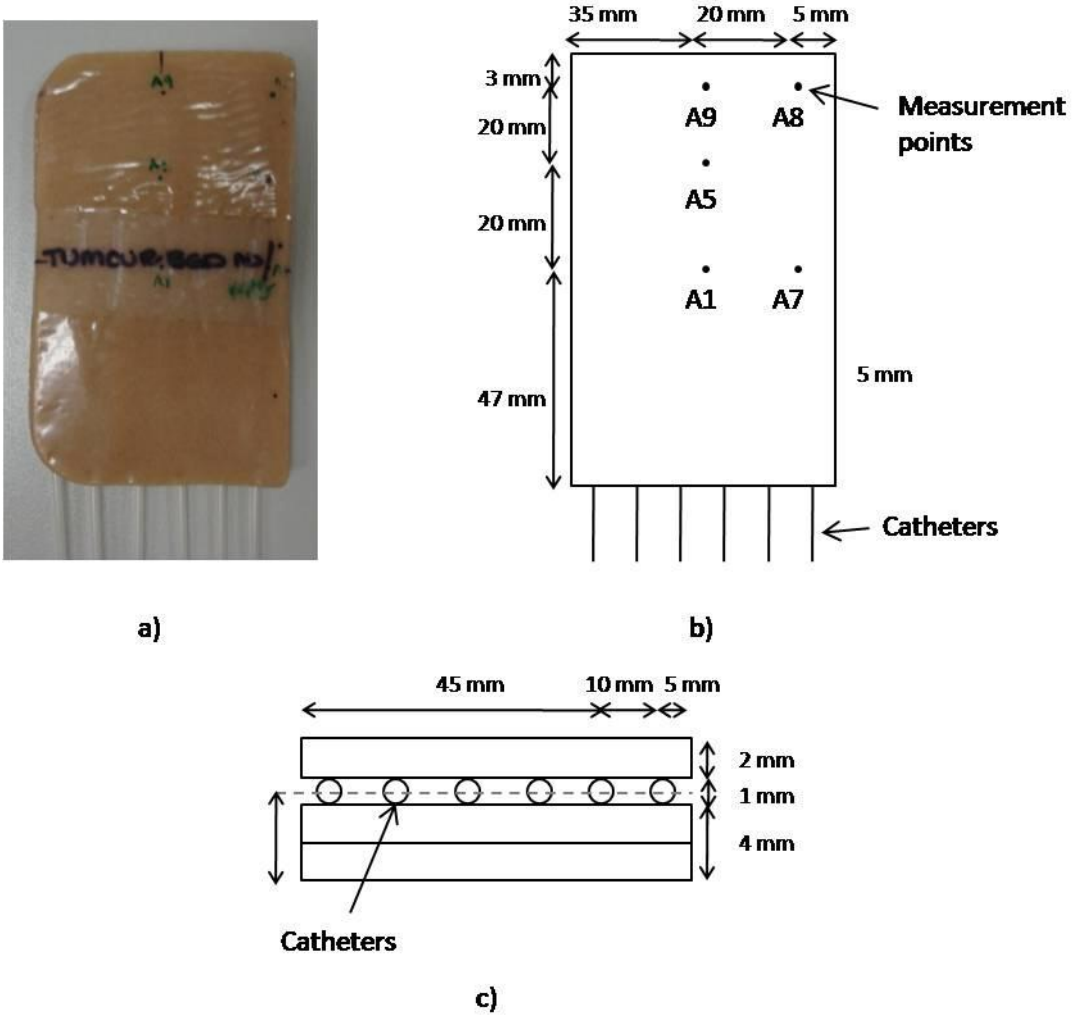

Figure 5.2 The five measurement positions on the IOBT applicator a) a photo of the five measurement positions marked on the underside of the applicator, b) a diagram of the applicator with the measurement positions marked, and c) cross section of the applicator.

Once constructed there is a 5 mm distance between the back of the applicator and the source position in the catheter, see Figure 5.2c.

The dose to the underside of the IOBT applicator was measured using TLD rods, MOSkins and dual MOSkins. The dose was measured in both the presence and absence of scatter material in the form of 80 mm of PTW RW3 slabs placed above the IOBT applicator.

The six catheters of the IOBT applicator were connected to six delivery tubes attached to the HDR unit containing the Ir-192 source. The applicator was placed on top of 10 mm of superflab material to prevent damage to the TLD rods, MOSkins and dual MOSkins. Below the superflab was 80 mm of PTW RW3 slabs. The TLD rods and MOSkins were attached directly to the underside of the applicator. Some wadded paper towel was used along the sides of the applicator to provide support for the PTW RW3 slabs placed above and to prevent the IOBT applicator from being compressed, as shown in Figure 5.3.

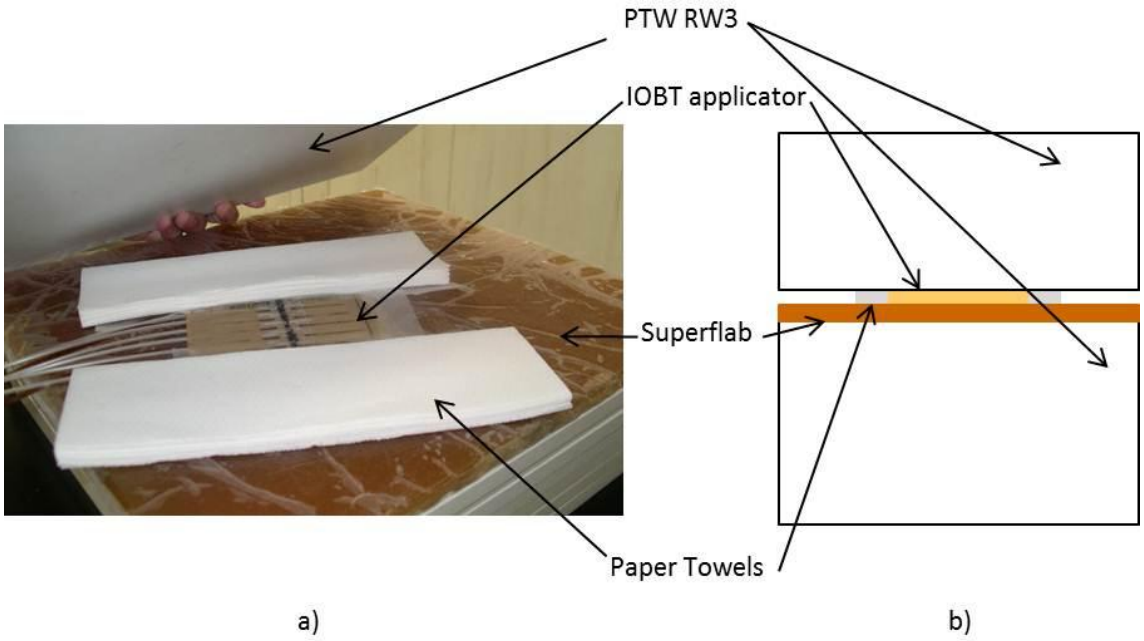

Figure 5.3 a) Photograph of the dose measurements with the IOBT applicator set up and b) diagram of set up showing applicator position, superflab, paper towels and PTW RW3 slabs.

A treatment plan was generated that would deliver a dose of 0.5 Gy to a plane parallel to the IOBT applicator at a distance of 5 mm below the IOBT applicator, the same distance the detectors would be placed.

5.3.1 Backscatter Factor

The backscatter factor for each measurement position was calculated using Equation 5.1.

$$Back\ Scatter\ Factor = \frac{Measurement\ with\ backscatter - Measurement\ without\ backscatter}{Measurement\ with\ backscatter} \times 100$$

Equation 5.1

5.3.2 TLD Measurements

Each TLD rod was first placed in a small plastic pocket. This was achieved by first thermally sealing the end of a thin plastic tube, inserting the TLD rod, then thermally sealing the other end and cutting the sealed pocket from the remaining plastic tube. This allowed the individual TLD rods to be labelled by writing on the plastic pockets.

A single TLD rod inside a plastic pocket was then taped directly to the underside of the IOBT applicator at each of the five measurement positions indicated in Figure 5.2b. The TLD rod packets were taped such that the long axis of the TLD rod was parallel to the long axis of the catheters, as shown in Figure 5.4. The measurements were repeated three times, each with one TLD rod at each measurement point. Measurements were made both with and without 80 mm of PTW RW3 slabs placed above the applicator as backscatter material. The treatment plan was used to deliver a dose of 0.5 Gy to 5 mm below the IOBT applicator, the same distance as the TLD rods. The measurements at each position with and without backscatter material were then averaged separately for each measurement position.

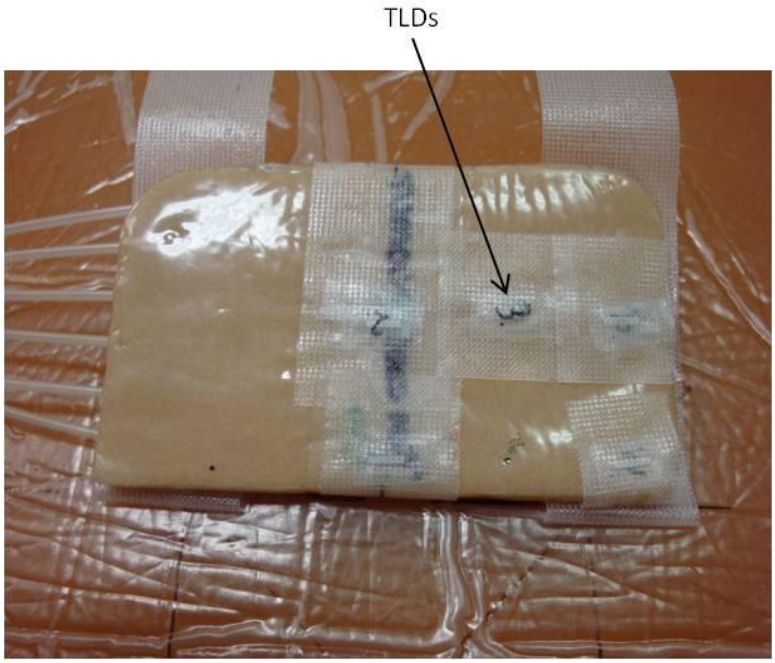

Figure 5.4 Photograph of TLD rods in individual plastic pockets taped to the underside of the IOBT applicator.

5.3.2.1 Uncertainty in TLD rod measurements

The uncertainty for each TLD rod measurement was calculated by summing in quadrature the individual uncertainty associated with each dosimetric characteristic and/or applying a correction factor where relevant.

The sensitivity, linearity, azimuthal angular response and dose rate response of the TLD rods was discussed in Section 3.4 of Chapter 3. The uncertainty associated with each of these dosimetric characteristics and how this uncertainty will be applied is summarised in Table 5.1.

Energy Response

The backscatter measurements with the IOBT applicator result in two different energy spectra from the Ir-192 source. At a depth of 5 mm in water, with full backscatter conditions, the spectrum of Ir-192 has an average energy of approximately 352 keV (D. Cutajar, personal correspondence) and a response factor of 1.014 relative to the 6 MV beam (see Section 3.5.4). The mean energy of the spectrum at a source to detector distance of 5 mm without 80 mm of

backscatter is unknown but we would expect the energy to be increased due to the absence of low energy scatter components. A conservative estimate of this increase would be a mean energy of 397 keV (which is the mean energy of Ir-192 in air). The response factor for an energy of 397 keV is 1.011, relative to the response at a 6 MV linac beam. A correction factor in the form of Equation 5.2 and 5.3 was applied to all measurements with and without backscatter respectively, to correct for the energy response of the TLD rods.

$$Energy\ Correction\ Factor_{with\ backscatter} = \frac{1}{Response\ at\ 352\ keV} = \frac{1}{1.014} = 0.986$$

Equation 5.2.

$$Energy\ Correction\ Factor_{without\ backscatter} = \frac{1}{Response\ at\ 397\ keV} = \frac{1}{1.011} = 0.989$$

Equation 5.3

5.3.3 MOSkin detector measurements

The MOSkins were taped directly to the underside of the IOBT applicator, as shown in Figure 5.5. At each of the five measurement positions a measurement was made with a single MOSkin for three separate treatment deliveries, both with and without 80 mm of PTW RW3 slabs as backscatter material. The three measurements at each position without backscatter material and with backscatter material were then corrected for accumulated dose response and averaged.

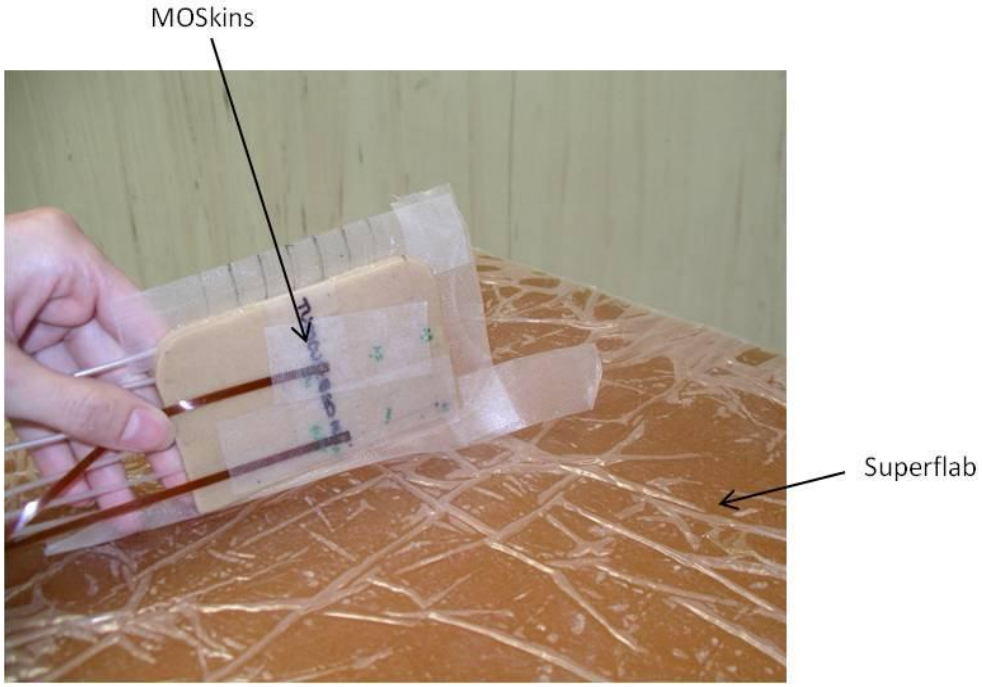

Figure 5.5 Photograph of two MOSkins taped to the underside of the IOBT applicator at measurement positions A1 and A7.

5.3.3.1 Uncertainty in MOSkin measurements

The uncertainty for each MOSkin measurement was calculated by summing in quadrature the individual uncertainty associated with each dosimetric characteristic and/or applying a correction factor where relevant.

The stability, linearity azimuthal angular response and dose rate response of the MOSkins was discussed in Section 4.4 of Chapter 4. The uncertainty associated with each of these dosimetric characteristics and how this uncertainty will be applied is summarised in Table 5.2.

Accumulated Dose Response

The accumulated dose response of the MOSkins was predictable, and was accounted for by applying a correction factor to each raw measurement. For measurements made using the Ir-192 source the correction factor was in the form of Equation 5.4.

$$Correction\ Factor = \frac{1}{\{1-(3.42\times10^{-3}\times Dose\ in\ Gray)\}} \qquad \text{Equation 5.4.}$$

Radial Angular Response

As the geometry of the experimental set up was known a range of relevant radial angles could be calculated. The maximum angle of 78.7^{o} occurred when the source was in the catheter furthest away from the MOSkin, the minimum angle of 0^{o} occurred when the source was in the catheter directly above the MOSkin, see Figure 5.6. For each MOSkin position a weighted angular response correction factor was calculated. This correction factor was calculated by taking the response, from the polynomial fit, at each radial angle made between the catheters and measurement positions and weighting them with the time the source spent in each catheter.

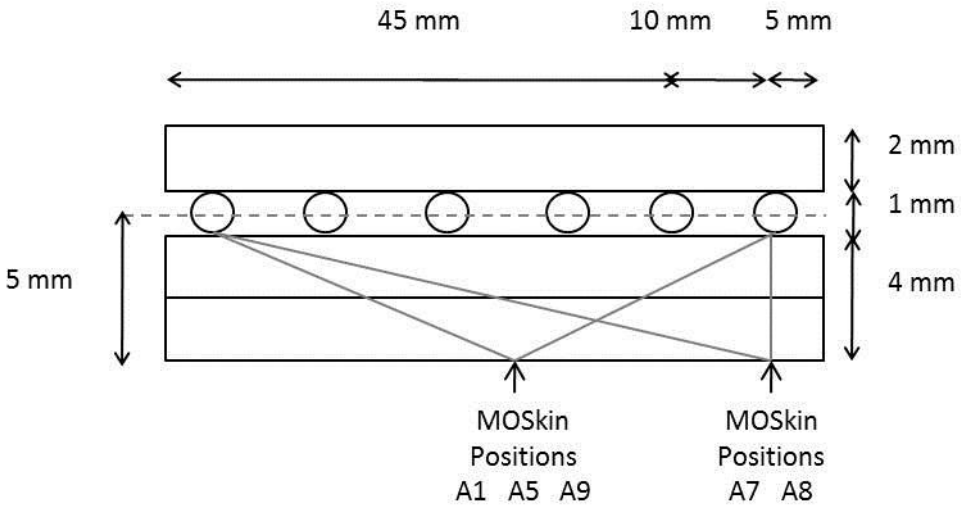

Figure 5.6 Diagram of the cross section of the IOBT applicator showing radial angles relevant to the backscatter factor measurements.

The weighted radial angular response correction factor for MOSkin positions A1, A5 and A9 was 1.076 and for MOSkin position A7 and A8 it was 1.074. However, as this correction factor would be applied to both the measurements with and without backscatter it would cancel out of the equation to calculate the backscatter factor (Equation 5.1).

Energy Response

The energy response of the MOSkins is discussed in Section 4.4.5 in Chapter 4. The backscatter measurements with the IOBT applicator result in two different energy spectra from the Ir-192 source, as explained for the TLD rods in Section 5.3.2.1. At a depth of 5 mm in water, with full backscatter conditions, the spectrum of Ir-192 has an average energy of approximately 352 keV (D. Cutajar, personal correspondence) and a response factor of 1.034 relative to the 6 MV linac beam (see Section 4.5.5). The response factor for an energy of 397 keV is 1.025, relative to a 6 MV linac beam. A correction factor in the form of Equation 5.5 and 5.6 was applied to all measurements with and without backscatter respectively, to correct for the energy response of the MOSkins.

$$Energy\ Correction\ Factor_{with\ backscatter} = \frac{1}{Response\ at\ 352\ keV} = \frac{1}{1.034} = 0.967$$

Equation 5.5

$$Energy\ Correction\ Factor_{without\ backscatter} = \frac{1}{Response\ at\ 397\ keV} = \frac{1}{1.025} = 0.976$$

Equation 5.6.

5.3.4 Dual MOSkin measurements

The dual MOSkins were taped directly to the underside of the IOBT applicator in the same way as the single MOSkins. At each of the five measurement positions three measurements were made both with and without 80 mm PTW RW3 slabs as backscatter material. The measurements were made using the MOSPLOT2 software developed by the (Centre for Medical Radiation Physics, University of Wollongong). The software takes a reading of the threshold voltage from up to five individual MOSkins every second and displays the information as a real time graph for a specified recording period. The data recorded can also be exported to a Microsoft Excel file. The dual MOSkins used to take these measurements had no previous dose history. The measurements were corrected for accumulated dose response and averaged.

5.3.4.1 Uncertainty in dual MOSkin measurements

The uncertainty for each dual MOSkin measurement was calculated by summing in quadrature the individual uncertainty associated with each dosimetric characteristic and/or applying a correction factor where relevant.

The accumulated dose response of the dual MOSkins was corrected using the same method as for the single MOSkins, see Section 5.3.3.1. The uncertainty due to stability, linearity, energy response and dose rate response were the same as for the single MOSkin, see Section 5.3.4.1. The azimuthal angular response of the dual MOSkins is discussed in Section 4.4.8.2 of Chapter 4.

Radial Angular Response

Weighted radial angular response correction factors were calculated using the same method as described for the single MOSkins (see Section 5.3.3.1). The weighted radial angular response correction factor for MOSkin positions A1, A5 and A9 was 1.021 and for MOSkin position A7 and A8 it was 1.019. However, as this correction factor would be applied to both the measurements with backscatter and the measurements without, it would cancel out of the equation to calculate the backscatter factor (Equation 5.1).

5.4 Results

Backscatter factors were measured at five positions on the IOBT applicator using TLD rods, MOSkins and dual MOSkins. For all detectors a lower dose was recorded at all positions in the absence of backscatter material. The uncertainty associated with each TLD rod, MOSkin and dual MOSkin measurement was calculated as shown in Tables 5.1 to 5.3.

TLD rod		
Dosimetric Characteristic	**Standard Uncertainty**	**How the uncertainty was applied**
Sensitivity	1.1 %	Summed in Quadrature
Linearity	2.8 %	Summed in Quadrature
Azimuthal Angular Response	4.6 %	Summed in Quadrature
Energy Response	ECF_{352keV}=0.986 ECF_{397keV}=0.989 1.2%	Applied as a correction factor Applied as a correction factor Summed in Quadrature
Dose Rate Response	1.8%	Summed in Quadrature
Total Uncertainty	**5.9%**	**1 Standard Deviation**

Table 5.1 Table showing a summary of the TLD rod measured total uncertainty for one backscatter factor measurement.

MOSkin		
Dosimetric Characteristic	**Standard Uncertainty**	**How the uncertainty was applied**
Accumulated Dose Response	0.0342 % per Gy	Applied as a correction factor to all raw measurements
Stability	0.9 %	Summed in Quadrature
Linearity	1.4 %	Summed in Quadrature
Radial Angular Response	$WCF_{A1,A5,A9} = 1.076$ $WCF_{A7,A8} = 1.074$ 2.1 %	Applied as a correction factor (but cancelled out of backscatter factor equation) Summed in Quadrature
Azimuthal Angular Response	2.1 %	Summed in Quadrature
Energy Response	$ECF_{352keV}=0.967$ $ECF_{397keV}=0.976$ 2.3%	Applied as a correction factor Applied as a correction factor Summed in Quadrature
Dose Rate Response	3.8 %	Summed in Quadrature
Total Uncertainty	**5.6%**	**1 Standard Deviation**

Table 5.2 Table showing a summary of the MOSkin measured total uncertainty for one backscatter factor measurement.

Dual MOSkin		
Dosimetric Characteristic	**Standard Uncertainty**	**How the uncertainty was applied**
Accumulated Dose Response	0.0342 % per Gy	A correction factor was applied to all raw measurements
Stability	0.9 %	Summed in Quadrature
Linearity	1.4 %	Summed in Quadrature
Radial Angular Response	$WCF_{A1,A5,A9} = 1.021$ $WCF_{A7,A8} = 1.019$ 0.5 %	Applied as a correction factor (but cancelled out of backscatter factor equation) Summed in Quadrature
Azimuthal Angular Response	2.5 %	Summed in Quadrature
Energy Response	$ECF_{352keV}=0.967$ $ECF_{397keV}=0.976$ 2.3 %	Applied as a correction factor Applied as a correction factor Summed in Quadrature
Dose Rate Response	3.8 %	Summed in Quadrature
Total Uncertainty	**5.4%**	**1 Standard Deviation**

Table 5.3 Table showing a summary of the dual MOSkin measured total uncertainty for one backscatter factor measurement.

The percentage reduction in dose, (backscatter factor), for each detector at each measurement position, along with the uncertainty, is shown in Table 5.4. Also shown are theoretical backscatter values that were calculated using the TG-43 formalism dose model[62] and backscatter factor model data obtained by Monte Carlo modelling reported by Poon et al[63].

Measurement Position	% Reduction in dose (Backscatter Factor)			
	TLD rod	MOSkin	Dual MOSkin	Calculated[63]
A1	6.9 ± 5.9%	8.5 ± 5.6%	5.5 ± 5.4%	4.6 ± 0.4%
A5	6.8 ± 5.9%	6.6 ± 5.6%	7.3 ± 5.4%	4.4 ± 0.4%
A7	4.6 ± 5.9%	8.8 ± 5.6%	5.6 ± 5.4%	4.0 ± 0.4%
A8	21.5 ± 5.9%	14.2 ± 5.6%	10.2 ± 5.4%	3.8 ± 0.4%
A9	1.9 ± 5.9%	9.1 ± 5.6%	9.6 ± 5.4%	4.6 ± 0.4%
Average	**8.3 ± 5.9%**	**9.4 ± 5.6%**	**7.4 ± 5.4%**	**4.3 ± 0.4%**
Average (Excluding A8)	**5.1 ± 5.9%**	**8.3 ± 5.6%**	**7.1 ± 5.4%**	**4.4 ± 0.4%**

Table 5.4 Table showing a summary of the measured backscatter factors at each measurement position for the TLD rods, MOSkins and dual MOSkins.

For all detectors a lower dose was recorded in the absence of scatter material above the applicator for all positions measured. Figure 5.7 to Figure 5.9 show the measured backscatter factors for each detector as well as the calculated backscatter factors.

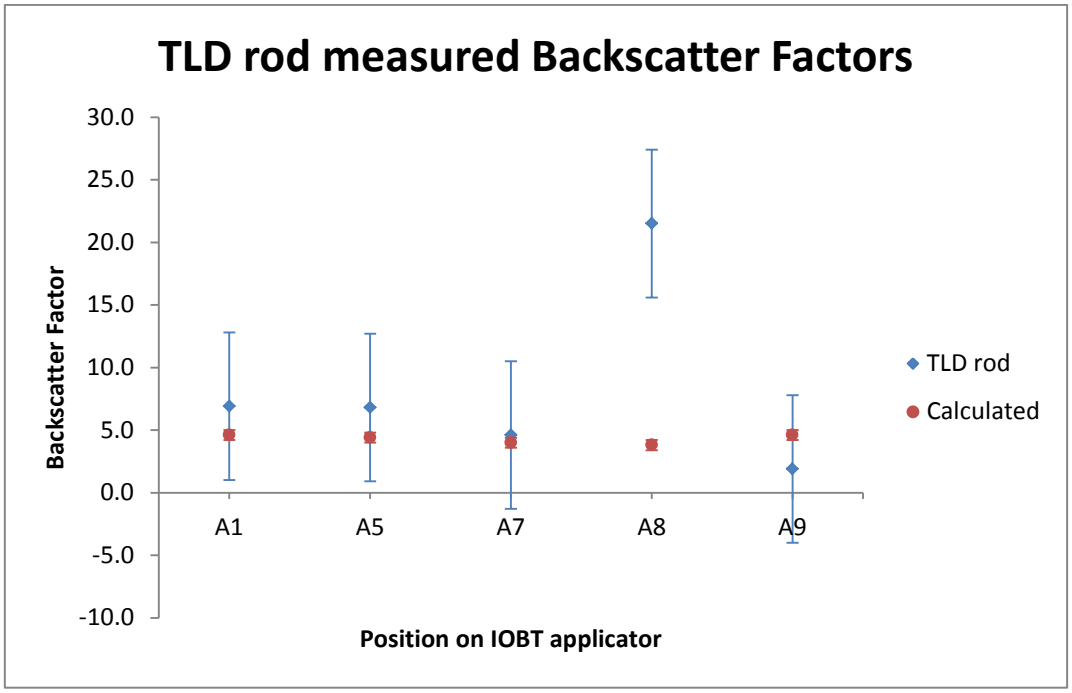

Figure 5.7 TLD rod measured backscatter factors plotted with the calculated backscatter factors[63] for comparison.

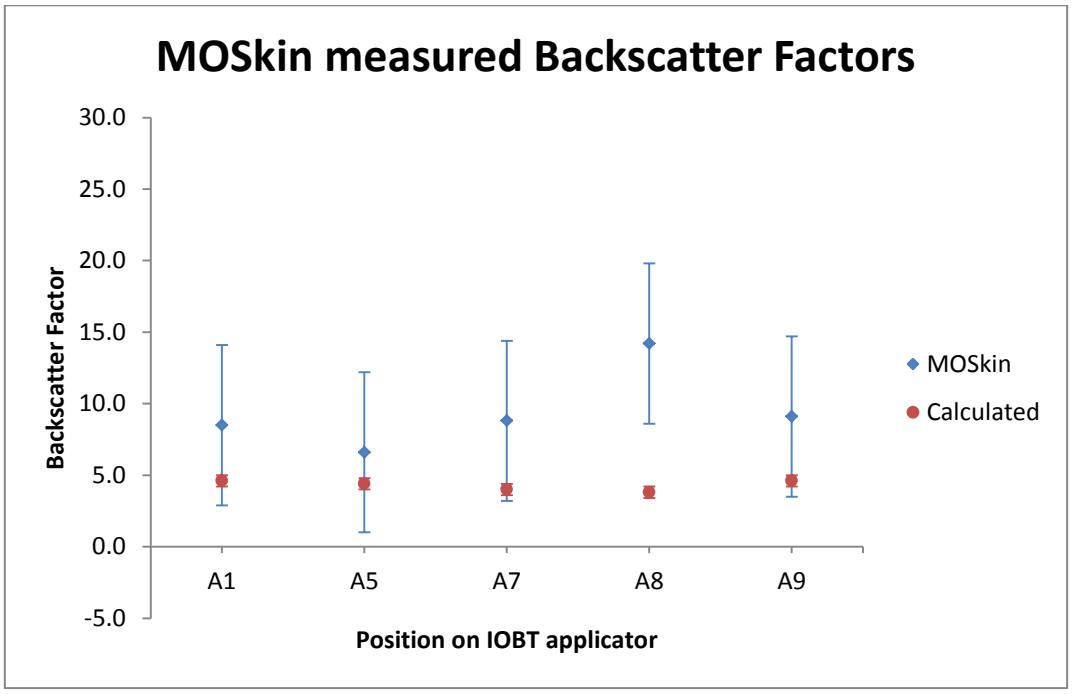

Figure 5.8 MOSkin measured backscatter factors plotted with the calculated backscatter factors[63] for comparison.

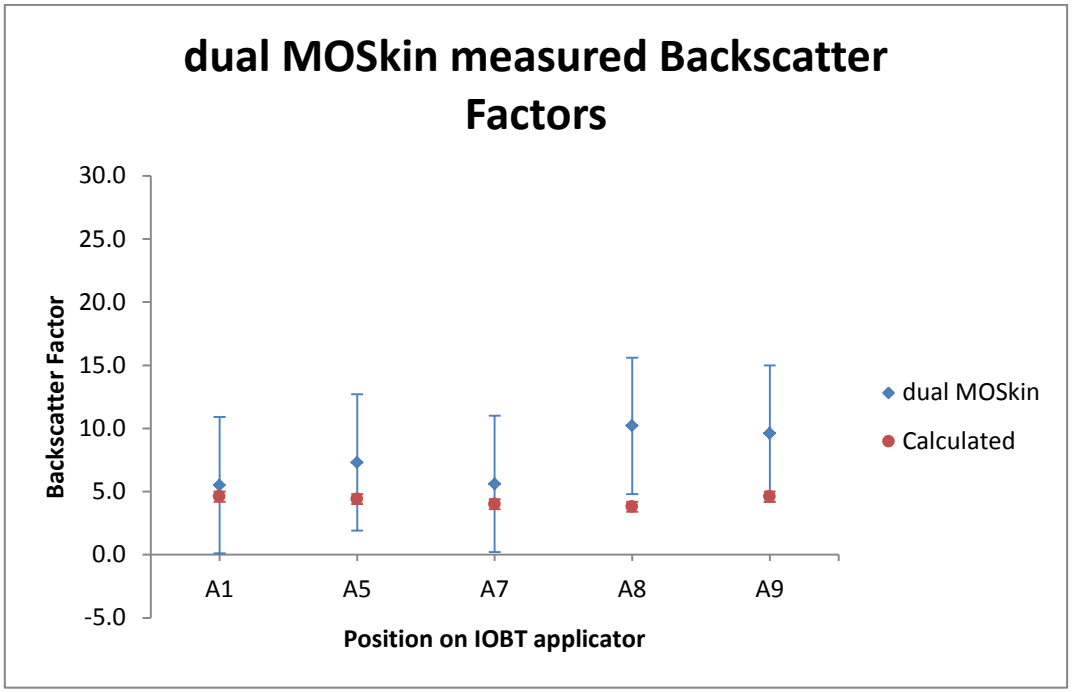

Figure 5.9 dual MOSkin measured backscatter factors plotted with the calculated backscatter factors[63] for comparison.

5.5 Discussion

Results show that measurements made using the IOBT applicator agree with calculations (apart from position A8) within measurement uncertainty. This is as expected, however, the magnitudes of the dose reductions measured in the absence of back scatter material, using the TLD rods, MOSkins and dual MOSkins were on average larger than predicted by the modified TG-43 model calculations.

5.5.1 TLD rod measurements

For four out of the five measurement positions the magnitude of the dose reductions agreed with the calculated reduction within experimental uncertainty. The average of these four measured reductions in dose was 5.1% in comparison to the average calculated value for the same four measurement points of 4.4%. At position A8, the measured dose reduction was significantly higher (21.5%), than at the other measurement points. The calculated dose reduction for this measurement point was in fact the lowest value of the five in question. The probable explanation for this is that position A8 is located on the corner of the IOBT applicator where it has the least surrounding scatter material and a close proximity to air gaps.

5.5.2 MOSkin measurements

For four out of five measurement positions the magnitude of the dose reductions agreed with the calculated reduction within experimental uncertainty. The measured reduction in dose at position A8 was again significantly higher (14.2%), than at the other four measurement positions. The average of these four reductions in doses was 8.3% in comparison to the average calculated reduction in dose of 4.4%.

5.5.3 dual MOSkin measurements

For four out of the five measurement positions the magnitude of the dose reductions agreed with the calculated reduction within experimental uncertainty. Again the greatest reduction in

dose was observed at position A8 (10.2%). The average measured reduction in dose of the other four points was 7.0% in comparison to the average calculated reduction in dose of 4.4%.

5.5.4 Summary

The average reduction in dose measured for positions A1, A5, A7 and A9 was 5.1% ± 5.9%, 8.3% ± 5.6% and 7.0% ± 5.4% for the TLD rods, MOSkins and dual MOSkins respectively. All these values are higher than the average calculated reduction in dose by 0.6%, 3.9% and 2.6% respectively. One possible explanation for this larger than anticipated dose reduction is the error associated with the energy correction. A correction factor was applied to all measurements without backscatter material to correct for the energy response of the detector. This correction factor was based on the assumption that the effective energy of the radiation from the Ir-192 source would change from 352 keV with full backscatter to 397 keV without backscatter. This is a conservative estimate and the actual change in the effective energy associated with our experimental set up is unknown. Future work could involve Monte Carlo modelling of the specific experimental set up to calculate the change in effective energy. Secondly, there is a degree of error associated with the response relation used to calculate response factors at the two effective energies. This leads to a large uncertainty in the gradient which gives a large uncertainty in energy correction factors used.

The measurement points used to calculate the energy response relation had an average of 1.2% and 2.3% uncertainty associated with them for the TLD rods (Figure 3.18) and the MOSkins (Figure 4.26) respectively. If this uncertainty is translated directly to the response values calculated for 352 keV and 397 keV a range of values for the energy correction factors are obtained. For the TLD rods the energy correction factors become 0.986 ± 0.012 and 0.989 ± 0.012 and for the MOSkins and dual MOSkins the energy correction factors become 0.967 ± 0.022 and 0.976 ± 0.022. Using energy correction factors within these ranges the average

backscatter factors for positions A1, A5, A7 and A9 do agree with the calculated average for the four positions

5.6 Conclusion

The reduction in dose due to lack of backscatter material was measured using an IOBT applicator and three different detectors. All measurements indicated a lower dose was delivered in the absence of backscatter material. The average reduction in dose for the four measurement points within the central part of the applicator (A1,A5, A7 and A9) was 5.1%, 8.3% and 7.0% for the TLD rods, MOSkins and dual MOSkins respectively. These values were within experimental uncertainty compared with the calculated value of 4.4%. The largest source of uncertainty for both the MOSkins and the TLD rods was the uncertainty in the energy response and this uncertainty could explain the systematic difference seen between the measured backscatter factors and the calculated backscatter values.

6 Discussion and Conclusion

6.1 Detector Characterisation

The dosimetric characteristics of MOSkin detectors were examined to assess their suitability for measurements relevant to dosimetry in brachytherapy. The dosimetric characteristics of TLD rods were also examined for comparison. Chapters 3 and 4 examined the dosimetric characteristics of TLD rods and MOSkins respectively. In Chapter 5 these detectors were used to measure backscatter factors for a clinical brachytherapy application. This provided an example of how correction factors and uncertainty estimates can be applied in this dosimetry application. In this chapter we bring together the results of measurements made with both detectors and form conclusions on their suitability for absorbed dose measurement in brachytherapy and suggest methods to further improve on the work presented in this thesis.

6.1.1 TLD rods

The following dosimetric characteristics were examined for the TLD rods: sensitivity, linearity, azimuthal angular response, energy response, dose rate response and temperature response. The characteristic making the largest contribution to uncertainty was energy response. The energy response was found to vary by 58.5% with the largest variation seen in the kilovoltage range, meaning measurements made in the kilovoltage range need to be corrected for energy or an overestimation of dose will be made. An equation involving four parameters was fit to the measurement points allowing the response at any energy to be calculated. In this way, a correction factor could be applied to measurements made at different energies. The uncertainty involved in the measurement points used to determine the parameters for the equation translates to an uncertainty in the response calculated using the equation. The variation, and hence uncertainty, is greatest for energies between 100 keV and 400 keV, which

also represents the energy range most relevant to measurements around an HDR Ir-192 source.

6.1.2 MOSkin detectors

The following dosimetric characteristics were examined for the MOSkins: stability, accumulated dose response, linearity, radial angular response, azimuthal angular response, energy response, dose rate response and temperature response. The characteristic making the largest contribution to uncertainty was energy response. The energy response was found to vary by 4.7 times the response at 6 MV, again with the largest variation seen in the kilovoltage range. An equation involving four parameters was also fit to the measurement points which allowed the response at any energy to be calculated. Similarly to the TLD rod measurements, the uncertainty involved in the measurement points used to determine the parameters for the equation translates to an uncertainty in the response calculated using the equation. The variation, and hence uncertainty, is greatest for energies between 100 keV and 600 keV, which again represents the energy range most relevant to measurements around an HDR Ir-192 source.

The accumulated dose response of the MOSkins used in this project was found to be almost equivalent for 6 MV linac radiation and radiation from an HDR Ir-192 source at a constant depth in water.

The radial angular response of the MOSkins varied by 19.0% over 360°. The response was symmetrical about 0°, with the minimum responses occurring at ± (156°). The shape of the radial angular response was fitted with a polynomial equation that could be used to calculate the response at any angle. This is useful if the source-detector geometry is known but can lead to large uncertainties if the geometry is unknown. For example if the accuracy of an angle of the source relative to the detector is known to within ± 5° the uncertainty in the MOSkin

response could vary between 0.03% - 2.10%. However, if the accuracy of the angle is known to within ± 20° the uncertainty in the MOSkin response could vary between 0.04% to 8.20%.

The dose rate response of the MOSkins was also a relatively large source of uncertainty. We would expect the response to be independent of dose rate using Ir-192 as demonstrated by Fagerstrom et al[37], Halvorsen et al[38] and Ramaeshan et al[32], however, the measurements made with the HDR Ir-192 source carried a large degree of uncertainty. This is because these measurements were made at different depths in PTW RW3 which required a correction for energy response. The energy response factors carry a large uncertainty. Future studies could investigate the dose rate response by taking measurements at a constant depth but at regular periods during the decay of the source, e.g. weekly, thus avoiding the need to apply energy response corrections and reducing the uncertainty.

6.1.3 Dual MOSkins

With the exception of radial and azimuthal response, the dosimetric characteristics of the dual MOSkins were found to be identical to those of the single MOSkin. The angular response characteristics of the single and dual MOSkins are summarised in Table 6.1.

Characteristic	Single MOSkin	Dual MOSkin
Radial Angular Response	Varied by 19.0% over 360°	Varied by 2.9% over 360°
Azimuthal Angular Response	Varied by an average of 2.1% between -29.4° and 36.4°	Varied by an average of 2.5% between -33° and 35°

Table 6.1 Table showing a comparison of angular response characteristics of the single and dual MOSkins.

The design of the dual MOSkins was intended to reduce the variation in the radial response of the detector and allow for angular-independent measurements[60]. The radial angular response measurements made using the dual MOSkins showed a variation in response of 2.9% over 360°, which is a reduction in variation of response by a factor of six in comparison to the variation in response of the single MOSkins of 19.0% over 360°, (Figure 6.1).

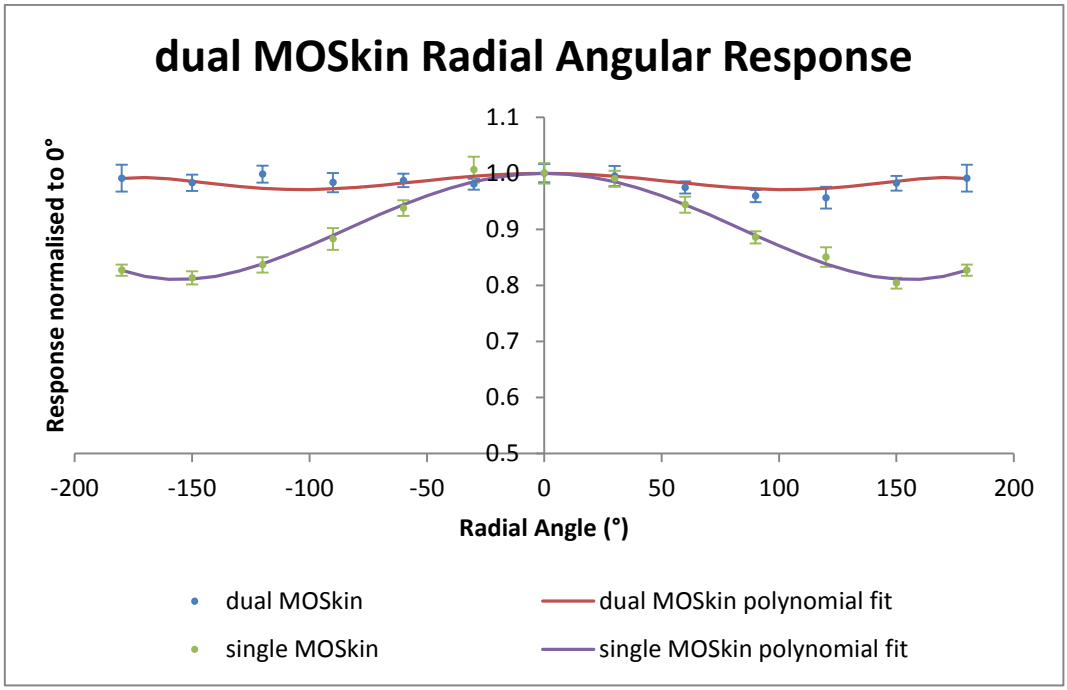

Figure 6.1 Comparison of the single and dual MOSkin radial angular response plotted as a function of radial angle. Note the truncated vertical axis.

The design of the dual MOSkin was not intended to reduce the variation in response in azimuthal direction. The average variation in the azimuthal angular response of 2.1% for the dual MOSkin and between 2.5% for the single MOSkin are consistent with this.

6.2 Lack of Backscatter Measurements with the IOBT applicator

From the examination of the dosimetric characteristics of the TLD rods, MOSkins and dual MOSkins, a summary of the relevant uncertainties associated with a single measurement of the backscatter factor made using the IOBT applicator were determined, see Section 5.4. The total uncertainty for each backscatter factor measurement was calculated as 5.9%, 5.6% and 5.4% for the TLD rods, MOSkins and dual MOSkins respectively.

A weighted radial angular correction factor was calculated for both the single and dual MOSkins, however, this factor cancelled out of the backscatter factor calculations as the same value was used for with backscatter material and without backscatter material.

The average backscatter factor was larger than the average calculated backscatter factor (4.4%) for positions A1, A5, A7 and A9 for the TLD rods (5.1%), MOSkins (8.3%) and dual MOSkins (7.0%). The most likely reason for this may be related to the uncertainty in the energy response of the detectors.

The absence of backscatter material above the IOBT applicator resulted in a higher effective energy than the measurements with backscatter material as low energy scatter components were not present. This meant the measurements made to calculate the backscatter factor with and without scatter material involved different effective energies. The exact difference in effective energy was unknown and so an estimate was made. This estimate was based on the change in effective energy between a depth of 5 mm in water with full scatter conditions and the effective energy of Ir-192 in air.

The response of both TLD rods and MOSkins increased for energies between 300 keV and 600 keV. To characterise the energy response, measurements were made between 15.7 keV – 108.8 keV, and at 6 MV and 18 MV. For the TLD rods it was also possible to make a measurement using Cs-137 (662 keV). However, measurements with the Cs-137 irradiator could not be made with the MOSkins because of the physical design of the irradiator that

requires the detector to be fully contained within the irradiation unit and therefore not suitable for use with MOSkins that have a cable linking them to the bias voltage. This leaves a large range of energies that were not measured including those most relevant to the backscatter factor measurements. Specifically, the effective energy from an HDR Ir-192 source at different depths in water has been calculated using Monte Carlo techniques[21], allowing measurements to be made at depths in water where the effective energy is known. Also, a measurement made using Cs-137 (662 keV) and Co-60 (1.17 MeV, 1.33 MeV) would be beneficial.

Energy correction factors were applied to both the measurements made with and without backscatter material to account for the change in energy. These energy correction factors were based on the effective energy at 5 mm depth in water with full backscatter, which does match the experimental set up, and the effective energy in air, which does not match the experimental set up. So there was an uncertainty in both the energy response and the estimated difference in effective energy for the experimental set up.

6.3 Suitability for measurements around HDR sources

The use of TLDs in medical dosimetry is well established owing to a list of suitable characteristics. For measurements around HDR brachytherapy sources the characteristics of most importance are the small physical size of the detector and the energy and dose rate response of the detector. The TLD rods used in this project had a total volume of 6 mm^3 (6 mm × 1 mm × 1 mm). This means that if the TLD rod was positioned with its long axis directed away from the source there could be a significant dose gradient across its length depending on its distance from the Ir-192 source. In close proximity to an Ir-192 HDR source, the dose rate and effective energy of the radiation are subject to large variations. TLD rods show no variation in response to changes in dose rates but they do display a large variation to changes in effective energy (58.5% between 15.7 keV and 18 MV). The energy response can be described by an equation but the accuracy of the fit is related to the number and accuracy of the measurement points used to calculate the parameters. The accuracy of the energy response could be improved by making more measurements in the energy range relevant to an Ir-192 HDR source. In particular a measurement made using Cs-137 (662 keV) would have been beneficial had access to a source been available.

MOSkins also display a number of characteristics indicating suitability for measurements around HDR sources. The first is that they have an extremely small detection volume (0.55 µm). The physical size of the entire MOSkin detector is also less than 1 mm thick. Whilst some MOSFET detector systems are available with a remote reader[38, 64], such a system was not available for this project. The MOSkin detectors used in this project were required to be connected to the bias supply during all measurements, meaning measurements could only be made in situations where the source and detector do not have to be completely isolated. Measurements made using the TLD rods are not subject to this issue as they do not require any auxiliary equipment to make a measurement.

The energy response of the MOSkin detector varies by 4.7 times the response at 6 MV in the range 15.7 keV to 18 MV, this is significantly larger than the variation in the TLD response of 58.5% over the same range. The energy response of the MOSkins could also be described by an equation but again the accuracy of the response calculated using this equation is subject to uncertainty from the number and accuracy of measurements made. The magnitude of the variation with energy of the MOSkins in comparison to that of the TLD rods indicates a larger uncertainty in the energy response, particularly if the true effective energy is unknown.

The MOSkins also display a significant variation in response to changing radial angles (19.0% over 360°). The design of the dual MOSkins is such that this variation in response is reduced to 2.9% over 360°. For measurements where the angle is unknown this is a significant reduction in uncertainty making the dual MOSkins a better choice for measurements around HDR sources than the single MOSkins.

TLD rods can be used repeatedly with proper annealing between measurements, whereas MOSkins have a limited useful lifetime. The useful lifetime of a MOSkin is a function of the total accumulated dose. The MOSkins used in this project had a useful lifetime of approximately 70 Gy. As each new batch of MOSkins would require commissioning, the limited useful lifetime of the detectors could prove a time and material consuming process.

6.3.1 Summary

This project has investigated the dosimetric characteristics of MOSkin detectors and TLD rods for the purpose of making backscatter factor measurements using an IOBT applicator and an HDR Ir-192 source. The characteristics making the largest contribution to measurement uncertainty were the energy response for both TLD rods and MOSkin detectors. The radial angular response of the MOSkin detectors also made a significant contribution to the measurement uncertainty. The small detection volume and ability to give an immediate reading of MOSkin detectors make them an attractive choice for measurements around HDR sources, however, the relatively large uncertainty as a result of energy and angular response mean they are not suitable for measurements when a correction for energy response is required or the angle of incidence to the source to detector is unknown. The limited useful lifetime of the MOSkin detector is also a draw back.

In conclusion, MOSkin detectors are shown to be suitable for measurements where both the geometry and radiation energy are known. Circumstances where uncertainties in the geometry and/or energy exist may result in an unacceptably large uncertainty in measurements. The dual MOSkin detector, with its reduced variation in angular response goes part way to solving the problem for angular response uncertainty.

7 Reference Pages

1. ICRU. Dose and Volume Specifications for Reporting Intracavitary Therapy in Gynecology; 1985.
2. Heriot AG, Byrne CM, Lee P, Dobbs B, Tilney H, Solomon MJ, et al. Extended Radical Resection: The Choice for Locally Recurrent Rectal Cancer. *Diseases of the Colon & Rectum* 2008;**51**(3):284-91 10.1007/s10350-007-9152-9.
3. Lambert J, Nakano T, Law S, Elsey J, McKenzie DR, Suchowerska N. In vivo dosimeters for HDR brachytherapy: A comparison of a diamond detector, MOSFET, TLD, and scintillation detector. *Medical Physics* 2007 May;**34**(5):1759-65.
4. Duggan L, Hood C, Warren-Forward H, Haque M, Kron T. Variations in dose response with x-ray energy of LiF : Mg,Cu,P thermoluminescence dosimeters: implications for clinical dosimetry (vol 49, pg 3831, 2004). *Physics in Medicine and Biology* 2004 Sep;**49**(18):4445-.
5. Kron T. Thermoluninescence dosimetry and its applications in medicine - Part 1: Physics, materials and equipment. *Australasian Physical and Engineering Sciences in Medicine* 1994;**17**(4):175-99.
6. Niroomand-Rad A, Blackwell CR, Coursey BM, Gall KP, Galvin JM, McLaughlin WL, et al. Radiochromic film dosimetry: Recommendations of AAPM Radiation Therapy Committee Task Group 55. *Medical Physics* 1998 Nov;**25**(11):2093-115.
7. Soares CG. Radiochromic film dosimetry. *Radiation Measurements* 2006 Dec;**41**:S100-S16.
8. Roozen K, Kron T, Haworth A, Franich R. Evaluation of EBT radiochromic film using a multiple exposure technique. *Australasian Physical & Engineering Sciences in Medicine* 2011;**34**(2):9.

9. Gotanda T, Katsuda T, Gotanda R, Tabuchi A, Yamamoto K, Kuwano T, et al. Evaluation of effective energy using radiochromic film and a step-shaped aluminum filter. *Australasian Physical & Engineering Sciences in Medicine* 2011;**34**(2):10.

10. Khan FM. *The Physics of Radiation Therapy*. Third ed. Philadelphia: Lippincott Williams and Wilkins; 2003.

11. Saini AS, Zhu TC. Energy dependence of commercially available diode detectors for in-vivo dosimetry. *Medical Physics* 2007 May;**34**(5):1704-11.

12. Rosenfeld AB, Cutajar D, Lerch MLF, Takacs G, Cornelius IM, Yudelev M, et al. Miniature semiconductor detectors for in vivo dosimetry. *Radiation Protection Dosimetry* 2006 Sep;**120**(1-4):48-55.

13. Kwan IS, Rosenfeld AB, Qi ZY, Wilkinson D, Lerch MLF, Cutajar DL, et al. Skin dosimetry with new MOSFET detectors. *Radiation Measurements* 2008 Feb-Jun;**43**(2-6):929-32.

14. Harvey JA, Haverland NP, Kearfott KJ. Characterization of the glow-peak fading properties of six common thermoluminescent materials. *Applied Radiation and Isotopes* 2010;**68**(10):1988-2000.

15. Horowitz YS. *Thermoluminescence and Thermoluminescent Dosimetry*. Florida, USA: CRC Press; 1984.

16. Mahesh K, Weng PS, Furetta C. *Thermoluminescence in solids and its applications*. Ashford, Kent, England: Nuclear Technology Publishing; 1989.

17. Tochilin E, Goldstein N. Dose rate and spectral measurements from pulsed x-ray generators. *Health Physics* 1966;**12**:9.

18. Kron T, Smith A, Hyodo K. Synchrotron Radiation in the Study of the Variation of Dose Response In Thermoluminescence Dosimeters with Radiation Energy. *Australasian Physical and Engineering Sciences in Medicine* 1996;**19**(4):225-36.

19. Physical Measurement Laboratoy N. Tables of X-Ray Mass Attenuation Coefficients and Mass Energy-Absorption Coefficients from 1 keV to 20 MeV for Elements Z = 1 to 92 and 48 Additional Substances of Dosimetric Interest. 2010 [cited 2011; Available from: http://www.nist.gov/pml/data/xraycoef/index.cfm

20. Jayachandran CA. Calculated effective atomic number and Kerma value for tissue-equivalent and dosimetry materials. *Physics in Medicine and Biology* 1971;**16**(4):617-23.

21. Meli JA, Meigooni AS, Nath R. On the choice of phantom material for the dosimetry of ^{192}Ir sources. *International Journal of Radiation Oncology Biology and Physics* 1988;**14**:8.

22. Meigooni AS, Meli JA, Nath R. Influence of the variation of energy spectra with depth in the dosimetry of ^{192}Ir using LiF TLD. *Physics in Medicine and Biology* 1988;**33**(10):12.

23. Thomason C, Higgins P. Radial dose distribtion of 192Ir and 137Cs seed sources. *Medical Physics* 1989;**16**(2):4.

24. Thomason C, Higgins P. Reply to comments of Meli, Meigooni, and Nath. *Medical Physics* 1989;**16**(5):1.

25. Meli J, Meigooni A, Nath R. Comment on "Radial dose distribution of 192Ir and 137Cs seed sources". *Medcical Physics* 1989;**16**(5):1.

26. Museum CH. The Silicon Engine: A Timeline of Semiconductors in Computers. 2007 [cited 2011; Available from: http://www.computerhistory.org/semiconductor/timeline/1960-MOS.html

27. Holmes-Siedle A. The space-charge dosimeter: General principles of a new method of radiation detection. *Nuclear Instruments and Methods* 1974;**121**(1):169-79.

28. Holmes-Siedle A, Menary P, Sharpe P, Mills JA. RADFET devices are they coming of age? *Scope* 2010:21-7.

29. Hughes RC. Theory of response of radiation sensing field-effect transistors in zero-bias operation. *Journal of Applied Physics* 1986;**60**(3):2.

30. Ramani R, Russell S, O'Brien P. Clinical dosimetry using MOSFETs. *International Journal of Radiation Oncology Biology and Physics* 1997;**37**(4):959-64.

31. Kwan IS, Wilkinson D, Cutajar D, Lerch M, Rosenfeld A, Howie A, et al. The effect of rectal heterogeneity on wall dose in high dose rate brachytherapy. *Medical Physics* 2009 Jan;**36**(1):224-32.

32. Ramaseshan R, Kohli KS, Zhang TJ, Lam T, Norlinger B, Hallil A, et al. Performance characteristics of a microMOSFET as an in vivo dosimeter in radiation therapy. *Physics in Medicine and Biology* 2004 Sep;**49**(17):4031-48.

33. Cheung T, Buston MJ, Yu PKN. Energy dependence corrections to MOSFET dosimetric sensitivity. *Australasian Physical and Enginerring Sciences in Medicine* 2009;**32**(1):5.

34. Kron T, Duggan L, Smith T, Rosenfeld A, Butson M, Kaplan G, et al. Dose response of various radiation detectors to synchrotron radiation. *Physics in Medicine and Biology* 1998 Nov;**43**(11):3235-59.

35. Lavallee MC, Gingras L, Beaulieu L. Energy and integrated dose dependence of MOSFET dosimeter sensitivity for irradiation energies between 30 kV and Co-60. *Medical Physics* 2006 Oct;**33**(10):3683-9.

36. Crook J. The role of brachytherapy in the definitive management of prostate cancer. *Cancer/Radiothérapie* 2011;**15**(3):230-7.

37. Fagerstrom JM, Micka JA, DeWerd LA. Response of an implantable MOSFET dosimeter to (192)Ir HDR radiation. *Medical Physics* 2008 Dec;**35**(12):5729-37.

38. Halvorsen PH. Dosimetric evaluation of a new design MOSFET in vivo dosimeter. *Medical Physics* 2005 Jan;**32**(1):110-7.

39. Daskalov GM, Loffler E, Williamson JF. Monte Carlo-aided dosimetry of a new high dose-rate brachytherapy source. *Medical Physics* 1998 Nov;**25**(11):2200-8.

40. Cheung T, Butson MJ, Yu PKN. Effects of temperature variation on MOSFET dosimetry. *Physics in Medicine and Biology* 2004 Jul;**49**(13):N191-N6.

41. Rosenfeld AB, Lerch MLF, Kron T, Brauer-Krisch E, Bravin A, Holmes-Siedle A, et al. Feasibility study of online high-spatial-resolution MOSFET dosimetry in static and pulsed X-ray radiation fields. *Ieee Transactions on Nuclear Science* 2001 Dec;**48**(6):2061-8.

42. Gupta VK. Brachytherapy - Past, Present and Future. *Journal of Medical Physics* 1995;**20**(2):8.

43. Kresl JJ. St. Joseph's Hospital and Barrow Neurological Institute stereotactic radiotherapy experience: comparison of Gamma Knife and CyberKnife. *Journal of Oncology* 2006;**56**(2):6.

44. Calvo FA, Meirino RM, Orecchia R. Intraoperative radiation therapy First Part: Rationale and techniques. *Critical Reviews in Oncology/Hematology* 2006;**59**:10.

45. Harrison LB, Minsky BD, Enker WE, Mychalczak B, Guillem J, Paty PB, et al. High dose rate intraoperative radiation therapy (HDR-IORT) as part of the management strategy for locally advanced primary and recurrent rectal cancer. *International Journal of Radiation Oncology Biology and Physics* 1998;**42**(2):325-30.

46. MRNI. Delivery of HDR - IORT for Advanced Tumors Via Remote Afterloading. The H.A.M Applicator Faciliates Delivery of HDR Intraoperative Radiation Therapy (HDR-IOR) for Superficial and Advanced Tumors Via Remote Afterloading. In: Mick Radio-

Nuclear Instruements I, editor. *wwwmicknuclearcom*. 521 Homestead Avenue, Mount Vernon, New York, USA; 2011.

47. Nuyttens JJ, Kolkman-Deurloo IK, Vermaas M, Ferenschild FT, Graveland WJ, De Wilt JH, et al. High-dose-rate intraoperative radiotherapy for close or positive margins in apteints with locally advanced or recurrent rectal cancer. *International Journal of Radiaiton Oncology Biology and Physics* 2004;**58**(1):106-12.

48. Kolkman-Deurloo IK, Nuyttens JJ, Hanssens PEJ, Levendag PC. Intraoperative HDR brachytherapy for rectal cancer using a flexible intraoperative template: standard plans versus individual planning. *Radiotherapy and Oncology* 2004;**70**:75-9.

49. ConvaTech, Stomahesive Skin Barrier. 2011 [cited 2011; Available from: http://www.convatec.co.uk/engb/cvtuk-productsuk/cvt-products/0/proddett/1973/401/822/stomahesive-skin-barrier.html/vote_zero/z?franchise=46&typesearch=20&proddett=822&prodfamily=85#

50. Martinez-Monge R, Nag S, Martin EW. Three Different Intraoperative Radiation Modalities (Electron Beam, High-Dose-Rate Brachytherapy, and Iodine-125 Brachytherapy) in the Adjuvant Treatment of Patients with Recurrent Colorectal Adenocarcinoma. *American Cancer Society* 1999:236-47.

51. Borg J, Rogers WO. Monte Carlo Calculations of Photon Spectra in Air from 192Ir Sources. *PIRS-629r*. Ottowa, Ontario, K1A 0R6, Canada: Ioizing Radiation Standards, Institute for National Measurement Standards, National Research Council; 1990.

52. IAEA. Absorbed dose determination in external beam radiotherapy: An International Code of Practice for dosimetry based on standards of absorbed dose to water. Vienna; 2000.

53. IAEA. Calibration of photon and beta ray sources used in brachytherapy; 2002.

54. Butler D, Haworth A, Sander T, Todd S. Comparison of 192Ir air kerma calibration coefficients derived at ARPANSA using the interpolation method and at the National Physics Laboratory using a direct measurement. *Australasian Physical and Engineering Science in Medicine* 2008;**31**(4):332-8.

55. PTW. User Manual IChamber Type 30010, 30011, 30012, 30013 Technical Specifications.

56. Hardcastle N, Soisson E, Metcalfe P, Rosenfeld AB, Tome WA. Dosimetric verification of helical tomotherapy for total scalp irradiation. *Medical Physics* 2008 Nov;**35**(11):5061-8.

57. DuPont. Summary of Properties for Kapton Polyimide Films. 2011 [cited; Available from: http://www2.dupont.com/Kapton/en_US/assets/downloads/pdf/summaryofprop.pdf

58. Cygler JE, Saoudi A, Perry G, Morash C, Choan E. Feasibility study of using MOSFET detectors for in vivo dosimetry during permanent low-dose-rate prostate implants. *Radiotherapy and Oncology* 2006;**80**:6.

59. Benevides LA, Hintenlang DE. Characterization of metal oxide semiconductor field effect transistor dosimeters for application in clinical mammography. *Medical Physics* 2006 Feb;**33**(2):514-20.

60. Hardcastle N, Cutajar DL, Metcalfe PE, Lerch MLF, Perevertaylo VL, Tome WA, et al. In vivo real-time rectal wall dosimetry for prostate radiotherapy. *Physics in Medicine and Biology* 2010 Jul;**55**(13):3859-71.

61. Hayton A, Haworth A, Waterhouse D, Todd S, Pillainayagam J. Lack of backscatter factor measurements in HDR applications with MOSkins. *Australasian Physical & Engineering Science in Medicine* 2011;**34**(4):8.

62. Nath R, Anderson LL, Luxton G, Weaver KA, Williamson JF, Meigooni AS. Dosimetry of interstitial brachytherapy sources: Recommendations of the AAPM Radiation Therapy Committee Task Group No. 43. *Medical Physics* 1995;**22**(2):209-34.

63. Poon E, Verhaegen F. Development of a scatter correction technique and its application to HDR Ir-192 multicatheter breast brachytherapy. *Medical Physics* 2009;**36**(8):3703-13.

64. Haughey A, Coalter G, Mugabe K. Evaluation of linear array MOSFET detectors for in vivo dosimetry to measure rectal dose in HDR brachytherapy. *Australasian Physical and Engineering Sciences in Medicine* 2011;**34**(3):6.

Appendix A ‘Lack of backscatter factor measurements in HDR applications with MOSkins’

Australas Phys Eng Sci Med (2011) 34:545–552
DOI 10.1007/s13246-011-0101-5

TECHNICAL PAPER

Lack of backscatter factor measurements in HDR applications with MOSkins

Anna Hayton · Annette Haworth · David Waterhouse · Stephen Todd · Joseph Pillainayagam

Received: 7 March 2011 / Accepted: 13 September 2011 / Published online: 4 October 2011

Abstract Measurements of backscatter correction factors for intra operative (IOBT) HDR brachytherapy applicators were made using Centre for Medical Radiation Physics (CMRP), MOSFET devices. In clinical use there is an absence of backscatter material above the IOBT applicator, leading to a lower dose than predicted by conventional TG-43 dose calculations. To estimate the uncertainty in the MOSFET measurements, the dosimetric characteristics, including reproducibility, stability, linearity, and angular and energy response were measured using a HDR Ir-192 source, kilovoltage treatment unit and a high energy linac. Measurements were compared with previously published Monte Carlo data. Variability of the response of the MOSFETs due to angular variation contributed the largest uncertainty in dose measurements. Using the IOBT applicator without adequate scatter material resulted in a reduction of delivered dose of on average 10%, but was dependent on the location on the applicator and the treatment field size. Theoretical calculations based on previously published study indicated an expected reduced dose of on average 4%. MOSFET devices provide an ideal measurement tool in the presence of high dose gradients, however, the dosimetric characteristics of the detector must be accounted for when estimating the uncertainty.

Keywords MOSFET · IOBT · Backscatter · HDR · Brachytherapy

Presented at the Australian Brachytherapy Group Meeting 2010, 19th Scientific Meeting of the Australasian Brachytherapy Group, Melbourne, Australia, 8–10th April 2010.
Presented at EPSM-ABEC 2010, annual conference of Engineering and Physical Sciences in Medicine, Melbourne, Australia, 5–9 December 2010.

A. Hayton (✉) · A. Haworth
School of Applied Sciences, RMIT University, Melbourne, VIC, Australia
e-mail: Anna.Hayton@arpansa.gov.au

A. Hayton
Medical Physics Section, Australian Radiation Protection and Nuclear Safety Agency, 619 Lower Plenty Road, Yallambie, Melbourne, VIC 3085, Australia

A. Haworth · D. Waterhouse · S. Todd · J. Pillainayagam
Department of Physical Sciences, Peter MacCallum Cancer Centre, Melbourne, VIC, Australia

Introduction

Intra Operative Brachy Therapy (IOBT) is the process whereby a dose of radiation is delivered to the tumour bed immediately following surgical removal of the tumour. The advantage of IOBT is that a high dose of radiation can be delivered while minimising the dose to surrounding healthy tissue. In the treatment of rectal tumours, an IOBT applicator is placed on the tumour bed and a high dose rate radioactive Ir-192 source steps through catheters implanted within the applicator to deliver the prescribed dose to the tumour bed. The IOBT applicator used at the Peter MacCallum Cancer Centre consists of catheters spaced 10 mm apart and sandwiched between layers of a semi rigid tissue-equivalent material. The applicator is placed on the tumour bed following surgical excision. As the prescribed radiation dose is delivered during surgery it is not practical to use CT images for treatment planning, instead a library plan is used. This method has limitations as it introduces differences between the planned and actual geometry of the catheters in respect to the treatment volume. Typically it is not practical to apply a large quantity of bolus material in the sterile field to provide adequate scatter material above

the applicator. The treatment planning system assumes that the Ir-192 source is completely surrounded by scatter material. During the treatment the patient's body provides scatter material below the applicator but absence of scatter material above the applicator can result in a tumour surface dose that is lower than predicted by the planning computer, and potential under dosing of the tumour.

Dose measurements in brachytherapy can be challenging for many reasons. High dose rate gradients around sources necessitate a dosimeter with a very small detection volume. Also, the logistics of placing a dosimeter in a clinically meaningful position requires that they have a very small physical size. Dosimeters currently in use in brachytherapy are TLDs, Gafchromic film and MOSFETs. TLDs have a well established history of use in medical dosimetry, they have a relatively small physical size, and an approximately tissue equivalent atomic number but require a careful annealing process [1]. Gafchromic film is growing in popularity but requires careful handling and calibration procedures [2]. MOSFETs are less commonly used but are capable of giving dose measurements in real time. For the purpose of this study we have investigated the use of a relatively new product, the MOSkin, developed by the Centre for Medical Radiation Physics (CMRP), University of Wollongong (UOW), NSW Australia. The effective measurement point of the MOSkin detectors is of a water equivalent depth of 70 μm, which corresponds to the most radiosensitive layer of the epidermis. Their detection volume thickness is 0.00055 mm [3].

In this project we investigated the reduction in HDR IOBT delivered dose that occurs in the absence of adequate scatter material at the tumour bed surface. To measure the dose reduction we used MOSkins and an IOBT applicator. We compare our measurements with calculations made using a modified TG-43 dose calculation algorithm and Monte Carlo modelling.

Materials and methods

The IOBT applicator

The IOBT applicator is used during surgery. In the case of colorectal cancer, the tumour is first excised then the IOBT applicator is placed directly on the tumour bed. During delivery of the radiation dose, the patient provides backscatter material below the applicator but typically there is only air, or sometimes a small amount of wet gauze, above the applicator.

Applicators used at the Peter MacCallum Cancer Centre are constructed in-house from Nucletron 6F flexible plastic catheters and a water equivalent wafer material (Stomahesive, ConvaTec, Princeton, NJ, USA). The applicators are constructed from $100 \times 100 \times 2$ mm^3 wafer sheets. The catheters are spaced 10 mm apart starting 5 mm inside the wafer edge, with the tips of the catheters placed 3 mm inside the wafer edge. The $100 \times 100 \times 2$ mm^3 sheet of wafer can be cut down to appropriate dimensions. The applicator used in this project had dimensions of $60 \times 90 \times 5$ mm^3 and contained 6 catheters sandwiched between wafer layers, one layer on top and two layers below the catheters, which will be in contact with the tumour during treatment (Fig. 1).

The tissue equivalent wafers are somewhat flexible but all measurements were made with the applicator laid flat. Measurements were made with the applicator placed on top of 80 mm solid water and 10 mm of an in-house manufactured bolus material (superflab). This provided an adequate depth of scatter material below the applicator and the superflab ensured the MOSkin detectors were not crushed. The catheters of the applicator were connected to a Nucletron microSelectron V2 Ir-192 source (Nucletron, Veenendaal, The Netherlands). A Plato treatment planning system (Version 14.3.2, Nucletron, Veenendaal, The Netherlands) was used to determine dwell times to deliver 0.5 Gy to 5 mm below the underside of the applicator. Measurements were taken at several positions on the IOBT applicator as indicated in Fig. 1.

Measurements were made by attaching the MOSkin detectors directly to the underside of the IOBT applicator, giving a nominal source to detector distance of 3 mm. Measurements were made with and without scatter material above the applicator. Scatter material in the form of 80 mm of solid water was placed directly on top of the applicator. Wadded paper towel was used along the sides of the applicator to provide support for the solid water placed on top, to prevent compression of the applicator and to provide some lateral scatter material.

The dose delivered, both in the presence and absence of backscatter material, was measured using MOSkins

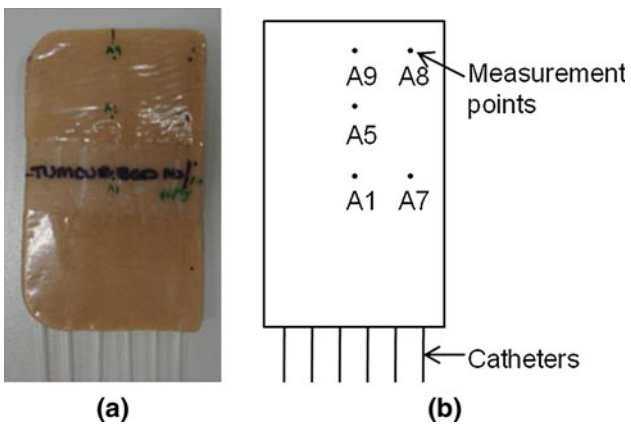

Fig. 1 **a** Underside of the IOBT applicator with measurement positions marked. **b** Diagram of measurement positions

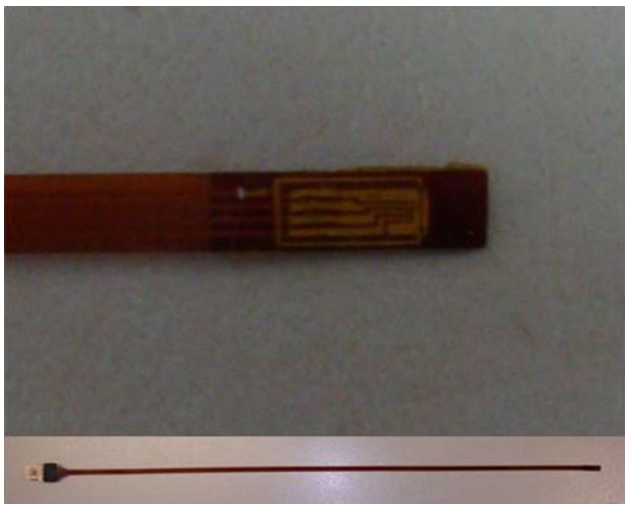

Fig. 2 The MOSkin dosimeter

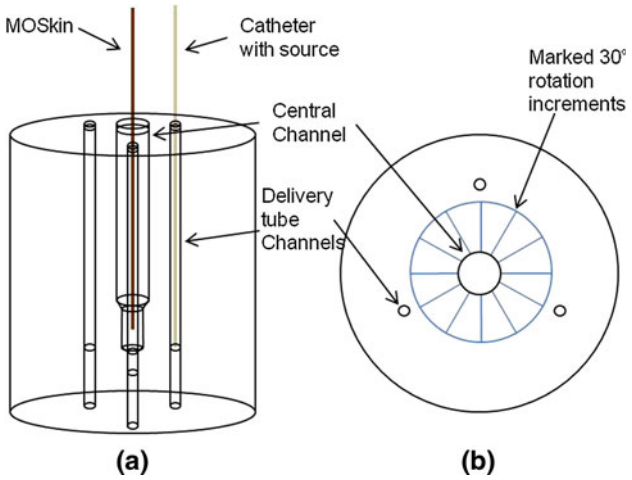

Fig. 3 The cylindrical water phantom **a** side view **b** top view

obtained from the Centre for Medical Radiation Physics (CMRP), University of Wollongong (UOW), NSW Australia. The MOSkin is a variation on the MOSFET dosimeter. Typically MOSFET dosimeters consist of a MOSFET sensor encapsulated in an epoxy bubble, the MOSkin dosimeter however, has the MOSFET sensor under a 0.020 mm thick build up layer of polyamide film giving a water equivalent detection depth of 0.070 mm. The entire MOSkin dosimeter is essentially a flat ribbon with dimensions 330 × 3 × 0.4 mm^3, as shown in Fig. 2.

MOSFETs are well known to vary in response due to a range of physical properties such as accumulated dose and angular and energy response [4–8]. To estimate the uncertainty and/or determine appropriate correction factors to be applied in the backscatter measurements, we first determined the change in response of the MOSkins under a variety of conditions. Wherever practical, measurements were made using a Nucletron microSelectron V2 HDR Ir-192 source in water, as this would be the source used clinically, however, some measurements were made using a Varian 600c and iX Linacs, (Varian, Palo Alto, CA), and slabs of solid water for convenience. A cylindrical PMMA water phantom was used with the Ir-192 source. The cylinder had a diameter of 200 mm and a depth of 300 mm. It contained a central channel in which a specially designed PMMA holder for the MOSkins could be inserted and three equally spaced channels at a radial distance of 50 mm in which catheters could be inserted (Fig. 3).

Stability

The stability of the MOSkins were measured over both short and long term time periods. Long term stability is an important consideration for MOSFETs as they are known to display a decreased response with total dose accumulated by the detector [7, 9, 10]. Long term stability was measured by comparing measurements from three MOSkins, from the same batch, at the start and end of a sequence of measurements using the Ir-192 source. A linear response was assumed and subsequent measurements corrected to account for the decreasing sensitivity with accumulated dose. The short term stability of the MOSkins was determined by measuring the random variation across five consecutive readings from a constant dose.

Linearity

Linearity was measured by irradiating two MOSkins using the 6MV linac. The MOSkins were irradiated at a depth of 50 mm in solid water using a field size of 100 × 100 mm^2 at a source to surface distance of 1000 mm. Three measurements were made with each MOSkin for doses ranging between 0.5 and 5.0 Gy. The average of the three measurements, normalised to the response at 1.0 Gy, was then plotted against the dose in Gy.

Angular response

The angular response of the MOSkins was measured in both the radial and azimuthal directions (Fig. 4). The cylindrical water phantom with the Ir-192 source was used to measure the radial angular response of the MOSkin as the MOSkin holder was rotated around the central axis (Fig. 3).

The azimuthal response of the MOSkin was measured by altering the position of the source in the catheter with the MOSkin in a constant position and correcting for source detector distance (Fig. 3).

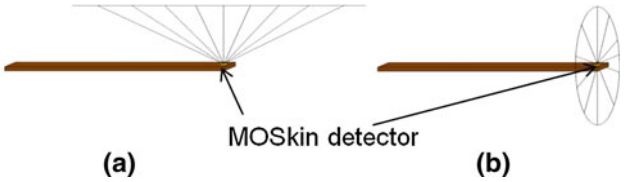

Fig. 4 Angular direction of the MOSkin **a** azimuthal **b** radial

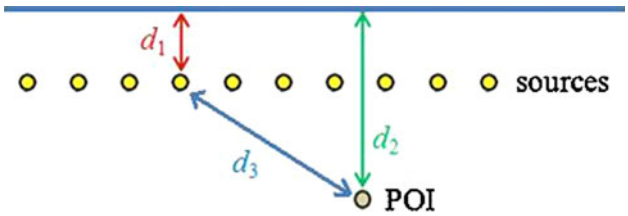

Fig. 5 Relevant parameters for a surface applicator

Energy response

MOSFETs are well known to have an energy response [4, 7–9]. The spectrum from an Ir-192 source changes according to its depth in water and the presence of backscatter material. For our backscatter measurements, the source detector distance was constant at 3 mm for all measurements, but the addition of scatter material above the applicator was expected to alter the spectrum. The backscatter components of the spectrum have low energies so the presence of backscatter material will lower the average energy of the spectrum. We therefore measured the energy response over a range of energies so that the difference in sensitivity of the MOSkins with the two measurement conditions, with and without backscatter, could be predicted.

The energy response was measured by irradiating the MOSkins over a range of energies using a Pantak Therapax X-ray unit Model MXT225, and a Varian iX linac. Kilovoltage X-ray machine spectra were filtered using Al and Cu to obtain mean beam energies between 15 and 100 kV. Peak photon energies from the linac (6 and 18 MV) are represented by mean beam energies of 2000 and 6000 kV, respectively.

Uncertainty

By examining the variation in response of the different dosimetric characteristics, an uncertainty for each characteristic was determined. The uncertainty associated with the short term reproducibility, linearity, radial and azimuthal angular response and energy response were summed in quadrature to estimate a total uncertainty in the backscatter measurements. The long term stability response of the MOSkins was predictable and as such a correction factor was applied to all raw measurements to account for this response.

Calculations

Dose calculations were initially made using the TG-43 [11] formalism and were implemented in a Microsoft Excel (Microsoft, Redmond, WA, USA) spreadsheet. The spreadsheet allowed the user to design a surface applicator of any smoothly varying shape and combination of source dwell positions, and was initially developed as a tool for real-time approximation of three-dimensional surface applicator shapes for export to commercial treatment planning software. It was also used as an independent check of the commercial treatment planning dose calculations. The spreadsheet model took into account the Ir-192 source orientation relative to the dose point of interest, and allowed the user to vary the source dwell time at any dwell position.

To include the effects of loss of backscatter material, the dose calculation spreadsheet was modified to include the TG-43 backscatter factor model and data obtained from Monte Carlo modelling reported by Poon et al. [12]. In their modified TG-43 model, the total dose to an interest point is the sum of a direct (primary) component plus a weighted proportion of a scatter dose component:

$$\dot{D} = \dot{D}_{\mathrm{TG-43,prim}} + \dot{D}_{\mathrm{TG-43,scat}} \cdot f_{\mathrm{scat}}$$

The weighting factor f_{scat} is called the scatter factor, and was tabulated by Poon et al. [12] for particular separations between the Ir-192 source and the applicator surface. The magnitude of the scatter factor varies from 1.0 for full scatter contribution, to 0.0 for no scatter contribution. The TG-43 radial dose function $g_{\mathrm{L}}(r)$ and anisotropy function $F(r,\theta)$ were also separated into primary and scatter components. Using the notation of Poon et al. [12] $f_{\mathrm{scat}} = f_{\mathrm{scat}}\ (d_1,\ d_2,\ d_3)$, and relevant parameters for a surface applicator are shown in Fig. 5.

As the distance d_1 is fixed in a flat surface applicator, the dose calculation is sufficiently simplified that inclusion of the Monte–Carlo determined scatter factor for depth d_1 tabulated as a function of d_2 versus d_3 can be implemented in a Microsoft Excel spreadsheet.

Results

Because MOSFETs are known to exhibit a variation in response with accumulated dose, energy and angle of incidence, we first measured each of these effects to estimate the overall uncertainty in our backscatter measurements.

Stability/linearity

The reproducibility of the MOSkin measurements was found to vary by up to 2.2% (1 SD) in the short term. Long term stability was measured by comparing measurements at the start and end of a sequence of measurements using the Ir-192 source. Assuming a linear decrease in detector sensitivity we found the decrease in response to be equivalent to 0.3% per Gy. The response of the MOSkins was found to be linear with dose in the range of 0.5 to 5 Gy corresponding to a change in voltage of 0.384 V per Gy ± 1.7% (1 SD) for the 6 MV beam.

Angular response

Raw measurements for the radial and azimuthal angular response were first corrected for accumulated dose response. In the azimuthal direction there was found to be no significant change in response over the range of angles measured, all measurements were within 2.7% (1 SD).

In the radial direction the response of the MOSkins varied with the radial angle. The response was greatest when the front of the MOSkin was facing the source and decreased as it was turned away both in the positive and negative angular direction. Measurements taken at 180° with the MOSkin holder orientation reversed indicated a slight offset in the position of the MOSkin in the MOSkin holder inside the cylindrical phantom. We found this offset to be equivalent to 0.23% which is equivalent to a physical distance offset of 0.082 mm. An individual correction factor for this offset was applied to each measurement at each position.

The radial response varied by 12.9% over the range of angles measured (Fig. 6), with the maximum response occurring between −30 and +60° depending on the individual MOSkin in use.

For the backscatter measurements, the geometry of the experimental set up was known, and the range of radial angles relevant to the backscatter measurements could be calculated. The maximum angle of 86.5° occurs when the source is in the catheter furthest away from the MOSkin, the minimum angle of 0° occurs when the source is in the catheter directly above the MOSkin (Fig. 7). Rather than apply multiple correction factors to each backscatter measurement to account for every source position, we instead calculated a single weighted radial uncertainty based on the length of time the source spent in each catheter and the response at that radial angle calculated from a polynomial fit to the radial angular response.

Energy response

Figure 8 shows the response of the MOSkins normalised to a mean beam energy of 2000 kV for mean beam energies between 15 and 6000 kV. The MOSkins over responded by a factor of 5 at 20 kV.

The backscatter measurements with the IOBT applicator result in two different energy spectra from the Ir-192 source. At a depth of 3 mm in water, with full backscatter conditions, the spectrum of Ir-192 has an average energy of approximately 353 keV (D. Cutajar, personal correspondence) and a response factor of 1.046 relative to the 6 MV beam (Fig. 8). The mean energy of the spectrum at a source-detector distance of 3 mm without 8 cm of backscatter is unknown but we would expect the energy to be *increased* due to the absence of low energy scatter components. Meigooni et al. reported the average energy for an ^{192}Ir source at a range of distances from the source [13]. A change of depth from 10 to 100 mm resulted in a change in average energy of 116 keV. Whilst this does not represent our experimental conditions it provides some indication that we might not expect a change in energy of more than 116 keV when removing the backscatter material. Using the data shown in Fig. 8, the response factor for an energy (353 + 116) 469 keV is 1.022. This represents difference in sensitivity of 2.4% We would not expect the difference between our two experimental conditions (with and without backscatter with constant source–detector distance) to

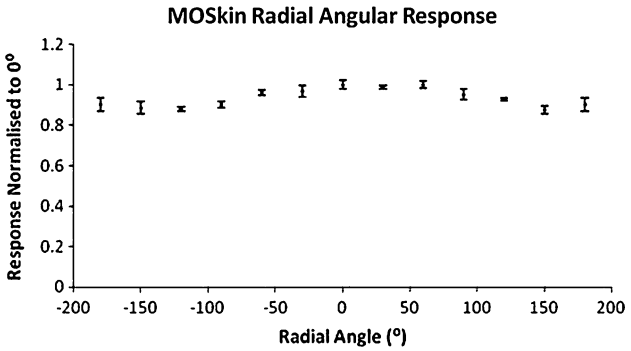

Fig. 6 MOSkin radial angular response. *Error bars* are 1 SD

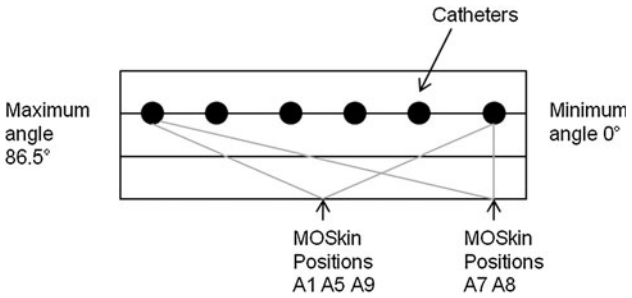

Fig. 7 Cross section of the IOBT applicator showing maximum and minimum radial angles

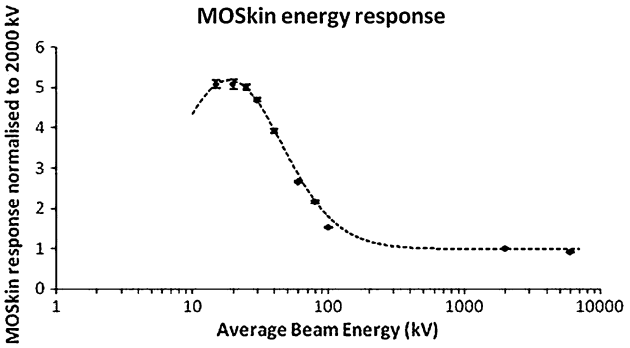

Fig. 8 MOSkin energy response. *Error bars* are 1 SD

Table 1 Dosimetric parameters and their uncertainties

Dosimetric parameter	Uncertainty	Comment
Short term reproducibility	2.2%	Summed in quadrature
Long term reproducibility	0.3% per Gy	Correction factor was applied to all raw measurements
Linearity	1.7%	Summed quadrature
Azimuthal angular response	2.7%	Summed in quadrature
Radial angular response	4.1%	Weighted uncertainty
Energy response	2.4%	Summed in quadrature
Total uncertainty	6.1%	1 Standard deviation

be this great however, we have assumed an uncertainty of 2.4% due to the energy response effect.

Table 1 shows a list of the dosimetric parameters measured, the uncertainty associated with each and how the uncertainty was applied. With the exception of long term reproducibility, for which a correction factor was applied to all raw measurements, the uncertainty from all dosimetric parameters was summed in quadrature to give a combined total uncertainty. This total uncertainty was applied to each backscatter measurement.

Calculations

Benchmarking tests showed that with the standard full scatter TG-43 dose model [11] and appropriate Ir-192 source data [14], the spreadsheet dose calculated to an array of reference points agreed to within 0.05% of that calculated with the Plato (Nucletron, Veenendaal, The Netherlands) treatment planning system, for any applicator shape up to 200 × 200 mm^2 that could be modelled as a smoothly-varying 3-dimensional surface. The spreadsheet calculations agreed within 0.5% with tabulated benchmark data available for download from the University of Valencia website http://www.uv.es/braphyqs/index2.htm.

The backscatter model used relevant scatter factor data for the Peter MacCallum Cancer Centre surface applicator, for which the thickness of backscatter material was assumed to be 3.0 mm. The modified spreadsheet was validated by comparing full scatter dose calculated using TG-43 parameters as tabulated by Poon et al. [12]. According to Poon et al. [12] the combined statistical and interpolation uncertainty in f_{scat} was <3%. Source orientation was not included in the calculation, since scatter dose is almost isotropic, and the maximum error from this approximation was expected to be <1.2% within 100 mm of the source. For a surface applicator and clinically relevant dose points, $d_2 < 20$ mm, $d_3 < 100$ mm we found the difference between Poon et al. [12] full scatter calculations and reference TG-43 data were generally <0.1%.

For the Peter MacCallum Cancer Centre surface applicator, the primary and scatter contributions to selected reference points that corresponded to the location of MOSkin detectors was calculated using the modified spreadsheet. The predicted primary dose contribution to each point was 75–87% of the total dose, while scatter dose accounted for 25–13% of the total dose. The full scatter TG-43 dose was also calculated at each point for comparison. The calculated backscatter factor shown in Table 2 is the difference between the TG-43 full scatter model and the backscatter model calculations.

Backscatter factors were measured at five positions on the IOBT applicator, as shown in Fig. 1. A correction factor was applied to all raw measurements to account for the accumulated dose response. At all positions, a lower dose was measured in the absence of scatter material above the applicator. The measured percentage reduction in dose, (backscatter factors) and those calculated are shown in Table 2 and Fig. 9. The average measured backscatter factor was 10.2 ± 6.1% and the average calculated backscatter factor was 4.3%.

Table 2 IOBT measured backscatter factors and calculated backscatter factors

Position	Measured backscatter factors (±1 SD)	Calculated backscatter factors	Difference between measured and calculated backscatter factor
A1	9.3 (±6.1)	4.6	4.7
A5	7.5 (±6.1)	4.4	3.1
A7	9.6 (±6.1)	4.0	5.6
A8	14.9 (±6.1)	3.8	11.1
A9	9.9 (±6.1)	4.6	5.3

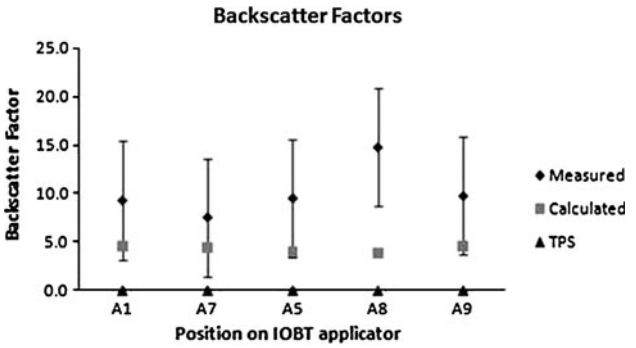

Fig. 9 The IOBT measured and calculated backscatter factors

Discussion

Stability short and long term/linearity

The short term stability of the MOSkins was found to be 2.2%, which is slightly higher than has been reported for other MOSFET devices [4, 5]. The linearly decreasing response of the MOSkins in the long term is similar to the findings of Cheung et al. [6], who found a slightly non linear decreasing response in the form of a low second order polynomial which was energy dependent. We had previously measured long term response through repeated measurements in a 6 MV beam and found a linearly decreasing sensitivity with accumulated dose which was equivalent to 0.5% per Gy. According to the findings of Cheung et al. [7], the percentage decrease from one beam energy will be proportional to the percentage decrease from a second beam energy according to the ratio of the energy response at the two beam energies. Using our results this would indicate a slightly higher percentage decrease of 0.52% per Gy for an Ir-192 source. In comparing our measurements at the start and end of a sequence of measurements, and assuming a linear decrease in detector sensitivity, we found the decrease in response to be equivalent to 0.3% per Gy, which is lower than predicted. We have assumed the difference between our measurements and the value predicted by Cheung et al. [7] is due to differences in MOSFET design and we chose to use our measured value to correct our backscatter measurements for long term sensitivity response.

The MOSkins displayed linearity with dose in the range of 0.5 to 5 Gy to within 1.7% (1 SD), and this is consistent with previous findings [4, 8].

Angular response

The maximum radial angular response for the MOSFET detectors used in this study was 12.9% which is consistent with the reported range of 2 to 15% for commercially available detectors [3, 4, 10, 15, 16]. New 'dual MOSkins', that take an average of the measurements from two MOSkins attached face to face, have reported angular variations between ±2.5% [5] and will be the subject of future investigations. To account for radial angular response we applied a single weighted uncertainty to our measurements taking into account the angle of the source to the MOSkin surface and time spent in each catheter. This uncertainty (4.1%) was the largest of all measurement uncertainties. The radial response was expected to be symmetric about 0° but the maximum response was found to vary between −30 and +60°. The asymmetry observed in the response could be due to geometrical variations in individual detectors. The general shape of the radial angular response is consistent with the physical design of the MOSkin with the response decreasing as the front of the detector is turned away from the source to a minimum response when the back of the detector is facing the source. The correction for the MOSkin holder offset of 0.23% corresponds to a physical offset of approximately 0.082 mm, so while we did apply individual correction factors to each measurement to account for this we did not confirm experimentally.

The angular response in the azimuthal direction was measured for angles of incidence from −31.0 to 35.0°, (90° refers to the cable end of the MOSkin). An angular dependence was not observed over this range, however, we would expect to observe a decrease in the response as we approach ±90°, particularly when the radiation is incident on the 'connection' end of the MOSkin where the MOSkin body and read-out cables will interfere with the dose.

Energy response

The MOSkins displayed an increased response in low energy X-rays. The maximum over response of five times occurred between the lowest mean beam energies measured, 15 and 20 kV. Kron et al. [9] found a maximum over response of 'epoxy bubble' style MOSFETs of seven times, normalised to 6 MV, at approximately 35 kV. The maximum response occurring at a higher energy for the 'epoxy bubble' style MOSFETs is most likely due to the 'epoxy bubble' filtering out the low energy part of the spectrum. As the MOSkins do not have this 'epoxy bubble' they are more sensitive to low energy beams, which explains our maximum response occurring at a lower energy. Our conservative estimation of the difference in energy response for no backscatter and full backscatter conditions using our IOBT applicator was less than 2.4%. This, along with the uncertainty associated with the linearity response, made the smallest contributions to our total uncertainty for the backscatter measurements.

IOBT applicator

Measurements made using the IOBT applicator indicate a reduced dose in the absence of back scatter material, this is as expected, however, the magnitudes of the dose reductions were larger than predicted by the modified TG-43 model calculations. While the magnitudes of the dose reductions do agree with the calculated reductions within experimental uncertainty, there is a systematic difference of on average 6.0%. The average calculated dose reduction for the five positions was $4.3 \pm 0.4\%$, the average dose reduction measured was $10.2 \pm 6.1\%$ (1 SD), more than twice as much, indicating the possibility of a systematic error. One possible explanation for this difference could be changes in the geometry of the experimental set up. When the scatter material was placed on top of the applicator it is possible the applicator was compressed leading to a shorter distance between source and detector, hence recording a higher dose than in the uncompressed state (assuming that the compression tends to spread the applicator laterally and make it thinner, rather than increase its density). Using the dose rate per unit air-kerma strength around an Ir-192 source as described by Daskelov et al. [14], we calculated the amount of compression needed to produce the appropriate increase in dose in the presence of scatter material is just 0.10 mm, and therefore a possible explanation for the difference between measured and calculated backscatter factors.

The backscatter factor for position A8 is significantly larger (14.8%) than measured at the other four positions. This measurement was repeated on two occasions with consistent results. One possible explanation for this is that position A8 is located on the corner of the IOBT applicator where it has the least surrounding scatter material and a close proximity to air gaps.

Conclusions

Dosimetric characteristics of MOSkin detectors were investigated using both an Ir-192 brachytherapy source and a 6 MV linac. The greatest source of uncertainty was found to be from radial angular dependence which contributed a total of 4.1% to the total measurement uncertainty of 6.1%. Measurements to ascertain the percentage dose reduction from lack of back scatter material were made using an IOBT applicator. All measurements made indicated a lower dose was delivered in the absence of back scatter material. The average measured backscatter factor was 10.2% with 6.1% experimental uncertainty. Four out of five measured backscatter factors were within experimental uncertainty of the calculated backscatter factors. A systematic difference was seen in the measured backscatter factors which could be accounted for by a small amount of compression in the experimental set up.

Acknowledgments The Authors would like to thank the Centre for Medical Radiation Physics at the University of Wollongong for the generous supply of the MOSkin devices used in this project and in particular we would like to thank Dr Dean Cutajar for his assistance. We would also like to thank the radiation therapists, especially Ms Sylvia van Dyk at the Peter MacCallum Cancer Centre for their careful construction of the IOBT applicator and helpful discussion in the clinical use of the applicator.

References

1. Kron T (1994) Thermoluninescence dosimetry and its applications in medicine-Part 1: physics, materials and equipment. Australas Phys Eng Sci Med 17:175–199
2. Niroomand-Rad A, Blackwell CR, Coursey BM, Gall KP, Galvin JM, McLaughlin WL, Meigooni AS, Nath R, Rodgers JE, Soares CG (1998) Radiochromic film dosimetry: Recommendations of AAPM Radiation Therapy Committee Task Group 55. Med Phys 25:2093–2115
3. Kwan IS, Rosenfeld AB, Qi ZY, Wilkinson D, Lerch MLF, Cutajar DL, Safavi-Naeni M, Butson M, Bucci JA, Chin Y, Perevertaylo VL (2008) Skin dosimetry with new MOSFET detectors. Radiat Meas 43:929–932
4. Ramaseshan R, Kohli KS, Zhang TJ, Lam T, Norlinger B, Hallil A, Islam M (2004) Performance characteristics of a micro-MOSFET as an in vivo dosimeter in radiation therapy. Phys Med Biol 49:4031–4048
5. Hardcastle N, Cutajar DL, Metcalfe PE, Lerch MLF, Perevertaylo VL, Tome WA, Rosenfeld AB (2010) In vivo real-time rectal wall dosimetry for prostate radiotherapy. Phys Med Biol 55: 3859–3871
6. Cheung T, Butson MJ, Yu PKN (2004) Effects of temperature variation on MOSFET dosimetry. Phys Med Biol 49:N191–N196
7. Cheung T, Buston MJ, Yu PKN (2009) Energy dependence corrections to MOSFET dosimetric sensitivity. Australas Phys Eng Sci Med 32:16–20
8. Benevides LA, Hintenlang DE (2006) Characterization of metal oxide semiconductor field effect transistor dosimeters for application in clinical mammography. Med Phys 33:514–520
9. Kron T, Duggan L, Smith T, Rosenfeld A, Butson M, Kaplan G, Howlett S, Hyodo K (1998) Dose response of various radiation detectors to synchrotron radiation. Phys Med Biol 43:3235–3259
10. Ramani R, Russell S, O'Brien P (1997) Clinical dosimetry using MOSFETs. Int J Radiat Oncol Biol Phys 37:959–964
11. Nath R, Anderson LL, Luxton G, Weaver KA, Williamson JF, Meigooni AS (1995) Dosimetry of interstitial brachytherapy sources: Recommendations of the AAPM Radiation Therapy Committee Task Group No. 43. Med Phys 22:209–234
12. Poon E, Verhaegen F (2009) Development of a scatter correction technique and its application to HDR Ir-192 multicatheter breast brachytherapy. Med Phys 36:3703–3713. doi:10.1118/1.3157105
13. Meigooni AS, Meli JA, Nath R (1988) Influence of the variation of energy spectra with depth in the dosimetry of ^{192}Ir using LiF TLD. Phys Med Biol 33:12
14. Daskalov GM, Loffler E, Williamson JF (1998) Monte Carlo-aided dosimetry of a new high dose-rate brachytherapy source. Med Phys 25:2200–2208
15. Roshau JN, Hintenlang DE (2003) Characterization of the angular response of an "isotropic" MOSFET dosimeter. Health Phys 84:376–379
16. Cygler JE, Saoudi A, Perry G, Morash C, Choan E (2006) Feasibility study of using MOSFET detectors for in vivo dosimetry during permanent low-dose-rate prostate implants. Radiother Oncol 80:296–301